averaging has occurred that the dynamical variables have become Gaussian distributed. Many random physical processes, because they meet the prerequisites of the central limit theorem of statistics, exhibit such a time regime.

Consider a random variable $v(t)$, whose probability distribution is $W(v,t)$, which is the result of random increments Δv (accumulated, say, over time interval Δt) that are themselves distibuted with probability distribution $\psi(v,\Delta v)$. This is known as a "random walk".

An example with non-trivial dependence on v is

$$\psi\left(v,\Delta v\right)=\frac{1}{\sqrt{4\pi\,q\,\Delta t}}\,\exp-\frac{\left(\Delta v+\beta\,v\,\Delta t\right)^{2}}{4q\,\Delta t}\ . \tag{5.1.1}$$

Moments of Δv are defined by

$$\begin{aligned}
&\int\Delta v^{0}\,\psi\left(v,\Delta v\right)\,d\left(\Delta v\right)=1\ ,\\
&\int\Delta v^{1}\,\psi\left(v,\Delta v\right)\,d\left(\Delta v\right)\equiv\left\langle v\right\rangle=-\beta\,v\,\Delta t\ ,\\
&\int\Delta v^{2}\,\psi\left(v,\Delta v\right)\,d\left(\Delta v\right)\equiv\left\langle v^{2}\right\rangle=2q\,\Delta t\ ,
\end{aligned} \tag{5.1.2}$$

where the final forms correspond to the example (5.1.1). The time evolution of $W(v,t)$ is governed by the consistency condition

$$W\left(v,t+\delta t\right)=\int W\left(v-\Delta v,t\right)\,\psi\left(v-\Delta v,\Delta v\right)\,d\left(\Delta v\right)\ . \tag{5.1.3}$$

Performing Taylor series expansions, this relation becomes

$$\begin{aligned}
W\left(v,t\right)+\frac{\partial W}{\partial t}\,\Delta t+\ldots=\int&\left(W\left(v,t\right)-\frac{\partial W}{\partial v}\,\Delta v+\frac{1}{2}\,\frac{\partial^{2}W}{\partial v^{2}}\,\Delta v^{2}+\ldots\right)\\
&\times\left(\psi\left(v,\Delta v\right)-\frac{\partial\psi}{\partial v}\,\Delta v+\frac{1}{2}\,\frac{\partial^{2}\psi}{\partial v^{2}}\,\Delta v^{2}+\ldots\right)\,d\left(\Delta v\right)\ .
\end{aligned} \tag{5.1.4}$$

Expanding the integrand, dropping terms proportional to Δv^3 and higher, and utilizing Eqs. (5.1.2), yields the so-called "Fokker-Planck" equation;

$$\frac{\partial W}{\partial t}\,\Delta t=-\frac{\partial\left(W\langle v\rangle\right)}{\partial v}+\frac{1}{2}\,\frac{\partial^{2}\left(W\langle v^{2}\rangle\right)}{\partial v^{2}}\ . \tag{5.1.5}$$

With the moments of example (5.1.1) this becomes

$$\frac{\partial W}{\partial t}=\beta\,\frac{\partial\left(W\,v\right)}{\partial v}+q\,\frac{\partial^{2}W}{\partial v^{2}}\ . \tag{5.1.6}$$

Some miscellaneous comments concerning the Fokker-Planck equation:

- When applied to a statistical problem, the word "solve" is not unambiguous. Often one is satisfied to find just the leading moment (average) though knowing the next moment (r.m.s. deviation) is typically also desireable. But there are many other properties, such as correlations, that may also be needed, the most ambitious being the detailed probability distribution. If one knows the probability distribution, it is straightforward to calculate the leading moments, but the converse is not true. Since the Fokker-Planck equation is satisfied by the probability distribution W it is, in principle, an extremely powerful expression of the statistical problem.
- Since the F-P equation is a partial differential equation (in one more variable as there are independent variables) its analytic solution is difficult. It may however be subject to numerical analysis.
- Other statistical methods, such as stochastic differential equations, can sometimes be formulated to give weaker information, such as low order moments, directly.
- In its full generality, the Fokker-Planck equation describes the evolution of a system from arbitrary initial conditions to its eventual equilibrium state. Typically it is the equilibrium distribution that is actually sought and, in that case, setting $\partial W/\partial t = 0$ results in a much more manageable equation. This is probably the main use of the F-P equation. Since the right hand side of the F-K consists of a linear operator operating on W, eigenfunction expansion methods are effective.
- Because the F-P equation is so powerful, its derivation depends on all statistical properties of the stochastic sources. This makes the valid derivation of the F-P equation very difficult in general. The derivation in the section has been as simple as it is only because of the special assumptions that are implicitly present in Eq. (5.1.3). The probability of transition depends only on the instantaneous state of the system, independent of the past. Processes satisfying this assumption are called Markov processes. Certain statistical methods, such as correlation functions, are introduced partly for the purpose of deriving the F-P equation appropriate for stochastic problems.

- Yet another weakness of the F-P equation is that its has been truncated after second derivatives. This may be a good approximation in many cases, but is unlikely to be any better than that.

The various calculations of distributions described in previous sections have been based on arguments and averagings which, though physically well motivated, were rather ad hoc. They involved calculating the statistical properties of random functions that depend on other random functions. One purpose for the discussion of stochastic physics in this chapter is that a rather powerful mathematical formalism based on "stochastic differential equations" has been developed for performing such calculations. We therefore proceed in this direction.

Another way of studying the distribution of v is to say that v satisfies the following stochastic differential equation or "Langevin equation",

$$\frac{dv}{dt} = -\beta\, v + A\,(t) \ , \tag{5.1.7}$$

where $A(t)$ is a random function (whose statistical properties are assumed to be known). v acquires random features By virtue of its satisfying this equation containing a random term, itself v acquires random features. If, for example, v were to stand for the velocity of a particle of mass m, $A(t)/m$ would be a random force acting on the particle. The term $-\beta\, v$, due, for example, to viscous drag, is determinative, not random.

Though $A(t)$ is assumed to fluctuate rapidly, its properties cannot be arbitrary if the motion it causes is to be physically realistic. Letting v_0 be an initial particle speed, Eq. (5.1.7) can be re-expressed as an integral equation

$$v - v_0\, e^{-\beta\, t} = e^{-\beta\, t} \int_0^t e^{\beta t'}\, A\left(t'\right)\, dt' \ . \tag{5.1.8}$$

Let us break up the range of that integral into a sum of uniform time intervals of length Δt assumed to be sufficiently short that all functions except $A(t')$ can be treated as constant over time intervals of this length;

$$e^{-\beta\, t} \sum_j e^{\beta j \Delta t} \int_{j\Delta t}^{(j+1)\Delta t} A\left(t'\right)\, dt' \ . \tag{5.1.9}$$

The integral in this expansion is (except for factor m) the impulse $B_{\Delta t}$ delivered to the particle during the time interval;

$$B_{\Delta t}\,(t) = \int_t^{t+\Delta t} A\left(t'\right)\, dt' \ . \tag{5.1.10}$$

$\Delta t\, B_{\Delta t}(t)$ is a "smoothed" version of $A(t)$, with the factor Δt being free, and somewhat arbitrary. Expressed in terms of $B_{\Delta t}$, Eq. (5.1.8) becomes

$$v - v_0\, e^{-\beta\, t} = \sum_j e^{-\beta(t-j\Delta t)}\, B_{\Delta t}\ . \tag{5.1.11}$$

In words, the deviation from where the particle would be in the absence of random force is a sum of impulses suffered, but with each derated by the time since it occurred. For $\beta = 0$ the formula amounts to dissipationless conservation of momentum , but with the built-in assumption that the impulses have no systematic dependence on t or v. "Solving" the stochastic equation amounts to imferring statistical properties of v from known statistical properties of A, or now B, and Eq. (5.1.11) represents substantial progress. For example, we can equate the variance (square of standard deviation) of left and right sides of the equation. To do this we use the rule that the variance of a sum is the sum of variances. This variance would be infinite in the special case $\beta = 0$, because of the infinite sum. But, for $\beta > 0$, the exponential factor damps the importance of fluctuations that occurred in the distant past. Quantitatively, using the abbreviation $\sigma^2_{B_{\Delta t}} = \mathrm{var}[B_{\Delta t}]$

$$\begin{aligned} \mathrm{var}\left[\sum_j e^{\beta(j\Delta t - t)}\, B_{\Delta t}\right] &= \sum_j e^{-\beta^2(t-j\Delta t)^2}\, \sigma^2_{B_{\Delta t}} \\ &\approx \frac{\sigma^2_{B_{\Delta t}}}{\Delta t} \int_0^\infty \exp\left(-\frac{\left(\sqrt{2}\,\beta\right)^2 \tau^2}{2}\right) d\tau \\ &= \frac{\sigma^2_{B_{\Delta t}}}{\Delta t}\, \frac{\sqrt{\pi}}{2\beta}\ . \end{aligned} \tag{5.1.12}$$

For large time, the left hand side of Eq. (5.1.11) approaches v which, according to statistical mechanics, should be temperature T, Maxwell-distributed;

$$W\,(v, t; v_0) \ \stackrel{t\to\infty}{\longrightarrow}\ \sqrt{\frac{m}{2\pi\, k\, T}}\, \exp\left(-\frac{m\, v^2/2}{k\, T}\right)\ , \tag{5.1.13}$$

independent of v_0. According to this,

$$\langle v^2 \rangle \equiv \sigma_v^2 \equiv \mathrm{var}\,[v] = \frac{kT}{m}\ . \tag{5.1.14}$$

To be consistent with this result, combining Eqs. (5.1.12) and (5.1.14) then yields

$$\langle B^2_{\Delta t} \rangle \equiv \sigma^2_{B_{\Delta t}} = \frac{2\beta k T \Delta t}{m}\ , \tag{5.1.15}$$

and the result that a distribution function for $B_{\Delta t}$ leading to distribution (5.1.13) is

$$w\left(B_{\Delta t}\right) = \frac{1}{\sqrt{2\pi\left(2\beta kT\Delta t/m\right)}} \exp\left(-\frac{B_{\Delta t}^2}{2\left(2\beta kT\Delta t/m\right)}\right) \ . \tag{5.1.16}$$

Chandrasekar proves this result in greater generality and with, perhaps, more rigor than has been exhibited here. The leading moments of this distribution are

$$\langle B_{\Delta t}\rangle = 0 \ , \quad \langle B_{\Delta t}^2\rangle = \frac{2\beta\, k\, T\, \Delta t}{m} \ . \tag{5.1.17}$$

The two approaches (random walk and Langevin) can be reconciled (for the special example discussed so far.) The Langevin equation has been approximated by

$$\Delta\, v = -\beta\, v\, \Delta t + B_{\Delta t} \ . \tag{5.1.18}$$

Identifying $w(B_{\Delta t})$ in Eq. (5.1.16) with $\psi(v, \Delta v)$ in Eq. (5.1.1), and using Eq. (5.1.18), the processes will be equivalent if

$$q = \frac{\beta kT\Delta t}{m} \ . \tag{5.1.19}$$

In preparation for exhibiting a close relationship between Brownian motion phenomena and quantum fluctuation electron beam phenomena, several comments can be made concerning this result:

- Eq. (5.1.15) is an example of a "fluctuation/dissipation" relation. This equation relates the "noise strength" σ_B and the "damping strength" β required for the phenomenon to be consistent with statistical thermodynamics. The temperature T is implicated in this relation. The equilibrium conditions represent a compromise between fluctuation and damping.
- With rapidly oscillatory, or short pulse, forces it is the the impulse integral $B_{\Delta t}$ that is more directly applicable than the instantaneous force $A(t)$.
- The ultimate distributions are largely independent of the detailed force variation, provided the time interval Δt can be chosen long enough to average over many noise pulses yet short compared to times over which v changes appreciably. Noise satisfying these requirements is known as "white noise."
- If the noise consists of disjoint pulses, it is only their rate and their r.m.s. strength that affect the ultimate distribution.

5.2. Statistical Properties of Systems of Random Points

A "system of random points (in time)" consists of random points t_j, having average rate $\mathcal{N}_1$ points per second. (The ordering of indices j is unrelated to the chronological order of arrival of the points.) If, as we assume, the times t_j are uncorrelated, it is a "Poisson system". During a time interval T the expected number of points is $\mathcal{N}_1 T$, but the actual number of arrivals, call it K, will be Poisson distributed. The probability P_K of exactly K arrivals is

$$P_K = \frac{(\mathcal{N}_1 T)^K}{K!}\, e^{-\mathcal{N}_1 T} \ . \tag{5.2.1}$$

This probability distribution has moments

$$\sum K^0\, P_K = 1 \ , \quad m_1 = \sum K^1\, P_K = \mathcal{N}_1 T \ , \quad m_2 = \sum K^2\, P_K = \mathcal{N}_1 T + (\mathcal{N}_1 T)^2 \ . \tag{5.2.2}$$

In spite of the pulse-like nature of such systems, the field $\xi(t)$ describing some phenomenon under study, that differs appreciably from zero only during time intervals close to one of the random points can also be thought of as a random function of time, or as a "random process". (Examples are molecular force $F(t)$ or synchrotron radiation power $P(t)$.) The values of $\xi(t)$ are almost zero most of the time, but occasionally they become large. Given many independent copies of the same process ξ_1, ξ_2, ξ_3, ..., their values $\xi_1(t_1)$, $\xi_2(t_1)$, $\xi_3(t_1)$, ..., at a particular time t_1 are random variables for which averages and r.m.s. values can be determined

$$\begin{aligned} k_1(t_1) = \langle \xi(t_1) \rangle &= \lim_{n\to\infty} \frac{\xi_1(t_1) + \xi_2(t_1) + \ldots + \xi_n(t_1)}{n} \ , \\ \langle \xi^2(t_1) \rangle &= \lim_{n\to\infty} \frac{\xi_1^2(t_1) + \xi_2^2(t_1) + \ldots + \xi_n^2(t_1)}{n} \ , \\ \sigma_\xi^2 \equiv k_{\xi,2} &= \langle (\xi - \langle \xi \rangle)^2 \rangle \ . \end{aligned} \tag{5.2.3}$$

These quantities are shown as potentially dependent on time t_1 but we will mainly be concerned with "stationary processes" for which these moment parameters are constant. We then define $m = k_1$, $k = k_2$.

From two random variables ξ_1 and ξ_2 one can form the "cross correlation"

$$\mathbf{K}[\xi_1, \xi_2] = \langle \xi_1, \xi_2 \rangle - \langle \xi_1 \rangle \langle \xi_2 \rangle \ . \tag{5.2.4}$$

In particular, the two random variables can be the values of random process $\xi(t)$ at times t and $t + \tau$. Abbreviating these values by ξ and ξ_τ, and assuming their correlation is

independent of t, we define "correlation function" $k_\xi(\tau)$ by[†]

$$k_\xi(\tau) = \mathbf{K}[\xi, \xi_\tau] \ , \quad \text{which implies} \quad k_\xi(-\tau) = k_\xi(\tau) \quad \text{and} \quad \sigma_\xi^2 = k_\xi(0) \ . \tag{5.2.5}$$

Digression concerning characteristic functions. I insert here material that will be needed later on, but recommend that it be skipped right over. From $w(\xi, t)$, the probability distribution of ξ at time t, one defines the "characteristic function", which is another name for Fourier transform;

$$\Theta(u;t) = \langle e^{iu\xi(t)} \rangle = \int w(\xi;t)\ e^{iu\xi}\, d\xi \ . \tag{5.2.6}$$

For the joint probability distribution, $w(\xi_1, \xi_2; t_1, t_2)$, of the two variables, $\xi(t_1)$ and $\xi(t_2)$, the characteristic function is

$$\Theta_2(u_1, u_2; t_1, t_2) = \langle e^{iu_1\xi(t_1) + iu_2\xi(t_2)} \rangle \ . \tag{5.2.7}$$

Assuming that all moments are independent of time and (optimistically) supposing that the Fourier transforms can be approximated by their leading terms, we have

$$\begin{aligned} \Theta(u;t) &\approx \exp\left(\langle\xi\rangle\, iu + \mathrm{var}(\xi)\ \frac{(iu)^2}{2!} \right) \ , \\ \Theta_2(u_1, u_2; t_1, t_2) &\approx \exp\left(i\langle\xi\rangle\ (u_1 + u_2)\right) \exp\left(-\frac{1}{2} \sum_{t_\alpha, t_\beta = 1}^{2} \mathbf{K}\left[\xi(t_\alpha), \xi\left(t_\beta\right)\right]\ u_\alpha u_\beta \right) \ . \end{aligned} \tag{5.2.8}$$

The motivation behind these formulas is that, knowing the low order moments of a function appearing in a stochastic equation one can obtain its Fourier transforms, which will then be transformed in some way, and then inverted to obtain some desired probability distribution. The mean $\langle\xi\rangle$ and the correlation function $k_\xi(\tau) = \mathbf{K}[\xi, \xi_\tau]$, appearing in Θ_2, are the leading players in this game. This is how Fokker-Planck equations can be derived. This ends the digression.

The Brownian motion and photon emission processes both have the property that the value at time t_1 within one pulse, say $F_j(t_1)$, correlates with the value $F_j(t_2)$ within the

[†] The term "correlation function" seems misleading to me. If there are no stochastic forces the value $\xi(t+\tau)$ differs neglibly from $\xi(t)$ for small τ, i.e. it "correlates" perfectly. The non-vanishing of $k_\xi(\tau)$ implies the loss of correlation in this sense.

same pulse at another time, but not with any value of any other pulse. A random function with these properties is

$$I(t) = \sum_k F(t - t_k) \overset{\text{e.g.}}{=} e \sum_k \delta(t - t_k) \ , \tag{5.2.9}$$

where the t_k are random times, occurring with average rate $\mathcal{N}_1$. In this final expression the "pulse-like" function represents the charge distribution of a point electron of charge e and $I(t)$ is the current passing a fixed point, due to randomly arriving electrons. For cases in which exactly K pulses occur during a time interval of length T, long compared to pulse lengths, the average current $\langle I_K \rangle$ is

$$\langle I_K \rangle = \int_0^T \frac{dt_1}{T} \int_0^T \frac{dt_2}{T} \cdots \int_0^T \frac{dt_K}{T} \sum_{k=1}^{K} F(t - t_k) \approx \frac{K}{T} \int_{-\infty}^{\infty} F(t)\, dt \ , \tag{5.2.10}$$

where the final expression is indicated as an approximation only to allow for points that happen to fall close to the ends of the interval. The "end-effect" error from this source can be made arbitrarily small. Averaging over all possible numbers of arrivals yields

$$\langle I \rangle = \sum_K P_K \langle I_K \rangle = \frac{1}{T} \int_{-\infty}^{\infty} F(t)\, dt \sum_K K \frac{(\mathcal{N}_1 T)^K}{K!} e^{-\mathcal{N}_1 T} \tag{5.2.11}$$

Since the final summation can be recognized as the expected number of arrivals in time T, which is $\mathcal{N}_1 T$, we obtain

$$\langle I \rangle = \frac{m_1}{T} \int_{-\infty}^{\infty} F(t)\, dt \ = \mathcal{N}_1 \int_{-\infty}^{\infty} F(t)\, dt \ . \tag{5.2.12}$$

For the example of the current made up of point electrons, the result is $\langle I \rangle = \mathcal{N}_1 e$. The reason for having followed this, seemingly circular, path, to find this obvious result, is to practice with a line of reasoning that will next be used to find the correlation function $k(\tau) = \langle I, I_\tau \rangle$ of a current of pulses. As in Eq. (5.2.10), for those cases in which exactly K pulses occur in time T, the mean of the product of current and current-delayed is

$$\langle I_K\, I_{K\tau} \rangle = \sum_{k=1}^{K} \sum_{m=1}^{K} \int_0^T \frac{dt_1}{T} \int_0^T \frac{dt_2}{T} \cdots \int_0^T \frac{dt_K}{T} F(t - t_k)\, F(t + \tau - t_m) \tag{5.2.13}$$

In all cases for which $k = m$ the integral is approximately

$$\int_0^{\infty} \frac{dt}{T} F(t)\, F(t + \tau)\ m \tag{5.2.14}$$

where, again, the approximation is arbitrarily good except at the ends. In cases for which $k \neq m$ the integral is approximately

$$\int_0^T \frac{dt_k}{T} F(t - t_k) \int_0^T \frac{dt_m}{T} F(t - t_m) \approx \left(\int_{-\infty}^{\infty} \frac{dt}{T} F(t) \right)^2 . \tag{5.2.15}$$

where, in the first step, dropping the τ is equivalent to a negligibly small shift in time t_k. Counting the terms of both types we obtain

$$\langle I_K \, I_{K\tau} \rangle = \frac{K}{T} \int_0^{\infty} F(t) \, F(t+\tau) \, dt + \frac{K(K-1)}{T^2} \left(\int_{-\infty}^{\infty} F(t) \, dt \right)^2 . \tag{5.2.16}$$

To complete the calculation as in Eq. (5.2.11), we sum over values of K, weighting each average with P_K,

$$\langle I \, I_\tau \rangle = \frac{m_1}{T} \int_0^{\infty} F(t) \, F(t+\tau) \, dt + \frac{m_2 - m_1}{T^2} \left(\int_{-\infty}^{\infty} F(t) \, dt \right)^2 . \tag{5.2.17}$$

Defining the correlation function as in Eq. (5.2.5) we obtain

$$\mathbf{K}[I, I_\tau] \equiv \langle I \, I_\tau \rangle - \langle I \rangle^2 = \mathcal{N}_1 \int_0^{\infty} F(t) \, F(t+\tau) \, dt , \tag{5.2.18}$$

where the cancellation of all but the surviving term follows from Eqs. (5.2.2).

For the special case given by the final form of Eq. (5.2.9), $I(t) = e \sum_k \delta(t - t_k)$, this result becomes

$$k(I, \tau) \equiv \mathbf{K}[I, I_\tau] = e^2 \mathcal{N}_1 \int_0^{\infty} \delta(t) \, \delta(t+\tau) \, dt = e^2 \mathcal{N}_1 \, \delta(\tau) . \tag{5.2.19}$$

The process is said to be "δ-correlated". The essential parameter of the process is the product $e^2\mathcal{N}_1$. In this limit, according to Formula Eq. (5.2.5), $\sigma_I^2 = k(I, 0)$ has become infinite, and hence unphysical. The problem is that the frequency spectrum of I extends to infinity. (Infinite bandwidth.) This may or may not be important, depending on the use to which the correlation function is put. Subsequent averaging over time or filtering of high frequencies could restore feasible behavior.

Within the formalism already described in this section, for any valid physical system, the function $F(t - t_k)$ would be less singular, and the result of evaluating the integral in Eq. (5.2.18) would replace the factor $\delta(\tau)$ in Eq. (5.2.19) by a less singular function. For example, approximating the δ-function by a Gaussian yields

$$k(I, \tau) = \frac{e^2 \mathcal{N}_1}{\sqrt{2\pi} \, \sigma_t} \exp\left(\frac{-\tau^2}{2\sigma_t^2} \right) , \tag{5.2.20}$$

which now has two essential parameters.

Can this process consisting of random points be cast into a form resembling the random walk discussed earlier? As it stands the answer is "no", because all pulses have the same polarity.

5.3. Nonidentical, Bipolar, Short Pulses, Random in Time

The only difference between the system of random points just discussed and either the Brownian motion or synchrotron radiation processes, is that the pulse amplitude (analogous to the coefficient e) is also random for those processes. Continuing with the example of a current made up of random charges, let us allow unequal charges, of either sign, starting with just two, say e_1 and e_2, occurring with rates $\mathcal{N}_1$ and $\mathcal{N}_2$. (Elsewhere in these notes the subscript 1 on $\mathcal{N}_1$ indicates unit time interval. This index is being comandeered only temporarily for the present discussion.) It is possible to distinguish the currents I_1 and I_2 corresponding to charges e_1 and e_2, and the formulas of the previous section apply to these currents separately. But we wish to find the statistical properties of $I = I_1 + I_2$. The mean current is

$$\langle I \rangle = \langle I_1 \rangle + \langle I_2 \rangle = e_1 \mathcal{N}_1 + e_2 \mathcal{N}_2 \ , \tag{5.3.1}$$

which vanishes if $e_1 \mathcal{N}_1 = -e_2 \mathcal{N}_2$. The correlation function is

$$\begin{aligned} k\,(I,\tau) &= \langle (I_1 + I_2)\,(I_{1\tau} + I_{2\tau}) \rangle - \langle I_1 + I_2 \rangle^2 \\ &= k\,(I_1,\tau) + k\,(I_2,\tau) + \langle I_1\, I_{2\tau} \rangle + \langle I_2\, I_{1\tau} \rangle - 2 \langle I_1 \rangle \langle I_2 \rangle \\ &= k\,(I_1,\tau) + k\,(I_2,\tau) \ . \end{aligned} \tag{5.3.2}$$

Let us apply the latter formula to a current consisting of randomly arriving delta functions;

$$I\,(t) = \sum_{k_1} e_1\, \delta\,(t - t_{k_1}) + \sum_{k_2} e_2\, \delta\,(t - t_{k_2}) \ . \tag{5.3.3}$$

We obtain

$$\begin{aligned} \langle I \rangle &= e_1\, \mathcal{N}_1 + e_2\, \mathcal{N}_2 \\ k\,(I,\tau) &= \left(e_1^2 \mathcal{N}_1 + e_2^2 \mathcal{N}_2 \right)\, \delta\,(\tau) \ . \end{aligned} \tag{5.3.4}$$

These formulas can be generalized to cover the case of charges that can take on a continuum of values, with $\mathcal{N}_1\, n_e(e)\, de \equiv (d\mathcal{N}_1/de)\, de$ being the rate of charges in the range e to $e + de$.

We obtain

$$I = \sum_k e_k \, \delta \left(t - t_k \right) \ ,$$

$$\langle I \rangle = \mathcal{N}_1 \int_0^\infty e \, n_e \left(e \right) \, de \equiv \mathcal{N}_1 \, \langle e \rangle_e \tag{5.3.5}$$

$$k \left(I, \tau \right) = \delta \left(\tau \right) \mathcal{N}_1 \int_0^\infty e^2 \, n_e \left(e \right) \, de \equiv \delta \left(\tau \right) \mathcal{N}_1 \, \langle e^2 \rangle_e \ .$$

Here the notation $\langle \rangle_e$ indicates averaging over the distribution of possible charges, which has to be distinguished from $\langle \rangle$ which indicates averaging over arrival times.

These formulas are directly applicable to the random emission of photons by circulating electrons. Of course e has to be identified as photon energy u, and I as radiated power. These formulas are then directly comparable to Eqs. (4.2.7), which gives actual numerical values for the stochastic parameters, $\langle e \rangle_e$ and $\langle e^2 \rangle_e$, in terms of critical energy u_c, which is a function of particle energy and local magnetic field. It is significant, and essentially simpler than might have been feared a priori, that all stochastic properties are parameterized by just two parameters.

5.4. Fokker-Planck Equation Derived From Stochastic Differential Equation

Can this process consisting of random points be cast into a form resembling the random walk discussed earlier? After introducing the averaging interval Δt, the randomness in the Langevin approach became parameterized by a single parameter, $\sigma^2_{B_{\Delta t}}$, (value given in Eq. (5.1.15).) If the assumptions needed to validate this introduction of Δt are satisfied by the system of random points, i.e. $\mathcal{N}_1 \Delta t >> 1$, the same parameterization should be applicable.

Basically we are faced with "integrating" the stochastic differential equation

$$\dot{Q} = I \left(t \right) \ , \quad \text{or} \quad Q = Q_0 + \int_0^t I \left(t' \right) \, dt' \ , \tag{5.4.1}$$

with I and its low order correlation functions given by Eqs. (5.3.5). We assume that all higher order moments vanish. Integrating the equation amounts to finding the probability distribution of $Q(t)$ and, in particular, its standard deviation at $t = \Delta t$.

The basic idea is that we know the moments of I and, using the equation, can figure out the moments of Q and, from them, the probability distribution of Q. The derivation

will be purely formal and heuristic. Increments to Q over time τ are given by

$$Q_\tau - Q = \int_t^{t+\tau} I\left(t'\right)\, dt' \ . \tag{5.4.2}$$

Define moments of these increments by $m_1 = \langle Q_\tau - Q \rangle$, and $m_2 = \langle (Q_\tau - Q)^2 \rangle$, and, from them, cumulants by $k_1 = m_1$, and $k_2 = m_2 - m_1^2$. All increase linearly with τ for small τ. In particular

$$\begin{aligned} k_1\left(Q\right) &= \langle \int_t^{t+\tau} I\left(t_1\right)\, dt_1 \rangle = \int_t^{t+\tau} k_{I,1}\left(t_1\right)\, dt_1 \\ k_2\left(Q\right) &= \int_t^{t+\tau} \int_t^{t+\tau} k_{I,2}\left(t_1, t_2\right)\, dt_1\, dt_2 \end{aligned} \tag{5.4.3}$$

Like the first of these equations, the second follows because the averages of integrals are equal to the integrals of the averages. Using Eq. (5.3.5) we obtain

$$k_1\left(Q\right) = \langle I \rangle\, \tau + \ldots \ , \quad k_2\left(Q\right) = \mathcal{N}_1 \left\langle e^2 \right\rangle_e \delta\left(\tau\right)\, \tau + \ldots \ . \tag{5.4.4}$$

Unfortunately it seems to be necessary to use the previously introduced characteristic function. If $w(I)$ is the probability distribution of I, then its characteristic function is

$$\Theta_I\left(u\right) = \int e^{iuI}\, w\left(I\right)\, dI \ , \tag{5.4.5}$$

i.e. $\Theta_I = \mathcal{F}(w)$, the Fourier transform. Conversely, then

$$w\left(I\right) = \frac{1}{2\pi} \int e^{-iuI}\, \Theta_I\left(u\right)\, du \ . \tag{5.4.6}$$

and, as Eq. (5.2.6) we approximate the characteristic function by its leading moments

$$\Theta\left(u; t\right) = \exp\left(k_1\left(Q\right) - k_2\left(Q\right)\, \frac{u^2}{2!} \right) \ . \tag{5.4.7}$$

Differentiating with respect to t yields

$$\dot{\Theta} = \left(\frac{dk_1}{dt} - \frac{u^2}{2}\, \frac{dk_2}{dt} \right)\, \Theta \tag{5.4.8}$$

The probability distribution of $Q - Q_0$ is given by a formula analogous to Eq. (5.4.6),

$$w\left(Q - Q_0, t\right) = \frac{1}{2\pi} \int e^{-iu\left(Q - Q_0\right)}\, \Theta_Q\left(u, t\right)\, du \ . \tag{5.4.9}$$

Differentiating this with respect to t and substituting from Eq. (5.4.8) yields

$$\begin{aligned} \dot{w} &= \sum_{s=1}^{2} \frac{\dot{k}_s}{s!} \int \left(iu\right)^s\, e^{-iu\left(Q - Q_0\right)}\, \Theta_Q\left(u, t\right)\, du \\ &= \sum_{s=1}^{2} \frac{\left(-1\right)^s}{s!}\, \dot{k}_s\, \frac{\partial^s w}{\partial Q^s} \ . \end{aligned} \tag{5.4.10}$$

This has illustrated how the Fokker-Planck equation is obtained from the correlation functions. (There may be a factor of 2 missing somewhere.)

Chapter 6.
Undulator Radiation

6.1. Introduction

A fundamental parameter characterizing an undulator (or wiggler) is K, where K/γ is the maximum angle of an electron passing through the device. Initially in this chapter the radiation into the lowest (or fundamental) interference maximum from an undulator will be calculated. This corresponds to the case $K << 1$. There will be occasional references to Jackson[2], as well as to Kim.[4] The word "frequency" (or its corresponding wavelength) seems most apt when discussing interference of X-rays, while the word "energy" seems most apt when discussing the detection of individual X-ray photons. Of course the Planck formula guarantees the essential equivalence (except for units) of frequency and energy, and the two terms will be used interchangeably.

By increasing K, high order diffraction maxima can be produced from the undulator that extend the produced spectrum to high energy, but the resulting beam has (undesirably) high power relative to the flux of useful X-rays. Making the undulator period short can concentrate the beam power in the useful spectral range, but a magnetic undulator with ideal radiation properties usually has a gap height too small for satisfactory operation at existing storage rings. These issues are discussed in chapter 7. Another (futuristic) approach to overcoming the problems is proposed in chapter 8 where the possibility is explored of replacing the magnetic undulator field by an electromagnetic wave, propagating in a waveguide that serves also as the accelerator vacuum pipe. This chapter discusses features that apply to any undulator.

There is a fairly narrow band of energies that is ideal for X-ray diffraction. The band is limited on the high energy side by difficulty in making optical elements in that range, by excessive heating, by long term radiation damage, and by unwelcome backgrounds. The low energy limit is due to excessive attenuation in vacuum windows, protective covers and thick samples—the attenuation length of few keV photons is so short as to cause unacceptable attenuation. But, because of the extremely rapid energy dependence of attenuation length, a factor of ten increase in energy largely overcomes this problem. One therefore seeks a

photon beam centered on, say, $E_\gamma = 12.4\,\mathrm{keV}$,[†] as brilliant as possible, consistent with being as monochromatic as possible.

The qualitative idea behind undulator radiation is familiar from the pattern produced by an optical diffraction grating, having multiple slits. Individual slits that are extremely thin and closely spaced produce single slit diffraction patterns that are very broad in angle and very nearly superimposed. As a result there is interference, which causes angular maxima that are narrow relative to their separation. The angular widths of the maxima are inversely proportional to the number of slits and, instead of being spread more or less uniformly in angle, the energy getting through the slits is concentrated in these maxima.

The primary element of a conventional undulator is a magnet having many, say, $2N_w$ magnetic poles, alternately north and south, with period λ_w. The trajectory of an electron through this magnet oscillates transversely about a straight central line, and this transverse acceleration of the electron results in synchrotron radiation. Though the radiation from different electrons is incoherent, the waves emitted from the same electron in different deflections interfere coherently. The fundamental interference maximum occurs when (because of the electron's speed deficit relative to c) the electron lags the radiated field by exactly one wavelength in passing through one period of the undulator. (Neglecting angular dependence and path length excess) this yields a condition

$$\lambda_{1,\mathrm{edge}} = \frac{\lambda_w}{2\gamma^2} \ , \tag{6.1.1}$$

giving $\lambda_{1,\mathrm{edge}}$, the short wavelength edge of the first order diffraction maximum, in the ideal limit of undulator operation. For numerical estimates in this chapter the value $\gamma = 10^4$, corresponding to 5.1 GeV operation, will be assumed. Then the choice $\lambda_w = 2\,\mathrm{cm}$ yields $\lambda_{1,\mathrm{edge}} = 1.0\,\mathrm{\AA}$, or about 12.4 keV.

It is difficult for λ_w to be as small as required by Eq. (6.1.1) because of the inevitable fringing between the poles and a correspondingly too-small gap height requirement. One can contemplate using higher order interference maxima but, since the electron's trajectory through a standard undulator is essentially sinusoidal, the higher orders are extremely weak unless $K > 1$.

[†] The choice of $E_\gamma = 12.4\,\mathrm{keV}$ as nominal energy corresponds to a wavelength $\lambda_{1,\mathrm{edge}} = 1\mathring{A}$ and to the (mnemonic) approximation $1\mathring{A} \to 12345\,\mathrm{eV}$.

Formula (6.1.1) can also be obtained using an elementary relativistic argument. Undulator "photons" of wavelength λ_w are foreshortened by a factor γ as observed in the electron rest system, where they are Thomson scattered, more or less isotropically, from the electron. In the electron rest system these photons are monochromatic but, when they are observed in the laboratory, their wavelengths are further foreshortened by a factor that varies from a maximum value of 2γ for perfect backscattering down to a value close to zero for glancing collision. This picture of the process is described more fully in the last section of this chapter.

A slightly different (but equivalent) approach is taken by Jackson. Working in the rest frame of the electron, where the undulator provides a sinusoidally varying transverse electric field, Jackson evaluates the electron's response (approximately simple harmonic) and from that the resulting (more or less isotropic) dipole radiation pattern of (monochromatic) photons. To find the laboratory distribution (no longer monochromatic, but with wavelength one-to-one and monotonically related to laboratory angle) Jackson transforms individual photons into the laboratory frame. (I think this analysis may be due to others, such as Hoffmann[5], originally.)†

† In anticipation of a seemingly contraversial issue, one can observe that N_w, the number of poles of the wiggler does not enter into the Hoffmann/Jackson picture. It is therefore not possible for the angular distribution of the radiated photons to depend on N_w, either in the electron or laboratory frame. Dependence on N_w enters only because, as viewed in the electron's frame, the undulator field is switched on for only a finite time—N_w cycles actually. Expressing the field as a wave packet, its frequency spread is proportional to $1/N_w$, and the laboratory X-ray spectrum inherits the effect of this spread. This spreading might be thought to be relatively insignificant, especially for large N_w, but that would be thoroughly incorrect. No matter how narrow the energy spread of the X-ray beam, the energy selectivity of the monochrometer preceding typical X-ray detection apparatus is usually even less. This amplifies the importance of the N_w poles of the undulator (by, roughly speaking, a factor of N_w), over and above the factor of N_w resulting from the fact that the radiation from every pole is aimed more or less toward the detection apparatus.

6.2. Semi-Quantitative Treatment of $K << 1$ Operation

6.2.1. Synchrotron Radiation From a "Short" Deflector

The following treatment of undulators is intended to complement the treatment in Jackson. It is based entirely on Maxwell's equations in the laboratory system and makes no explicitly relativistic arguments. There are several motives for this independent development. One is to develop and exploit the analogy between undulators and diffraction gratings; for this it is necessary to represent the undulator as a sequence of $2N_w$ short, alternating-sign, deflectors, rather than as harmonic oscillation. It is also valuable to have an independent formulation so that essential results can be cross checked. Another motive is to investigate certain features of Jackson's treatment that appear to contradict part of the lore of the field. I refer here to the "angular narrowing" of the forward peak, making its angular width proportional to $1/\sqrt{N_w}$, as described initially by Attwood, Halbach, and Kim.[6] This feature is (superficially) absent from Jackson's result. Since this section is concerned only with deriving analytical expressions with semi-quantitative accuracy, it contains fairly crude approximations.

In section 6.4 below, a more nearly exact, and far more general, theory will be applied to undulators having arbitrary K-value. The formulas derived there will superceed all preceeding formulas at the cost of being rather more formal and mathematical. The essential feature permitting a more general treatment is that the radiation from a full rather than a half period will be evaluated by integration. The interference over multiple periods will still be handled by phasor summation however.

The formalism to be employed has been described in chapter 2. The fundamental relationship governing synchrotron radiation is Eq. (2.1.2), which relates observation time t to "retarded time" t_r:

$$t = t_r + \frac{\mathcal{R}}{c} \ , \tag{6.2.1}$$

where $\mathcal{R}$ is the distance from source point to observation point P, located at angle ψ above an arbitrary tangent to the circular orbit. Using Eq. (2.1.14) (or equivalently approximating formulas from Jackson[7] fairly radically) the electric field at P, due to an electron

traveling in a circle of radius R is

$$E_x(\mathbf{r},t) \approx \frac{q}{4\pi\epsilon_0}\frac{4\gamma^4}{\mathcal{R}R}\left(1+\gamma^2\psi^2+\left(\frac{2c\gamma^3/R}{1+\gamma^2\psi^2}\right)^2 t^2\right)^{-2}\left(U(t-t_{\rm in})-U(t-t_{\rm out})\right)\ . \tag{6.2.2}$$

This field is appreciable only for emission directions within a range of vertical angles $|\psi|\tilde{<}1/\gamma$ about a central peak and for a correspondingly short time interval, centered on the time $t=0$ when the electron's velocity vector points toward P. The final factor $U(t-t_{\rm in})-U(t-t_{\rm out})$ is a "window function", equal to 1 when the electron is being deflected and zero otherwise. This factor is needed if the deflection interval is "short", $L<2R/\gamma$, which will be the case for small K. Then, even though the true longitudinal field dependence is sinusoidal, the deflection from each half period will be treated as a short impulse.

Three important approximations have been made in obtaining Eq. (6.2.2). Fortunately, the least-controlled of these approximations, namely dropping a term proportional to t_r^3 in the relation between retarded time t_r and observation time t, is valid for short magnets. This is because, being cubic, the excess length of a curved path in a short magnet is even less important than in a long magnet, relative to the effects of vertical angle and electron speed deficit. Another approximation in Eq. (6.2.2) amounts to having neglected vertically polarized radiation altogether. For "in-plane" radiation this is an excellent approximation, but the integrated, vertically polarized intensity can be something like 10 or 20% of the total intensity. The same approximation causes Eq. (6.2.2) to over-estimate the horizontally polarized intensity by a similar amount.

I will be prepared to make an even more extreme approximation, that will be valid in the pure undulator regime. Suppose the "window function" is non-vanishing for a time so short that the angle subtended by the electron's velocity vector is small compared to ψ. Then, in Eq. (6.2.2), we can make the replacement

$$\gamma^2\psi^2+\left(\frac{2c\gamma^3/R}{1+\gamma^2\psi^2}\right)^2 t^2 \to \gamma^2\vartheta^2 \tag{6.2.3}$$

where ϑ is the polar angle relative to the beam axis. The basis of this approximation is that, with the electron's direction being treated as constant, the horizontal and vertical angles can be added quadratically, as in Eq. (6.2.3) to give the polar angle, and the

retarded time correction becomes azimuthally symmetric. Since this approximation is rather drastic, it should be applied only when strictly necessary. (It will be useful when discussing the angular width of the forward peak produced by a multiperiod undulator in the pure undulator limit.)

The magnetic field of an undulator has the form $B(z)\hat{\mathbf{y}}$, where $B(z)$ is periodic with period λ_w. The equation of motion in this field, of a particle whose orbit lies in the x, z plane is

$$m\gamma \frac{d}{dt}\left(v_x\hat{\mathbf{x}} + v_z\hat{\mathbf{z}}\right) = q\mathbf{B}\left(z\right)\left(v_x\hat{\mathbf{x}} + v_z\hat{\mathbf{z}}\right) \times \hat{\mathbf{y}} \ , \tag{6.2.4}$$

which yields

$$\frac{dv_x}{dt} = \frac{-qB\left(z\right)}{m\gamma} v_z, \quad \frac{dv_z}{dt} = \frac{qB\left(z\right)}{m\gamma} v_x \ . \tag{6.2.5}$$

The constancy of γ, or of v^2, can be expressed as $v_x dv_x + v_z dv_z = 0$, which follows from these equations. By using z instead of t as independent variable, Eqs. (6.2.5) become

$$\frac{dv_x}{dz} = \frac{-qB\left(z\right)}{m\gamma}, \quad \frac{dv_z^2}{dz} = \frac{2qB\left(z\right)}{m\gamma} v_x \ . \tag{6.2.6}$$

Integrating the first of these, with the origin placed at a position z_0 where $v_x(z_0) = v_{x0}$, yields

$$v_x = v_{x0} - \frac{q}{m\gamma}\int_{z_0}^{z} B\left(z'\right)\, dz', \quad v_z^2 = v^2 - v_x^2 \ . \tag{6.2.7}$$

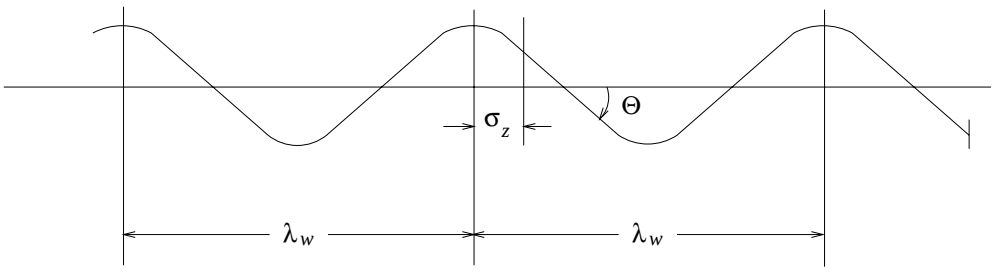

Figure 6.2.1: The electron orbit through the undulator is treated as a sequence of impulses, each bending through 2Θ. In the "ideal undulator limit", $\Theta = K/\gamma << 1/\gamma$, i.e. small compared to the half-angle of a cone containing most of the synchrotron radiation.

In practical wigglers the magnetic profile varies from "square saw-tooth" for large λ_w, to essentially sinusoidal for small λ_w. The undulator parameter K is traditionally defined

in the latter limit, and related to the peak magnetic field B_0. Then performing the integral in Eq. (6.2.7) over a half-period in which the field is positive yields

$$2\Theta \equiv \frac{2K}{\gamma} = \frac{\Delta v_x}{c} = \frac{e}{mc\gamma}\, B_0\, \frac{\lambda_w}{2}\, \frac{2}{\pi}, \quad \text{or} \quad K = \frac{eB_0}{mc}\, \frac{\lambda_w}{2\pi} = 93.4\, B_0\,[\mathrm{T}]\, \lambda_w\,[\mathrm{m}]\,. \tag{6.2.8}$$

One reason K is such a useful parameter is that it is independent of electron energy. The K value of a given undulator remains constant as the machine energy changes, or even if the undulator is moved from one storage ring to another.

It will simplify the calculations (especially in cases where the total undulator length is comparable with the distance to the observation point) if we can suppose that the deflecting element is "very short", in the sense explained above. In fact, as well as being short, to avoid the need for step functions, the deflecting field can be approximated as having Gaussian longitudinal profile such that the inverse bending radius is given by†

$$\frac{1}{R\,(z)} = \frac{1}{R_w}\, \exp\left(\frac{-z^2}{2\sigma_z^2}\right). \tag{6.2.9}$$

In passing one quarter of a wiggler period, an electron's angular deflection is

$$\Theta = \frac{1}{R_w} \int_0^\infty \exp\left(\frac{-z^2}{2\sigma_z^2}\right) dz = \sqrt{\frac{\pi}{2}}\, \frac{\sigma_z}{R_w} \equiv \frac{K_{\text{eff.}}}{\gamma}\ , \tag{6.2.10}$$

where the "effective wiggler strength parameter" $K_{\text{eff.}}$ has been introduced to facilitate comparison with magnetic undulators for which the maximum orbit angle relative to the undulator center line is traditionally defined as K/γ. Though $K_{\text{eff.}}$ is approximately equal to K, they are logically not identical, (in fact, with $\sigma_z = \lambda_w/(2\pi)$, it follows from Eq. (6.2.10) that $K_{\text{eff.}} \approx \sqrt{\pi/2}\, K$) but we will not distinguish between these definitions for the time being. For reference, a sinusoidal orbit having maximum slope K/γ is

$$x = \frac{\lambda_w}{2\pi}\, \frac{K}{\gamma}\, \cos\frac{2\pi\, z}{\lambda_w}\ , \quad \text{or} \quad \frac{1}{R\,(z)} = \frac{2\pi}{\lambda_w}\, \frac{K}{\gamma}\, \frac{\cos\left(2\pi z/\lambda_w\right)}{\left(1 + K^2 \sin^2\left(2\pi z/\lambda_w\right)\right)^{3/2}}\ , \tag{6.2.11}$$

where the latter relation (presumably more accurate than Eq. (6.2.9)) is obtained from a standard formula for curvature. This curve can be matched approximately by choosing R_w and σ_z appropriately, using the approximation

$$\sin x \approx -\sum_{i=-\infty}^{\infty} (-1)^i \exp\left(-\frac{\left(x + (2i+1)\,\pi/2\right)^2}{2}\right)\ . \tag{6.2.12}$$

† What with fringe fields being inevitable, treating the field shape of a short magnet as Gaussian could provide an accurate approximation, but we are intending to apply these formulas to a sinusoidal deflection field.

This is illustrated in Fig. 6.2.2, and the parameters are related by

$$\sigma_z = \frac{\lambda_w}{2\pi} \ . \tag{6.2.13}$$

For our nominal 12.4 keV energy, $\sigma_z = 1/\pi$ cm.

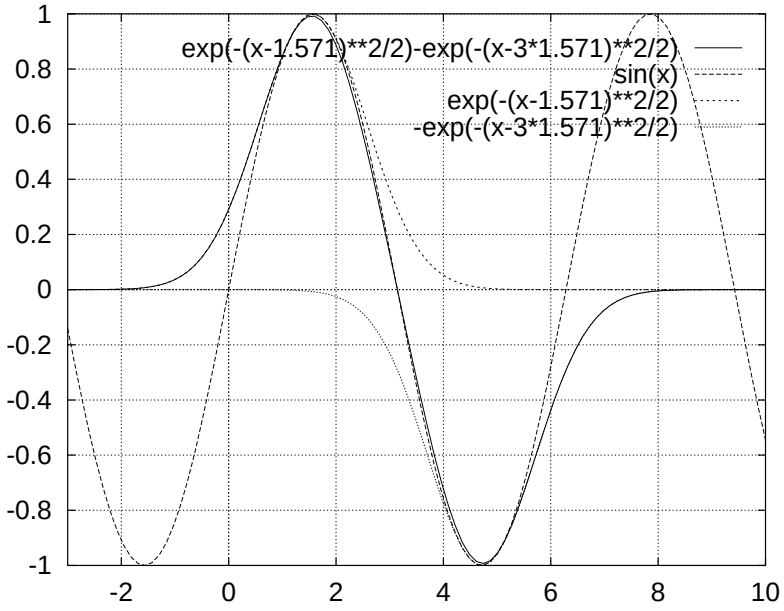

Figure 6.2.2: Plot illustrating a sinusoid matched by a series of alternate sign Gaussians, of which only two are shown. See key in upper right for analytic forms. The standard deviations are related to undulator wavelength by $2\pi\sigma_z = \lambda_w$ in order to match curvatures at the peaks. Though the true trajectory is sinusoidal, radiation integrals will be based on the Gaussian pulses, so radiation deficiency or excess from the tail regions will require (modest) correction.

With this (somewhat unconventional) approximation, the ends of the undulator can be represented by simply truncating the sum in Eq. (6.2.12). Also, after having sliced the undulator longitudinally, coherent superposition can be handled by the vector addition of phasors, one per deflection arc, or $2N_w$ in all. By using a Gaussian shape, the artificial high frequency components that would accompany using truncated half-sinusoids are largely suppressed. For long undulators it may be necessary to incorporate longitudinal dependency by making the phasor magnitude depend on longitudinal position.

According to Sands[8] the energy dissipated per unit length in a region with bending radius R_0 is given by

$$\frac{dU}{dz} = \frac{q^2\gamma^4}{6\pi\epsilon_0 R_0^2} \ . \tag{6.2.14}$$

This is sometimes known as "Schott's formula", though it is due to Liénard. The energy U_1 radiated by an electron in traversing our thin element is therefore given by

$$U_1 = \frac{q^2\gamma^4}{6\pi\epsilon_0 R_w^2} \int_{-\infty}^{\infty} \exp\left(\frac{-z^2}{\sigma_z^2}\right) dz = \frac{1}{6\sqrt{\pi}} \frac{q^2\gamma^4}{\epsilon_0} \frac{\sigma_z}{R_w^2} \ . \tag{6.2.15}$$

This can be compared to the more accurate result obtained using the second of Eqs. (6.2.11);

$$\begin{aligned} U_1' &= \frac{q^2\gamma^4}{6\pi\epsilon_0} \frac{2\pi}{\lambda_w} \frac{K^2}{\gamma^2} 2 \int_0^{\lambda_w/4} \frac{\cos^2\left(2\pi z/\lambda_w\right)}{\left(1 + K^2 \sin^2\left(2\pi z/\lambda_w\right)\right)^3} d\left(\frac{2\pi z}{\lambda}\right) \\ &= \frac{\pi}{24} \frac{q^2\gamma^4}{\epsilon_0} \frac{\sigma_z}{R_w^2} + O\left(K^4\right) \ , \end{aligned} \tag{6.2.16}$$

where λ_w has been replaced using Eq. (6.2.13), and the last of Eqs. (6.2.10) has been used. Since $(1/6\sqrt{\pi})/(\pi/24) = 0.72$ our formulas will underestimate the total energy radiated by this factor (which is comparable to the over-estimate built into Eq. (6.2.2).) This defect could be rectified by altering the definition of R_w or σ_z but I prefer to maintain the definitions given so far. Also, to permit working in terms of familiar quantities, U_1 can be expressed as a fraction of U_0 (the energy radiated as an electron travels in a complete circle of radius R_0)[†]

$$U_1 = \frac{1}{2\sqrt{\pi}} \frac{R_0\,\sigma_z}{R_w^2} U_0 = \frac{1}{\pi^{3/2}} \frac{U_0 R_0}{\sigma_z} \Theta^2 = \frac{1}{\pi^{3/2}} \frac{C_\gamma E_e^4}{\lambda_w/\left(2\pi\right)} \left(\frac{K}{\gamma}\right)^2 \ . \tag{6.2.17}$$

The essential qualitative feature of this formula is that, with undulator period held fixed, the radiation comes in $2N_w$ pulses of energy, each with energy given by Eq. (6.2.17). All that remains is to determine how this energy is distributed in direction and wavelength.

[†] Eq. (6.2.14) gives the energy radiated as a 5.1 Gev electron travels in a complete circle of radius $R_0 = 89\,\mathrm{m}$, to be $U_0 = 0.67\,\mathrm{MeV}$. Numerical estimates can be scaled to U_0. Though this is artificial, it has mnemonic value, since it relates quantities to that feature of synchrotron radiation which imposes itself most emphatically upon the operation of storage rings—the average energy loss. For accurate calculation one should use $U_0 R_0 = C_\gamma E_e^4$, where $C_\gamma = 0.885 \times 10^{-4}\,\mathrm{m/GeV^3}$; this formula gives $U_0 R_0$ in units of m-GeV.

6.2.2. Spectral Analysis of the Single Pole Radiation

The orbit and detection point P geometry is illustrated in Fig. 6.2.3. At $t = t_r = 0$ the electron passes O and its velocity vector points toward the origin O' in the plane of detection. The detection point P is displaced from O' by horizontal angle θ and vertical angle ψ. The instantaneous radius of curvature is R. The most important difference of the geometry here, from that of Chapter 2, concerns the placement of the origin O' in the detector plane. Now it lies on the undulator centerline extended. In Chapter 2 the origin O' lay on a tangent to the circular orbit, at arbitrarily chosen angle θ_h, and the observation point P lay directly above O', subtending angle ψ at O. Now the detector point P subtends vertical angle ψ and horizontal angle θ at O. So the undulator intensity depends on both ψ and θ, whereas, for pure circular motion, the intensity depended only on ψ and was independent of θ_h.

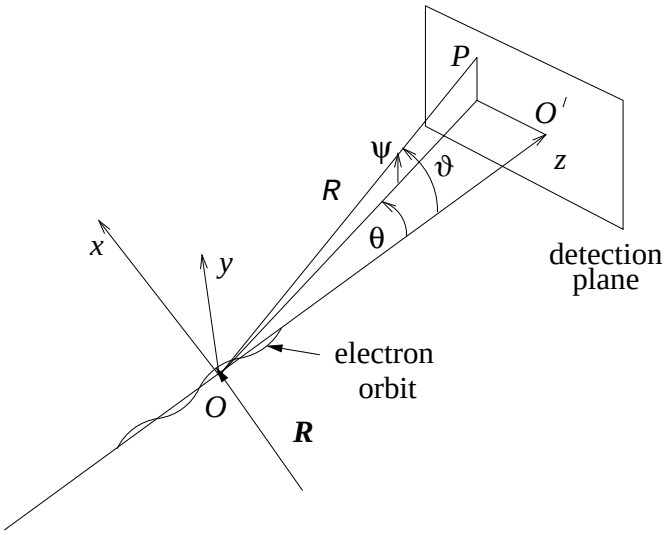

Figure 6.2.3: Orbit geometry and definition of horizontal angle θ and vertical angle ψ locating the detector position P relative to the $t = t_r = 0$ orbit position.

A fundamental assumption that will be made initially, and is only valid for $K << 1$, is that the electon's longitudinal position advances at constant speed, $z = \overline{v}t_r$. For values of K approaching and exceeding 1 this approximation will have to be improved later on, especially when it comes to forming the coherent sum of the amplitudes from more than one pole of the undulator.

Apart from the fundamental Eq. (6.2.1) relating t and t_r, the formulas needed from Chapter 2 are the analogs of Eq. (2.1.12), which gives their functional relationship,

$$t \approx t_r \left(\frac{1}{2\gamma^2} + \frac{\vartheta^2}{2} + \frac{c^2 t_r^2}{6R^2} \right) \quad , \quad \text{where} \quad \vartheta^2 = \theta^2 + \psi^2 \ , \tag{6.2.18}$$

where ϑ is the angle between $\mathbf{v}$ and $\widehat{\mathcal{R}}$, and Eq. (2.1.4),

$$\frac{dt}{dt_r} = 1 - \widehat{\mathcal{R}} \cdot \frac{\mathbf{v}\left(t_r\right)}{c} \ . \tag{6.2.19}$$

We also had Eqs. (2.1.5) and (2.1.6);

$$\frac{\mathbf{E}\left(\mathbf{r},t\right)}{\frac{q}{4\pi\epsilon_0 c\mathcal{R}}} = \left[\frac{\widehat{\mathcal{R}} \times \left(\left(\widehat{\mathcal{R}} - \frac{\mathbf{v}}{c} \right) \times \frac{\dot{\mathbf{v}}}{c} \right)}{\left(1 - \widehat{\mathcal{R}} \cdot \frac{\mathbf{v}}{c} \right)^3} \right]_{\text{ret.}} = \left[\frac{1}{1 - \widehat{\mathcal{R}} \cdot \frac{\mathbf{v}}{c}} \frac{d}{dt} \left(\frac{\widehat{\mathcal{R}} \times \left(\widehat{\mathcal{R}} \times \frac{\mathbf{v}}{c} \right)}{1 - \widehat{\mathcal{R}} \cdot \frac{\mathbf{v}}{c}} \right) \right]_{\text{ret.}} . \tag{6.2.20}$$

To simplify the triple cross product, let $\mathbf{v}_\perp$ stand for the component of $\mathbf{v}$ normal to $\widehat{\mathcal{R}}$. The Fourier transform of $\mathbf{E}$ is then given by

$$\begin{aligned} \frac{\widetilde{\mathbf{E}}\left(\omega,\theta,\psi\right)}{\frac{q}{4\pi\epsilon_0 c\mathcal{R}}} &= \frac{-1}{\sqrt{2\pi}} \int_{-\infty}^{\infty} e^{i\omega t} \left[\frac{1}{1 - \widehat{\mathcal{R}} \cdot \frac{\mathbf{v}}{c}} \frac{d}{dt} \left(\frac{\mathbf{v}_\perp / c}{1 - \widehat{\mathcal{R}} \cdot \frac{\mathbf{v}}{c}} \right) \right]_{\text{ret.}} dt \\ &= \frac{-1}{\sqrt{2\pi}} \int_{-\infty}^{\infty} e^{i\omega t_r \left(\frac{1}{2\gamma^2} + \frac{\vartheta^2}{2} + \frac{c^2 t_r^2}{6R^2} \right)} \frac{d}{dt_r} \left(\frac{\mathbf{v}_\perp / c}{1 - \widehat{\mathcal{R}} \cdot \frac{\mathbf{v}}{c}} \right) dt_r \ , \end{aligned} \tag{6.2.21}$$

where the integration variable has been changed from t to t_r. This integral can be further simplified using integration by parts to yield

$$\frac{\widetilde{\mathbf{E}}\left(\omega,\theta,\psi\right)}{\frac{q}{4\pi\epsilon_0 c\mathcal{R}}} \approx \frac{i\omega}{\sqrt{2\pi}} \int_{-\infty}^{\infty} \exp\left(i\omega t_r \left(\frac{1}{2\gamma^2} + \frac{\vartheta^2}{2} + \frac{c^2 t_r^2}{6R^2} \right) \right) \frac{\mathbf{v}_\perp}{c} \, dt_r \ . \tag{6.2.22}$$

(In this step the factor dt/dt_r has been replaced by $1 - \widehat{\mathcal{R}} \cdot \mathbf{v}/c$. Since Eq. (6.2.18) is only approximate, so also is this replacement. For undulators with small λ_w, the integral is dominated by the small t_r region where the term $c^2 t_r^2/(6R^2)$ is unimportant. This makes the approximation especially valid and, in what follows, the $\approx$ will be replaced by $=$.) For working out individual components we use the formulas

$$\begin{aligned} &\widehat{\mathcal{R}} \approx \theta \hat{\mathbf{x}} + \psi \hat{\mathbf{y}} + \left(1 - \frac{\vartheta^2}{2} \right) \hat{\mathbf{z}}, \\ &\frac{\mathbf{v}}{c} \approx -\sin\frac{vt_r}{R} \, \hat{\mathbf{x}} + \cos\frac{vt_r}{R} \, \hat{\mathbf{z}}, \\ &\widehat{\mathcal{R}} \cdot \frac{\mathbf{v}}{c} \approx -\theta \sin\frac{vt_r}{R} + \cos\frac{vt_r}{R}, \\ &\frac{\mathbf{v}_\perp}{c} = \frac{\mathbf{v}}{c} - \left(\widehat{\mathcal{R}} \cdot \frac{\mathbf{v}}{c} \right) \widehat{\mathcal{R}} \approx -\left(\sin\frac{vt_r}{R} + \theta \cos\frac{vt_r}{R} \right) \hat{\mathbf{x}} - \psi \, \cos\frac{vt_r}{R} \, \hat{\mathbf{y}} \ . \end{aligned} \tag{6.2.23}$$

It seems to be conventional in the field to call the x-component the "σ-mode" and the y-component the "π-mode", but I will continue to use x and y. From Eq. (6.2.22) one obtains

$$\begin{aligned}
\widetilde{E}_x(\omega,\theta,\psi) &= \frac{-i\omega q}{\sqrt{2\pi}4\pi\epsilon_0 c\mathcal{R}}\int_{-\infty}^{\infty} dt_r\, \exp\left(i\omega t_r\left(\frac{1}{2\gamma^2}+\frac{\vartheta^2}{2}+\frac{c^2t_r^2}{6R^2}\right)\right)\left(\sin\frac{vt_r}{R}+\theta\right) \\
&\approx \frac{-i\omega q}{\sqrt{2\pi}4\pi\epsilon_0 c\mathcal{R}}\int_{-\infty}^{\infty} dt_r\, \left(\frac{ct_r}{R(t_r)}+\theta\right)\exp\left(i\omega t_r\left(\frac{1}{2\gamma^2}+\frac{\vartheta^2}{2}\right)\right) \\
\widetilde{E}_y(\omega,\theta,\psi) &= \frac{-i\omega q}{\sqrt{2\pi}4\pi\epsilon_0 c\mathcal{R}}\int_{-\infty}^{\infty} dt_r\, \exp\left(i\omega t_r\left(\frac{1}{2\gamma^2}+\frac{\vartheta^2}{2}+\frac{c^2t_r^2}{6R^2}\right)\right)\psi\cos\frac{vt_r}{R}\ . \\
&\approx \frac{-i\omega q}{\sqrt{2\pi}4\pi\epsilon_0 c\mathcal{R}}\int_{-\infty}^{\infty} dt_r\, \psi\,\exp\left(i\omega t_r\left(\frac{1}{2\gamma^2}+\frac{\vartheta^2}{2}\right)\right)\ .
\end{aligned} \tag{6.2.24}$$

Because (for $K << 1$) the integrals are thoroughly dominated by regions in which $vt_r << R$ the trigonometric factors have been approximated by their leading terms, and the cubic terms in the exponents have been dropped for the same reason. Also, since there has been nothing in the derivation so far requiring the bending radius R to be independent of position (i.e. independent of t_r) this has been acknowledged by expressing R as $R(t_r)$; in an undulator the spatial variation of R is essential.

One reason for having derived these formulas in detail, rather than adapting them from Jackson's Eqs. (14.79), has been to justify including the factor $1/R(t_r)$ in the integrands. In the integrals of Eq. (6.2.24) the factors θ and ψ are constant, and could be moved outside the integral signs, but they have been left inside to facilitate comparison of two modes. A curious feature of the formulas (which is shared by Jackson's Eq. (14.79), is that the integrals proportional to θ and to ψ do not vanish in the limit $R\to\infty$. Though for practical parameter values these contributions are small compared to the $ct_r/R(t_r)$ contribution, this appears to predict radiation even with the undulator turned off. At the moment I don't understand this seeming paradox.

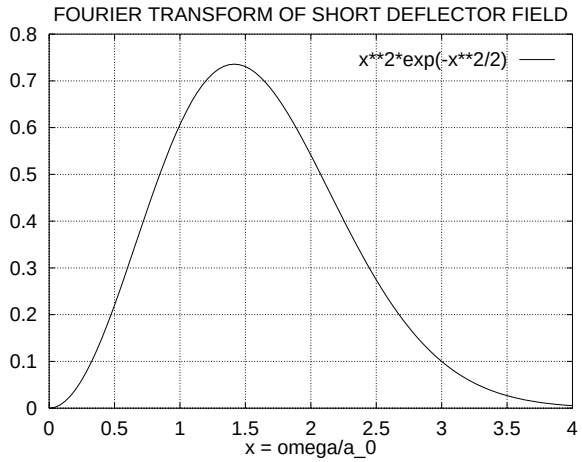

Figure 6.2.4: Fourier transform (Eq. (6.2.25)) of deflecting force due to a short Gaussian deflecting element for $\vartheta = 0$. The horizontal axis is ω/a_0. According to Eq. (6.2.25), the spectral shape for $\vartheta \neq 0$ is the same, provided the horizontal axis is interpreted as ω/a_ϑ.

Retaining only the dominant mode E_x and only its dominant part we obtain

$$\begin{aligned}
\frac{\widetilde{\mathbf{E}}_x(\omega,\vartheta)}{\frac{q}{4\pi\epsilon_0\mathcal{R}}} &\approx -\frac{i\omega}{R_w}\sqrt{\frac{2}{\pi}}\int_0^\infty t_r\,\exp\left(\frac{-t_r^2}{2\,(\sigma_z/c)^2}\right)\sin\left(\omega t_r\left(\frac{1}{2\gamma^2}+\frac{\vartheta^2}{2}\right)\right)\,dt_r \\
&= -\frac{i\omega}{R_w}\sqrt{\frac{2}{\pi}}\left(\frac{1}{2\gamma^2}+\frac{\vartheta^2}{2}\right)^{-2}\int_0^\infty t\,\exp\left(\frac{-t^2}{2\,(\sigma_z/c)^2\left(\frac{1}{2\gamma^2}+\frac{\vartheta^2}{2}\right)^2}\right)\sin\omega t\,dt\ . \\
&= -\frac{i\omega}{R_w}\sqrt{\frac{2}{\pi}}\,\frac{\sigma_z^2}{c^2}\,a_\vartheta^2\int_0^\infty t\,e^{\frac{-a_\vartheta^2 t^2}{2}}\sin\omega t\,dt \\
&= -\frac{i}{R_w}\,\frac{\sigma_z^2}{c^2}\,a_\vartheta\left(\frac{\omega}{a_\vartheta}\right)^2\exp\left(\frac{-\omega^2}{2\,a_\vartheta^2}\right)
\end{aligned} \tag{6.2.25}$$

where a function a_ϑ, with dimensions of frequency, has been defined by

$$a_\vartheta = \frac{a_0}{1+\gamma^2\vartheta^2} \quad \text{where} \quad a_0 = \frac{2\gamma^2 c}{\sigma_z} = \frac{4\pi\gamma^2 c}{\lambda_w}\ . \tag{6.2.26}$$

The spectrum given by Eq. (6.2.25), with $\vartheta = 0$, is plotted in Fig. 6.2.4. The radiated power is obtained from the Poynting vector which is proportional to the square of the function plotted. This gives the radiated power one has "to work with". As in an optical diffraction grating, though interference effects can "concentrate" the power into the form of photons centered on one or more diffraction maxima, such effects cannot alter the total power.

We can regard a_0 as a frequency typical of the radiation from a single deflection of r.m.s. length σ_z; it can play a role much like $\omega_c = (3/2)c\gamma^3/R_0$, the "critical frequency" traditionally defined for synchrotron radiation from bend radius R_0.† The maximum of the single deflector Fourier transform can be seen to be at $1.45\,a_0$. This defines a_ϑ to be a kind of "typical" X-ray frequency at angle ϑ. It will prove to be significant that the spectral shape is a universal function of the ratio ω/a_ϑ. (The extra multiplicative factor a_ϑ causes a further modest angular-dependent modulation of the radiated energy.) The energy radiated from a single undulator pole is distributed according to

$$\begin{aligned}\frac{d^2U_1}{d\omega d\Omega} &= \frac{2\mathcal{R}^2}{\mu_0 c}\,\tilde{E}_x(\omega)\,\tilde{E}_x(-\omega) = \frac{2\mathcal{R}^2}{\mu_0 c}\left(\frac{q}{4\pi\epsilon_0\mathcal{R}}\right)^2\left(\frac{\sigma_z^2}{R_w c^2}\right)^2\frac{\omega^4}{a_\vartheta^2}\exp\left(-\frac{\omega^2}{a_\vartheta^2}\right)\\ &= \frac{1}{\pi^2c^2}\,\frac{q^2}{4\pi\epsilon_0 c}\left(\frac{\lambda_w}{2\pi}\right)^2\left(\frac{K}{\gamma}\right)^2\frac{\omega^4}{a_\vartheta^2}\exp\left(-\frac{\omega^2}{a_\vartheta^2}\right)\end{aligned} \tag{6.2.27}$$

where the initial factor 2 accounts for restriction of ω to positive values. The second moment of ϑ for fixed ω is given by

$$\sigma_\vartheta^2(\omega) = \frac{\int_0^\infty\left(\vartheta^3+\gamma^2\vartheta^5\right)\exp\left(-\frac{\omega^2\gamma^2\vartheta^2}{a_0^2}\right)d\vartheta}{\int_0^\infty\left(\vartheta+\gamma^2\vartheta^3\right)\exp\left(-\frac{\omega^2\gamma^2\vartheta^2}{a_0^2}\right)d\vartheta} = \frac{1}{\gamma^2}\,\frac{a_0^2}{\omega^2}\,\frac{\omega^2+2a_0^2}{\omega^2+a_0^2}\ . \tag{6.2.28}$$

As a check on the consistency of our formulas we calculate the total energy radiated per deflection to be

$$\begin{aligned}U_1'' &= \frac{\mathcal{R}^2}{\mu_0 c}\int d\Omega\int d\omega\,\tilde{E}_x(\omega)\,\tilde{E}_x(-\omega)\\ &= 2\,\frac{\mathcal{R}^2}{\mu_0 c}\left(\frac{q}{4\pi\epsilon_0\mathcal{R}}\right)^2\left(\frac{\sigma_z^2}{R_w c^2}\right)^2\int\frac{d\Omega}{a_\vartheta^2}\int_0^\infty\omega^4\exp\left(-\frac{\omega^2}{a_\vartheta^2}\right)d\omega\\ &= \frac{3\sqrt{\pi}}{4}\,\frac{1}{\mu_0 c}\left(\frac{q}{4\pi\epsilon_0}\right)^2\left(\frac{\sigma_z^2}{R_w c^2}\right)^2\left(\frac{2\gamma^2 c}{\sigma_z}\right)^3\int_0^\infty\frac{2\pi\vartheta d\vartheta}{\left(1+\gamma^2\vartheta^2\right)^3}\\ &= \frac{3}{16\sqrt{\pi}}\,\frac{q^2\gamma^4}{\epsilon_0}\,\frac{\sigma_z}{R_w^2}\ .\end{aligned} \tag{6.2.29}$$

Numerically $3/(16\sqrt{\pi}) = 0.1058$, not quite the same as $1/(6\sqrt{\pi}) = 0.0940$, which is the corresponding coefficient of U_1. This disagreement is comparable with the inaccuracy of our other results,

† Because of its stronger dependence on γ one might be misled into believing that ω_c corresponds to a more "Lorentz contracted" and hence shorter wavelength than the wavelength $\lambda_0 = 2\pi c/a_0$, but this is wrong. In fact, the "short magnet effect" make the opposite true in a true undulator. For magnetic wigglers there is some point to evaluating ω_c from the peak magnetic field but, for the undulator we are discussing, ω_c is unrelated to the radiation spectrum.

Since the intended purpose of the undulator is to produce X-rays, it is important to estimate typical wavelengths. The wavelength corresponding to a_0 is

$$\lambda_0 = 2\pi \frac{c}{a_0} = \frac{\lambda_w}{2\gamma^2} \ , \tag{6.2.30}$$

and comparison with Eq. (6.1.1) shows that $\lambda_0 = \lambda_{1,\text{edge}}$. Of course this is no coincidence, but neither is it tautological. $\lambda_{1,\text{edge}}$ is a characteristic of the radiation from a full periodic structure, while λ_0 is characteristic of the radiation from one half-wiggle.† With the wiggler field shape being treated as a sinuisoid with wavelength equal to the wiggler period the (near) equality of λ_0 and $\lambda_{1,\text{edge}}$ is assured. The importance of their having comparable values is that there is a substantial flux of photons having wavelengths capable of constructive interference with the radiation from all the other "poles" of the wiggler.

Because positive and negative wiggles are being treated independently, the diffraction maxima occurs at $\omega = na_0$, where $n = 1, 3, 5, \ldots$. (This will be confirmed below.) From Fig. 6.2.4 one sees that there is appreciable amplitude only up to two or three times a_0. One concludes that the amplitudes of diffraction maxima of order higher than, say, $n = 3$, will be negligible (for the case $K << 1$ being analysed.)

λ_0 has the remarkable feature of being independent of R_w, the central deflecting radius of curvature. The first person to emphasize the experimental significance of this feature was apparently R. Coisson,[9] Unlike regular arc radiation, the short magnet spectrum extends to high energies even if the deflection angle is arbitrarily small. (This refers to the spectral *shape*; of course the total intensity goes to zero as the deflection angle approaches zero.) The theory has been amply corroborated at CERN, as part of diagnostics of the SPS, a 400 GeV proton accelerator, R. Bossart et. al,[10]

That the wakefield undulator produces high energy X-rays has been established. It remains to be seen how monochromatization occurs and whether sufficiently great intensities can be obtained to make a useful device.

† In principle the length of half-wiggle sections of a wiggler could be very short compared to the wiggler period. Then we would have $\lambda_0 << \lambda_{1,\text{edge}}$, and high order diffraction maxima would become significant. The same would be true if the wiggler field shape were more nearly an ideal square wave.

6.2.3. Coherence From Multiple Deflections

The coherence of amplitudes from different poles of an undulator depend critically on the average velocity of the electron. The electron's orbit will otherwise be treated as a straight line, with longitudinal velocity altered to account for the increased arc length of the actual (approximately sinusoidal) orbit;

$$\frac{\overline{v_z}}{c} \approx \sqrt{\frac{v^2}{c^2} - \overline{(\Theta\,\cos k_w z)^2}} \approx 1 - \frac{1}{2\gamma^2} - \frac{\Theta^2}{4}. \tag{6.2.31}$$

A single electron is subject to $2N_w$ undulator pulses, of alternating polarity, with each pulse having r.m.s. (retarded time) duration σ_z/c. All radiation sources are centered on the same straight line. Consider a component of the radiation having wavelength λ and direction ϑ. A reference wavefront is defined to be the plane passing through the emission point and perpendicular the photon's direction. As the electron advances the distance $\lambda_w/2$ from one deflection to the next, its travel time is $(\lambda_w/2)/\overline{v_z}$. Meanwhile the reference wavefront (traveling at the speed of light in the photon's direction) has traveled a distance $(\lambda_w/2)(c/\overline{v_z})$. Referring to Fig. 6.2.5, consider another wavefront which is parallel to the original wavefront, but emerges from the new emission point. The distance of this wavefront from the first emitter is $(\lambda_w/2)\cos\vartheta \approx (\lambda_w/2)(1-\vartheta^2/2)$. The phase difference between these two wavefronts is

$$\Delta\phi\,(\vartheta) = 2\pi\,\frac{\lambda_w}{2}\,\frac{c/\overline{v_z} - 1 + \vartheta^2/2}{\lambda} = \pi\,\frac{\lambda_w/\left(2\gamma^2\right)}{\lambda}\,\left(1 + K^2/2 + \gamma^2\vartheta^2\right)\ . \tag{6.2.32}$$

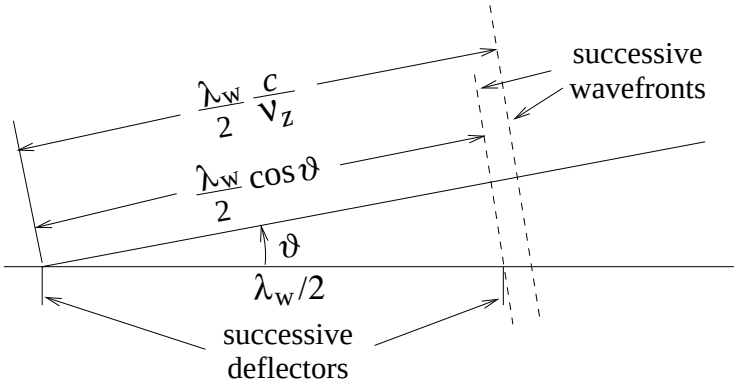

Figure 6.2.5: Geometry illustrating the condition for interference maximums observed at vertical angle ϑ.

In a "Fraunhofer approximation", in which all emission at angle ϑ is "focused at infinity" the condition for the two waves to interfere constructively is that this phase shift be $\pi\, n$ where n is any *odd* positive integer. That is

$$\lambda_n(\vartheta) = \frac{\lambda_w/\left(2\gamma^2\right)}{n}\left(1 + K^2/2 + \gamma^2\vartheta^2\right) \ , \quad \text{or} \quad \omega_n(\vartheta) = \frac{n a_0}{1 + K^2/2 + \gamma^2\vartheta^2} \ . \tag{6.2.33}$$

(Values of $\lambda_n(0)$ and $\omega_n(0)$ with $K = 0,\ n = 1$ have previously been denoted $\lambda_{1,\text{edge}}$ and $\omega_{1,\text{edge}}$.) According to Eq. (6.2.17), the total energy radiated is proportional to K^2. We see now, that there is a trade-off between intensity and shift to reduced energy. It is this trade-off that has often pushed beamline designs from the undulator regime into the wiggler regime, since the desired X-ray energies are only present in harmonics above the fundamental.

Due to betatron oscillation, the electron's angle θ_e, relative to the central axis, though small, will not be zero, and there is a longer effective deflector spacing, obtained by $\lambda_w \to \lambda_w/\cos\theta_e$. But, because λ_w appears only as a multiplicative factor in Eq. (6.2.33), this is a relatively insignificant effect.† For the same reason, though the term $K^2/2$ gives an (undesirable) shift to reduced energy, it does not cause the (typically more significant) energy broadening‡ caused by the $\vartheta^2/2$ term, due to finite out-of-plane acceptance of the detector. To avoid unacceptably large shift of interference maxima it will be necessary to check a condition such as

$$\Theta \stackrel{\sim}{<} \frac{1}{2\gamma} \ , \quad \text{or} \quad K \stackrel{\sim}{<} \frac{1}{2} \ . \tag{6.2.34}$$

that limits the shift to the 10% level. This will be referred to as the "ideal undulator condition". For a conventional magnetic undulator this condition typically corresponds to a low, and hence easily achievable, magnetic field. It will be comfortably satisfied for any feasible level of microwave power in a microwave undulator.

† Of course, the angular divergence of the radiated photon beam cannot be less than the angular divergence of the electron beam. This would only be possible if the radiation from different electrons were coherent; this would be true only at absurdly long wavelengths, as in a free electron laser.

‡ Because there is a functional relation between production angle and wavelength, the beam brilliance could, in principle, be infinite, in spite of the "Doppler" spread, since the detection apparatus could be designed to exploit this correlation. For example, if the beam is shone directly on a crystal, without having passed through a monochromator of other filter, the program analysing the diffraction pattern could exploit its full knowledge of the correlation. In practice the detection apparatus will usually sum incoherently over a finite range of ϑ, which will smear the energies and reduce the brilliance.

In the limit $\Theta << 1$, from Eq. (6.2.33), the relation between production angle and frequency of the fundamental $n = 1$ line is

$$\omega_1(\vartheta)|_{K<<1} = \frac{a_0}{1+\gamma^2\vartheta^2} \ , \tag{6.2.35}$$

This function is plotted in Fig. 6.2.6. Note, from this equation and Eq. (6.2.26), that the angular dependence of $\omega_1(\vartheta)$ (diffraction maximum of the multisource pattern) and of a_ϑ (characteristic frequency of the single source pattern) are the same. This causes the diffraction maximum to retain its same position relative to the single source spectrum, independent of ϑ.

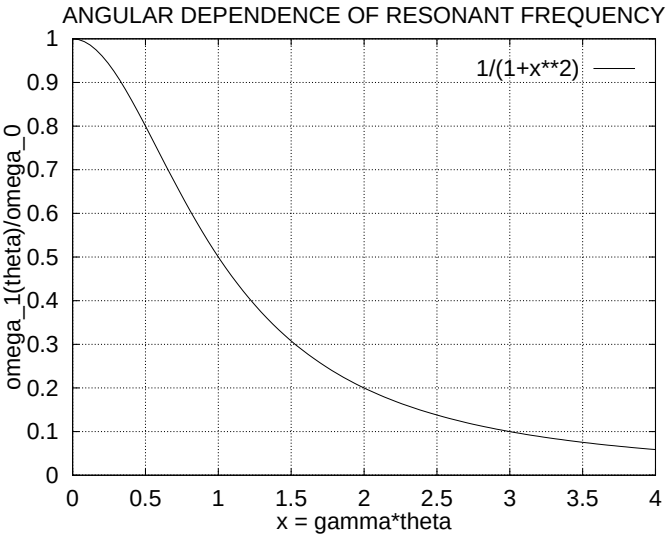

Figure 6.2.6: Angular dependence $\omega_1(\vartheta)|_{K<<1}$, the frequency of the fundamental undulator line with $K << 1$. The horizontal axis is $\gamma\vartheta$. Some people refer to this as a "Doppler shift", based on an analysis in which the radiation is first evaluated in the rest frame of the electron, and then transformed to the laboratory frame.

To calculate the multiple source interference pattern we sum the amplitudes from $2N_w$ deflectors, using the phasor construction of Fig. 6.2.7. The phase slip per deflection can be expressed in terms of ω by substituting the second of Eqs. (6.2.33) back into Eq. (6.2.32);

$$\Delta\phi(\vartheta) = \pi\, n\, \frac{\omega}{\omega_n(\vartheta)} = \pi\, n\, \nu \ , \tag{6.2.36}$$

where relative energy variable

$$\nu = \frac{\omega}{\omega_n(\vartheta)} \tag{6.2.37}$$

has been introduced. In the forward direction, for $n = 1$, Eq. (6.2.36) yields $\Delta\phi(0) = \pi\omega/a_0$, so ν is the coordinate along the horizontal axis in Fig. 6.2.4 in this case. Though ν is a fractional energy, it might be better to designate it as $\nu_n(\vartheta)$ since it is a fraction of the energy of the n'th harmonic peak in the energy spectrum viewed at angle ϑ. These dependencies will be suppressed for brevity. A variable that is equivalent to ν, but is useful for expressing dependencies close to a resonance peak, is

$$\Delta\nu = \nu - 1 = \frac{\omega - \omega_n(\vartheta)}{\omega_n(\vartheta)} \tag{6.2.38}$$

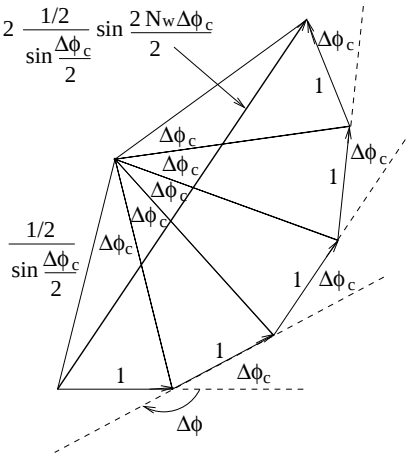

Figure 6.2.7: Phasor diagram with $2N_w$ arrows to calculate the coherent sum of waves from $2N_w$ sources, or N_w undulator periods. The directions of alternate phasors are reversed to account for the half period phase shift. $\Delta\phi_c = \pi - \Delta\phi$ where $\Delta\phi$ is the phase advance per half period of the undulator. Though $2N_w$ is necessarily even, the total number of deflections can actually be odd, as in the figure,

As shown in Fig. 6.2.7, the result of the phasor summation is a "grating amplitude"

$$G(2N_w, \Delta\phi) = \frac{\sin(2N_w(\pi/2 - \Delta\phi/2))}{\sin(\pi/2 - \Delta\phi/2)} \ , \tag{6.2.39}$$

which will later be squared to obtain an intensity. Though functions resembling G arise in a variety of multisource situations, its detailed interpretation requires a certain amount of

care. We will substitute for $\Delta\phi$ from Eq. (6.2.36), and then for ν from Eq. (6.2.37);

$$\begin{aligned} G\left(2N_w, \Delta\phi\right) &= \frac{\sin\left(N_w\pi\left(1-n\,\nu\right)\right)}{\sin\left(\pi/2-\pi\,n\,\nu/2\right)} = \pm\frac{\sin\left(N_w\pi n\nu\right)}{\cos\left(\pi\,n\,\nu/2\right)} = \pm\frac{\sin\left(N_w\pi n\left(1+\Delta\nu\right)\right)}{\cos\left(\pi\,n\,\left(1+\Delta\nu\right)/2\right)} \\ &= \begin{cases} \pm\frac{\sin(N_w\pi n\Delta\nu)}{\cos(\pi\,n\,\Delta\nu/2)} & n=0,2,4,\ldots \\ \pm\frac{\sin(N_w\pi n\Delta\nu)}{\sin(\pi\,n\,\Delta\nu/2)} & n=1,3,5,\ldots \end{cases} \\ \overset{\Delta\nu\to 0}{\longrightarrow} &\begin{cases} \pm\sin\left(N_w\pi n\Delta\nu\right) & n=0,2,4,\ldots \\ \pm 2N_w\,\frac{\sin(N_w\pi n\Delta\nu)}{N_w\pi\,n\,\Delta\nu} & n=1,3,5,\ldots \end{cases} \end{aligned} \tag{6.2.40}$$

The simplification in the last step is applicable only for $\pi\Delta\nu << 1/n$, which is to say, for energies very close to a interference maximum. (It is not necessary to keep track of the signs more carefully since the result will be squared, and a simpler yet more accurate formula will be derived later.) From this equation one sees that the only constructive interference maxima occur for $n = 1, 3, 5, \ldots$.

For $2N_w = 20$, the function $G^2(20, \Delta\phi)\widetilde{\mathbf{E}}_x^2(\omega, 0)$ is plotted in Fig. 6.2.8 with, as yet, arbitrary units for the vertical scale. A logarithmic scale is used, to make the third harmonic peak more visible, and to show that its amplitude is small compared to the fundamental peak, but the absolute widths of first and third harmonic are the same. This makes the third three times narrower in relative terms—like a grating spectrometer, the resolution is better in higher order. The replacement of the true transverse deflection profile by a Gaussian profile (Eq. (6.2.9)) has caused the higher order peak to be underestimated, but not by a large factor. No line spreading due to finite vertical acceptance is included in this spectrum.

The (squared) grating function, as approximated by the last expression in Eq. (6.2.40), near the $n = 1, 3, 5, \ldots$ resonance peaks, is a narrow positive definite function, having area $4N_w/n$. It is conveniently further approximated by a Dirac delta function or by a Gaussian;

$$G^2\left(2N_w, \Delta\phi\right) \approx \frac{4N_w}{n}\,\delta\left(\Delta\nu\right) \approx 4N_w^2\,\exp\left(-\frac{\Delta\nu^2}{2\left(\sqrt{2\pi}N_w n\right)^{-2}}\right)\;; \tag{6.2.41}$$

for the Gaussian approximation, the central value has been matched to the central value and the r.m.s. width $\sigma_{\delta\nu} = 1/(\sqrt{2\pi}N_w n)$ has been adjusted to give the correct area. An alternative definition of "width" is the value of $\Delta\nu$ at the first diffraction minimum—this would yield $\Delta\nu_{\text{width}} = 1/(N_w n)$. Whatever way it is defined, the relative width of the energy peak observed at fixed angle is inversely proportional to n and to N_w.

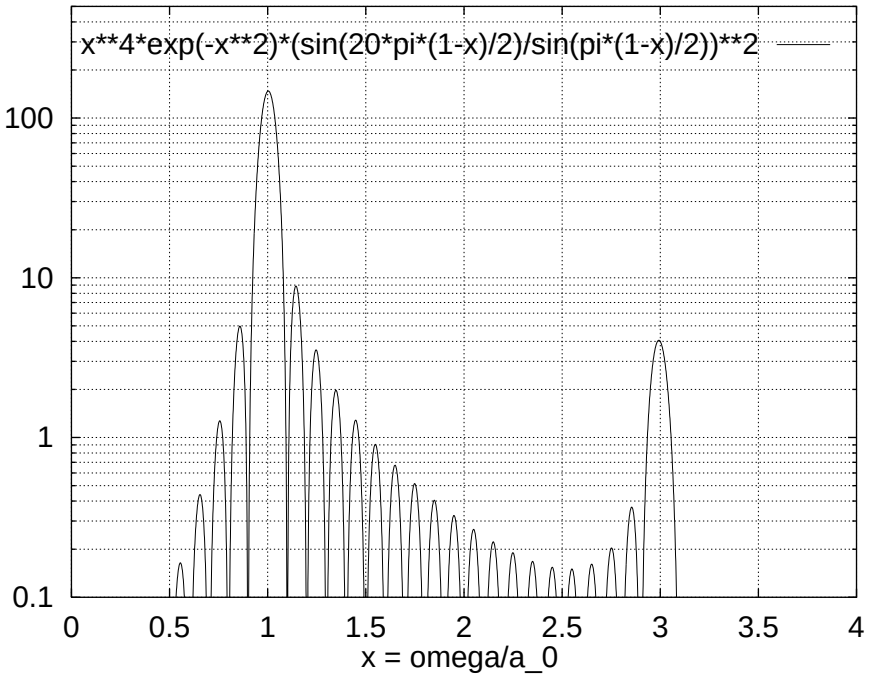

Figure 6.2.8: Energy spectrum for $N_w = 10$ undulator periods, with $\vartheta = \Theta = 0$. The horizontal axis is ω/a_0.

Combining Eqs. (6.2.27), (6.2.33), and Eq. (6.2.41), and substituting for λ_w from Eq. (6.2.30), the distribution of energy radiated by a single electron passing through the undulator into the n'th harmonic, for $n = 1, 3, 5, \ldots$, is given by the following alternative expressions, of which the first is most accurate, and all assume $K << 1$;

$$\begin{aligned}
\frac{d^2U_n}{d\omega d\Omega} &= \frac{4K^2\gamma^2}{\pi^2}\,\frac{q^2}{4\pi\epsilon_0 c}\,\frac{\omega_n^4(\vartheta)}{a_0^2 a_\vartheta^2}\,\exp\left(-\frac{\omega_n^2(\vartheta)}{a_\vartheta^2}\right)\,G^2\left(2N_w,\Delta\phi\right) \\
\overset{\text{or}}{\approx}\ & \frac{16}{\pi^2}\,N_w K^2\gamma^2\,\frac{q^2}{4\pi\epsilon_0 c}\,\frac{n^3}{\left(1+\gamma^2\vartheta^2\right)^2}\,\exp\left(-\frac{\omega_n^2(\vartheta)}{a_\vartheta^2}\right)\,\delta\left(\Delta\nu\right) \qquad (6.2.42) \\
\overset{\text{or}}{\approx}\ & \frac{16}{\pi^2}\,N_w^2 K^2\gamma^2\,\frac{q^2}{4\pi\epsilon_0 c}\,\frac{n^4\exp\left(-n^2\right)}{\left(1+\gamma^2\vartheta^2\right)^2}\,\exp\left(-\left(\Delta\nu\sqrt{\pi}\,N_w n\right)^2\right)\ .
\end{aligned}$$

(For reference, the closest corresponding formula from Jackson, namely his Eq.(14.114), after various notational changes (which should be checked), becomes

$$\frac{d^2U_1}{d\omega d\Omega} = N_w K^2\gamma^2\,\frac{q^2}{4\pi\epsilon_0 c}\,\frac{\left(1-\gamma^2\vartheta^2\right)^2+4\gamma^2\vartheta^2\sin^2\phi_J}{\left(1+\gamma^2\vartheta^2\right)^4}\,\delta\left(\Delta\nu\right)\ . \qquad (6.2.43)$$

Exact comparison of this formula with the central equation of (6.2.42) is made difficult by the fact that it includes dependence on Jackson's azimuthal angle ϕ_J and sums over both

polarization states. Also, inclusion of the $K^2/2$ terms in Eq. (6.2.42) may not be justified, since the small K approximation may not have been handled consistently.

6.3. Energy Interval Definitions

An absurdly small fraction of the energy emitted from a storage ring, or even from any one undulator, actually contributes to any X-ray diffraction exposure. Perhaps the greatest inefficiency is due to the extremely narrow energy acceptance window of typical detection apparatus. This makes it important to define, evaluate, and compare various energy intervals. It is important to distinguish between *absolute* and *relative* energy intervals. In practice it is usually relative energy intervals, ratios of energy width to central energy, that are most significant.

To calculate either "flux" or "brilliance" it is necessary to integrate $d^2U_n/d\omega d\Omega$, as given in Eq. (6.2.42), over an actual detection apparatus. The δ-function form can only be used for apertures that are large compared to the natural spreads. Otherwise, for example, arbitrarily small aperture could lead to infinite brilliance. Similarly, since the Gaussian approximation does not convey the true diffraction pattern, it can only be used to *estimate* the brilliance unless the aperture size is large compared to diffractive structure.

In spite of this cautionary sentence, there is picture of the forward distribution of photons, due to Kim, based on a formula very similar to the Gaussian approximation, the last of Eqs. (6.2.42). I find this picture confusing and misleading, but it seems to be popular with workers in the field, so I will try to construct an analogous picture. Imagine an apparatus tuned to accept an infinitessimal band of energies centered on $na_0/(1+K^2/2)$, which is the central frequency of the peak, in the forward direction, for the n'th harmonic. Let us suppose that the apparatus measures production angles with perfect angular resolution, and is used to measure the dependence of radiated power on ϑ. Substituting the second of Eqs. (6.2.33) into Eq. (6.2.38) yields the fractional deviation from resonance of this detector, at angle ϑ, to be

$$\Delta\nu\,(\vartheta) = -\frac{\gamma^2\vartheta^2}{1+K^2/2}\ . \tag{6.3.1}$$

Retaining only the (dominant) final factor of the final version of Eq. (6.2.42), the angular dependence of energy striking the detector is given by

$$\frac{d^2U_n}{d\omega d\Omega} \sim \exp\left(-r^4\vartheta^4\right) \quad \text{where} \quad r^2 = \frac{\gamma^2}{1+K^2/2}\sqrt{\pi}N_w n \ . \tag{6.3.2}$$

Since this formula has a "hyper-Gaussian" dependence, with ϑ^4 in the exponent, it disagrees with Kim, whose exponent is proportional to ϑ^2. Nevertheless we can use it to "calculate" an angular variance;

$$\sigma_\vartheta^2 = \frac{\int_0^\infty \vartheta^3 \exp\left(-r^4\vartheta^4\right)\, d\vartheta}{\int_0^\infty \vartheta \exp\left(-r^4\vartheta^4\right)\, d\vartheta} = \frac{1}{\Gamma\left(1/2\right)}\frac{1}{r^2} = \frac{1}{\pi}\frac{1+K^2/2}{\gamma^2}\frac{1}{N_w n} \ . \tag{6.3.3}$$

This agrees with formula Eq.(4.33) of Kim, except the factor $1/\pi$ is replaced by $1/4$ in his formula. This discrepancy may be due to slightly different definition of the parameters and, in any case, constitutes good agreement within the spirit of the approximation. The same formula appears in "X-Ray Data Handbook", Berkeley, 1986, and in the Wiedemann contribution, "Undulator and Wiggler Radiation", to the "Handbook of Accelerator Physics and Engineering", A. Chao and M. Tigner, editors. See, for example, page 189 of Wiedemann (or page 4-7, Kim).

The reason I disapprove of this analysis is that it begs to be misinterpreted as showing that coherence from the N_w undulator poles causes the radiation cone to "narrow" as N_w increases. In fact, if the full energy spread is accepted at every angle, the angular pattern from the whole undulator is the same as would come from any one of its poles in isolation. Speaking loosely, the mathematics of this is that a practical experimental monochrometer is "even narrower than a δ-function". This is to say that, even though it is usually legitimate to approximate a narrow line whose width is, say, 1%, (typical for undulators) by a δ-function (as in the second of Eqs. (6.2.42) or Jackson's Eq. (6.2.43)), this is *not* valid for apparatus having acceptance of, say, 0.1%. In the following more detailed description of actual detection apparatus, it may become understandable how this misinterpretation of the effect of coherence in the forward direction seems not to have led to experimental contradictions for present-day (not very large N_w) undulators.

Some of the points that have been raised are illustrated in Fig. 6.3.1 which shows little parallelograms at the intersections of the narrow, fixed-energy acceptance of a detector and the radiation bands of the lowest three undulator resononances. In greater detail,

the parallelograms are defined by contours of constant photon energy forming two sides and undulator band edges forming the other sides. At fixed energy, lines from undulator harmonics appear at angles increasing monotonically with n. Single source diffraction structure (corresponding to $G(2N_w, \Delta\phi)$, as defined in Eq. (6.2.39)) is not shown; the effect of this dependence would be to produce fringes at the edges of the little acceptance parallelograms. The actual pattern observed by the detector would consist of rings; Fig. 6.3.1 just shows the intersections of these rings with one coordinate plane.

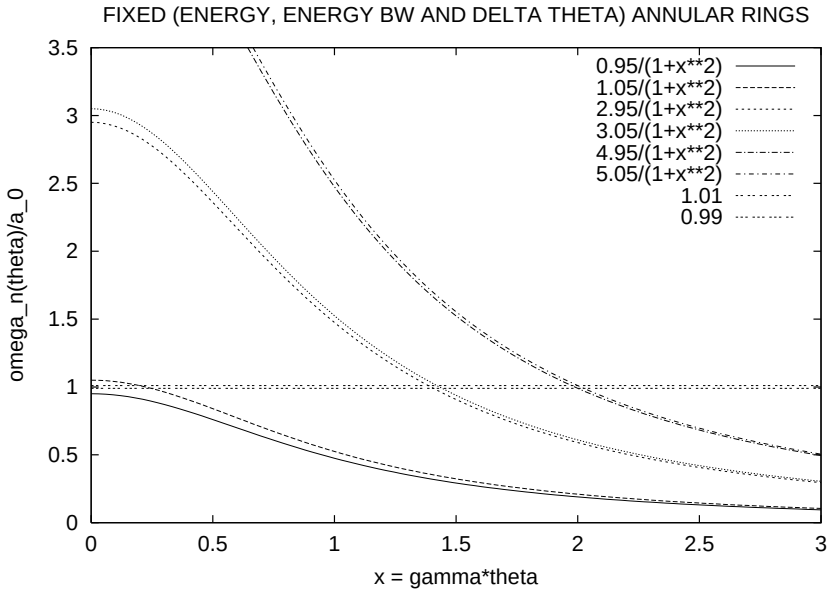

Figure 6.3.1: The photon flux into a detector having fixed central energy, fixed energy acceptance and full angular acceptance is proportional to the areas of the little parallelograms whose sides are contours of constant n resonance (Eq. (6.2.33)) and whose bottoms and tops are contours of constant photon energy. There is no significance to the solid, broken, etc. curves other than to correlate with the mathematical form shown in the key.

The radii of the annular rings increase monotonically with n. If the energy window were reduced slightly from the value shown, even the $n = 1$ resonance would give an annular ring, and if the window were raised the central spot would vanish. The setting shown, with the energy window centered on the $n = 1$ resonance, is optimal for achieving maximum brilliance. It is also the configuration for which Formula (6.3.3) is most nearly valid. But one sees that the vanishing of $d\omega_n/d\vartheta$ at this point complicates the mathematics.

It would be unreasonable to suppose that, in such a situation, a formula for the variance (Eq. (6.3.3)) will yield anything better than a semi-quantitative indication of the nature of the distribution near this point. An equation providing the same qualitative content could just as well have been derived by finding the intersection of the constant energy line with the resonator band edge. This amounts to finding the angle $\vartheta_{\text{typ.}}$ at which the numerator factor in the last form of Eq. (6.2.42) has fallen by the same amount the numerator factor is reduced for a typical value $\Delta\nu = 1/(2N_w n)$;

$$\vartheta_{\text{typ.}}^2 = \frac{1}{4\gamma^2 N_w n} \ . \tag{6.3.4}$$

This is in semiquantitative agreement with Eq. (6.3.3), and with Kim's Eq.(4.33).

The fractional energy band from an undulator was calculated in the previous section. Expressed in terms of ν, defined in Eq. (6.2.37), the fractional energy band for the n'th undulator line is $-1/(2N_w n) < \Delta\nu < 1/(2N_w n)$. There are also other fractional energy bands that can be introduced, some to be defined and evaluated later:

- $\Delta\nu_{\text{nom.}}$=0.001 is a nominal fractional spread, which is presumably typical of X-ray detection apparatus, since terms like "brightness" and "brilliance use it in their definition.
- $\Delta\nu_{\text{monochrom.}}$ is the fractional energy transmission window of a monochrometer placed in the beamline upstream of the particular detection apparatus. The monochrometer acceptance window is assumed to be independent of X-ray position and angle. For present purposes we will make the (obviously incorrect) assumption that all apparatus is typical, so $\Delta\nu_{\text{monochrom.}}$ and $\Delta\nu_{\text{nom.}}$ will be at least approximately equal.
- $\Delta\nu_{\text{collim.}}$ is the fractional energy spread defined by a collimator that limits X-ray angles at the front end of the detection apparatus. In the angle-energy plane there is (especially for $K << 1$) a strong correlation between X-ray angle and energy, but contours of equal angle are not the same as contours of equal energy so the bands passed by collimator and monochrometer do not match perfectly. In practice, a collimator will typically define a considerably broader energy window than does the monochrometer.

- $\Delta\nu_{N_w} \equiv 1/(N_w n)$ is a fractional energy spread characteristic of the number of undulator periods N_w, at the n'th harmonic. This is equivalent in spirit, though not exactly in value, to either of the two widths defined below Eq. (6.2.41). For undulators of modest length this width will typically be much greater than $\Delta\nu_{\text{monochrom.}}$

The energy spectrum (for $N_w = \infty$, $K << 1$, and integrated over production angle) is shown in Fig. 9.1, from Jackson. Defining† $\nu_{\text{J}} = \omega/a_0$, and P to be the total beam power, Jackson gives the spectrum to be

$$\frac{dP}{d\nu_{\text{J}}} = 3P\left(\nu_{\text{J}} - 2\nu_{\text{J}}^2 + 2\nu_{\text{J}}^3\right) \ , \quad \text{for} \quad 0 < \nu_{\text{J}} < 1 \ . \tag{6.3.5}$$

(Of course the discontinuous drop to zero at $\nu_{\text{J}} = 1$ is valid only as $N_w \to \infty$. For finite N_w the spectrum at fixed angle falls continuously over a range $\approx 1/N_w$. Relative to (6.3.5), the number spectrum acquires a factor of ν_{J} and is hence more nearly flat over the range $0 < \nu_{\text{J}} < 1$ than is the curve in Fig. 9.1. (It would be exactly flat if the distribution were uniform in the electron rest system.) But, for purposes of accounting, we can count photons as if they all had the full energy and restore appropriate angle and energy dependencies later. (Certainly this yields an undercount of actual photons, and a serious overcount of useful photons.) Because of the correlation between energy and angle, the actual number of useful photons depends on the detailed experimental setup. From Eq. (6.3.5), the fractional power in the range $1 - \Delta\nu_{\text{J}} < \nu_{\text{J}} < 1$ works out to be

$$\frac{\Delta P}{P} = 3\Delta\nu_{\text{J}} \ . \tag{6.3.6}$$

As will be explained, it is sensible to first narrow the energy spectrum by collimating the beam to pick out a central circular cone. From Eq. (6.3.1), close to the forward direction,

$$\nu_{\text{J}} \approx 1 - \gamma^2\vartheta^2, \quad \text{or} \quad \Delta\nu_{\text{J}} = \gamma^2\vartheta^2, \quad \text{or} \quad \vartheta = \frac{\sqrt{\Delta\nu_{\text{J}}}}{\gamma} \ , \tag{6.3.7}$$

and the solid angle within this collimation angle is $\Delta\Omega = \pi\vartheta^2$. (The term $K^2/2$, suppressed to make the next few formulas look simpler, should be restored if K approaches or exceeds 1.) Then the fractional beam power and fractional energy width are related to $\Delta\Omega$ by

$$\Delta\Omega_{\text{collim.}} = \frac{\pi}{\gamma^2}\,\Delta\nu_{\text{J,collim.}} = \frac{\pi}{3\gamma^2}\,\frac{\Delta P}{P} \ . \tag{6.3.8}$$

† The quantities ν, defined in Eq. (6.2.37), and ν_{J} defined here, though similarly motivated, are not equal, because ν_J (J for Jackson) refers ω to the peak frequency while ν refers ω to the resonant frequency at ϑ.

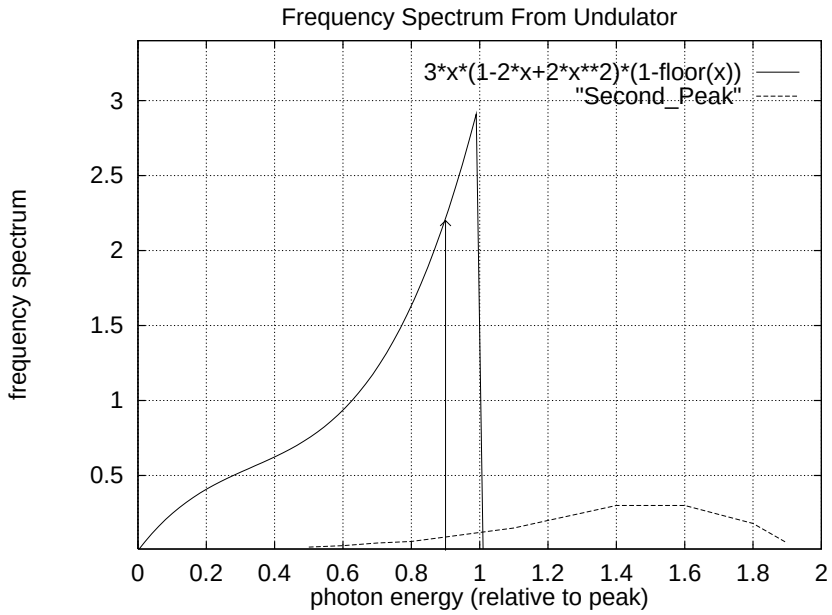

Figure 6.3.2: Undulator frequency spectrum plots copied (combined and somewhat garbled) from figures in Jackson, *Classical Electrodynamics*. The spectra plotted assume the production angle has been integrated over. The $K = 0$ functional form can be read from the key in the upper right corner. Preceeding the apparatus by a collimator that stops angles greater than one third of the cone angle of the radiation, would allow only the narrow energy band above the arrow to be transmitted. The second interference maximum is shown corresponding to $K = 0.5$.

By convention the "useful for X-ray physics" fractional energy range is taken to be $\Delta\nu_{\mathrm{J,nom.}} = 0.001$. Eq. (6.3.6) shows therefore, that photons making up only three parts in one thousand of the beam power in a pure ($N_w = \infty$) undulator beam lie within the nominal energy bandwidth. The "useful" power flux therefore is therefore less than the total power by a factor of 300. Corresponding to the nominal energy width we can define a "nominal collimation angle" $\vartheta_{\mathrm{nom.}}$ and a "nominal solid angle" $\Delta\Omega_{\mathrm{nom.}}$

$$\vartheta_{\mathrm{nom.}} = \sqrt{0.001}/\gamma \ , \quad \Delta\Omega_{\mathrm{nom.}} = 0.001\pi/\gamma^2 \ . \tag{6.3.9}$$

Most of the photons at fixed angle lie in the fractional range $\Delta\nu_{J,N_w}$. For $N_w \approx 1000$, $\Delta\nu_{J,N_w}$ and $\Delta\nu_{\mathrm{J,nom.}}$ would be equal, and the collimation could be established such that $\Delta\nu_{\mathrm{J,collim.}} \approx \Delta\nu_{\mathrm{J,nom.}} \approx \Delta\nu_{J,N_w}$. But most undulators have far fewer periods, so $\Delta\nu_{\mathrm{J,nom.}} << \Delta\nu_{J,N_w}$. Also, in practical setups, $\Delta\nu_{J,N_w} < \Delta\nu_{\mathrm{J,collim.}}$, by a conservatively large factor.

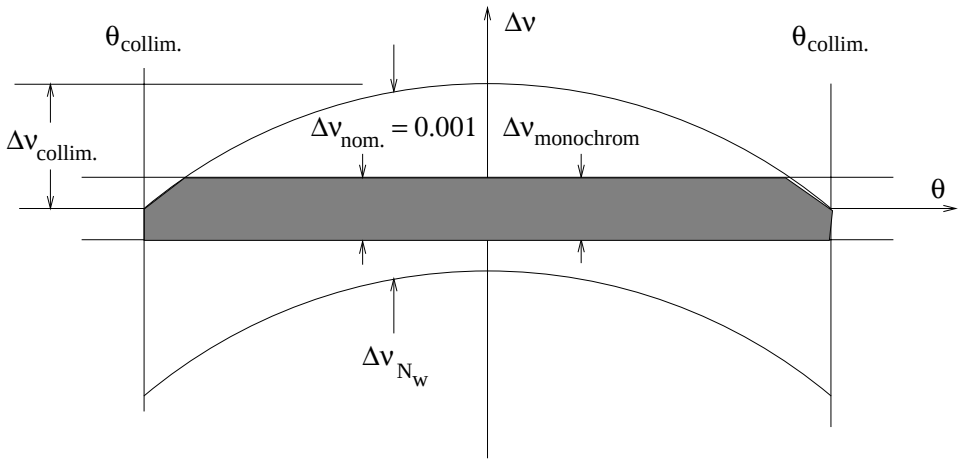

Figure 6.3.3: In the $\nu_{\rm J}, \vartheta$ plane apertures are defined by monochromatization, by collimation, and by the undulator characteristics (i.e. number of poles N_w.) For the relative sizes of these apertures suggested in the text as typical, useful photons populate the shaded region.

The apertures that have been defined are illustrated in Fig. 6.3.3. It is the photons falling within the shaded region that make up the useful flux. If the relative magnitudes are as illustrated by this figure, it can be seen that the "useful flux" is proportional to $\Delta\nu_{\rm J,nom.}\Delta\Omega_{\rm collim.}$ where $\Delta\Omega_{\rm collim.} = \pi\theta^2_{\rm collim.}$. Approximating the grating function to be uniform within the band $\Delta\nu_{J,N_w}$, and using Eq. (6.3.8), the flux is given (approximately) in terms of P_1, the beam power in the fundamental $n = 1$ line, by

$$\mathcal{F}_1 = 3\frac{\gamma^2}{\pi}\,\Delta\Omega_{\rm collim.}\,\frac{P_1}{E_\gamma}\,\frac{\Delta\nu_{\rm J,nom.}}{\Delta\nu_{J,N_w}}\ . \tag{6.3.10}$$

The beam brilliance is then given by

$$\mathcal{B}_1 = \frac{\mathcal{F}_1}{\Delta\nu_{\rm J,nom.}\Delta\Omega_{\rm collim.}A} = \frac{3N_w\gamma^2}{\pi}\,\frac{P_1}{E_\gamma}\,\frac{1}{\pi\sqrt{\beta_x\epsilon_x}\,\sqrt{\beta_y\epsilon_y}}\ , \tag{6.3.11}$$

where $A = \pi\sqrt{\beta_x\epsilon_x}\sqrt{\beta_y\epsilon_y}$ is the "spot area". Since P_1 is proportional to N_w the brilliance is (superficially) proportional to N_w^2. Since, according to Eq. (6.2.17), the total power radiated from the undulator is proportional to K^2 there is a low-K regime in which the brilliance is proportional to K^2, but since Eqs. (6.3.10) and (6.3.11) are valid only for $K << 1$, the range over which this variation holds requires further analysis. These equations also neglect any contribution to the X-ray angular spread coming from the angular spread of the electron beam. Therefore, they provide approximate upper limits for the flux and brilliance.

6.4. Undulator Radiation For Arbitrary K Values

Since the formulas in this section will eventually have to be evaluated numerically, approximations will be avoided to the extent possible. Also, at the expense of repetition, to emphasize the surprisingly small number of steps needed to derive the main result, intermediate formulas already given in earlier sections will be repeated. In writing this section I have profited from conversations with, and numerical calculations using MAPLE by, Lewis Kotredes.

The approach so far has been to represent a single pole by one phasor and to evaluate the total amplitude as the vector sum of $2N_w$ such phasors. We should now note that what was called the "long magnet condition" in Eq. (2.2.1), namely $L > 2R/\gamma$, in undulator terminology corresponds to $K > 1$. As K increases from zero it becomes increasingly less valid to represent the radiation from a single pole by a single phasor amplitude. Rather, one should break the entire undulator into sufficiently short intervals, then form their phasor sum. For large N_w this would be a formidable task, requiring the summation over large numbers of nearly-canceling quantities.

Because the undulator structure is most naturally specified in terms of z we will eventually change the integration variable from t_r to z. The extreme dependence of t upon t_r has been noted previously, and now the dependence of t_r upon z becomes progressively more influential as K increases.

For a purely sinusoidal orbit, using Eq. (6.2.7), the velocity components are given by

$$\frac{v_x}{c} = \frac{v}{c}\,\Theta\,\cos k_w z, \quad \frac{v_z}{c} \approx 1 - \frac{1}{2\gamma^2} - \frac{\Theta^2}{2}\,\cos^2 k_w z\ . \tag{6.4.1}$$

This formula gives v_z the correct maximum value, $v/c \approx 1 - 1/(2\gamma^2)$, and the correct average value as given by Eq. (6.2.31), and corresponds to having chosen the z-origin at a point where v_z is minimum. Inverting the second of Eqs. (6.4.1) to give dt_r/dz, and then integrating and setting $t_r = 0$ at $z = 0$, yields

$$t_r \approx \left(1 + \frac{1 + K^2/2}{2\gamma^2}\right)\,\frac{z}{c} + \frac{(K/\gamma)^2}{8k_w c}\,\sin\left(2k_w z\right)\ . \tag{6.4.2}$$

This gives the laboratory frame time of arrival of a reference electron at z. Referring again to Fig. 6.2.3 and dropping factors that are cubic or higher in small quantities, the factors

governing radiation are

$$\begin{aligned}
&\widehat{\mathcal{R}} \approx \theta\hat{\mathbf{x}} + \psi\hat{\mathbf{y}} + \left(1 - \frac{\vartheta^2}{2}\right)\,\hat{\mathbf{z}},\\
&\frac{\mathbf{v}}{c} = \frac{v}{c}\,\Theta\,\cos k_w z\,\hat{\mathbf{x}} + \left(1 - \frac{1}{2\gamma^2} - \frac{\Theta^2}{2}\,\cos^2 k_w z\right)\,\hat{\mathbf{z}},\\
&1 - \widehat{\mathcal{R}}\cdot\frac{\mathbf{v}}{c} \approx -\theta\Theta\,\cos k_w z + \frac{1}{2\gamma^2} + \frac{\vartheta^2}{2} + \frac{\Theta^2}{2}\,\cos^2 k_w z,\\
&\frac{\mathbf{v}_\perp}{c} = \frac{\mathbf{v}}{c} - \left(\widehat{\mathcal{R}}\cdot\frac{\mathbf{v}}{c}\right)\,\widehat{\mathcal{R}} \approx (\Theta\,\cos k_w z - \theta)\,\hat{\mathbf{x}} - \psi\,\hat{\mathbf{y}} + \left(-\theta\Theta\,\cos k_w z + \vartheta^2\right)\,\hat{\mathbf{z}}\ .
\end{aligned} \tag{6.4.3}$$

Substituting into Eqs. (6.2.19) and using Eq. (6.4.2) yields

$$\frac{d\,(ct)}{dz} = \frac{dt}{dt_r} = -\theta\Theta\,\cos k_w z + \frac{1 + K^2/2}{2\gamma^2} + \frac{\vartheta^2}{2} + \frac{\Theta^2}{4}\,\cos 2k_w z\ . \tag{6.4.4}$$

Only the leading term of Eq. (6.4.2) has survived in this formula because it is of order 1 times z/c, making the other term negligible. This means that it has not really been essential to distinguish between t_r and z/c. But this *does not* mean that the phase shift depending on the longitudinal position of the electron can be neglected. Integrating Eq. (6.4.4) and requiring $t = 0$ at $z = 0$ yields

$$ct = \frac{1}{2\gamma^2}\,\left(1 + \frac{K^2}{2} + \gamma^2\vartheta^2\right)\,z - \frac{\theta\Theta}{k_w}\,\sin k_w z + \frac{\Theta^2}{8k_w}\,\sin 2k_w z\ . \tag{6.4.5}$$

Position, velocity and acceleration components, as well as the trigonometric terms appearing in Eq. (6.4.5) are plotted as a function of z in Fig. 6.4.1. Regions of the trajectory that dominate $E(t)$ (because B_y and hence transverse acceleration a_x is large) are indicated in the top figure. These regions are centered alternately on the north and south magnet poles.

Following Kim[4](though not in detail) as well as (and more closely) Als-Nielsen and McMorrow,[11] to interpret Eq. (6.4.5) it is useful to re-arrange it so that the linear term is the same as the arguments of the trigonometric factors. Toward that end, copying from Eqs. (6.2.33) and (6.2.26), we introduce

$$\omega_1\,(\vartheta) = \frac{2\gamma^2}{1 + K^2/2 + \gamma^2\vartheta^2}\,ck_w, \quad \phi_t = \omega_1\,(\vartheta)\ t, \quad \text{and} \quad \phi_z = k_w z \approx k_w c t_r\ . \tag{6.4.6}$$

The newly introduced quantity ϕ_t is the observation time expressed as a phase angle, where the phase is referred to the $n = 1$ undulator resonance frequency *at the particular angle* ϑ.

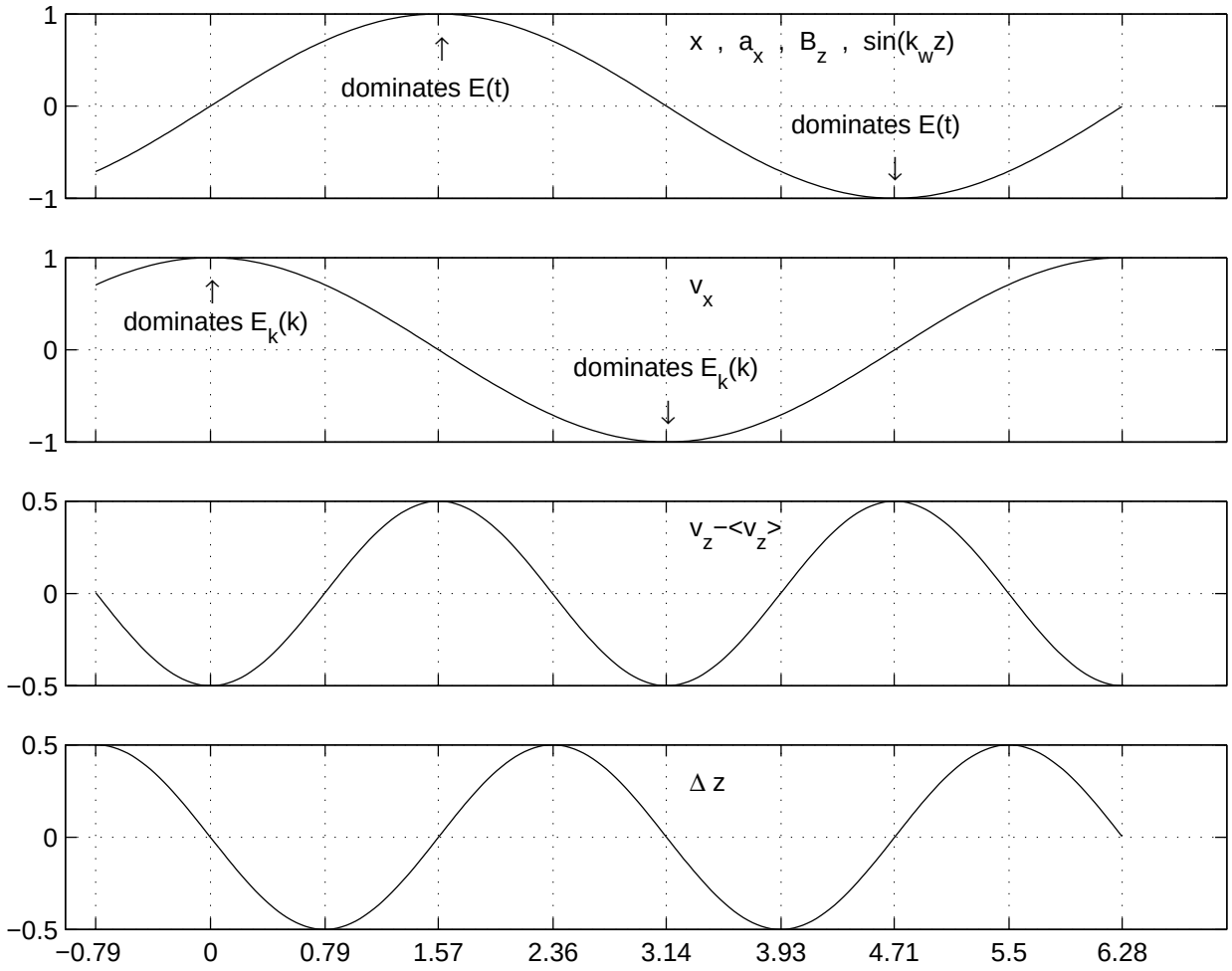

Figure 6.4.1: Graphs showing the correlations among various quantities as a function of longitudinal position in the undulator. Vertical scales can be reconstructed using formulas in the text.

Then we obtain[†]

$$\begin{aligned}\phi_t &= \phi_z - \frac{2\gamma\theta K}{1+K^2/2+\gamma^2\vartheta^2}\,\sin\phi_z + \frac{K^2/4}{1+K^2/2+\gamma^2\vartheta^2}\,\sin 2\phi_z \\ &\equiv \phi_z + p\,\sin\phi_z + q\,\sin 2\phi_z\ .\end{aligned} \tag{6.4.7}$$

An example of this dependence is plotted in Fig. 6.4.2.

The electron's motion is a periodic function of ϕ_z with period 2π. As ϕ_z advances by 2π, the first term on the right hand side of Eq. (6.4.7) advances by 2π while the other

[†] Apart from different symbols, my p and q need to be multiplied by $\mp\omega/\omega_1(\vartheta)$ respectively to be the same as Kim's p and q. It appears that Kim's Eq.(4.23) has a typographical error—in his factor $\phi/K - \cos\xi$ the first term is of order $1/\gamma$ relative to the second, and hence would be neglible according to the usual approximation. To be consistent with my formulas his K should be replaced by Θ. Kim corrects this error in the equation below his Eq.(4.51).

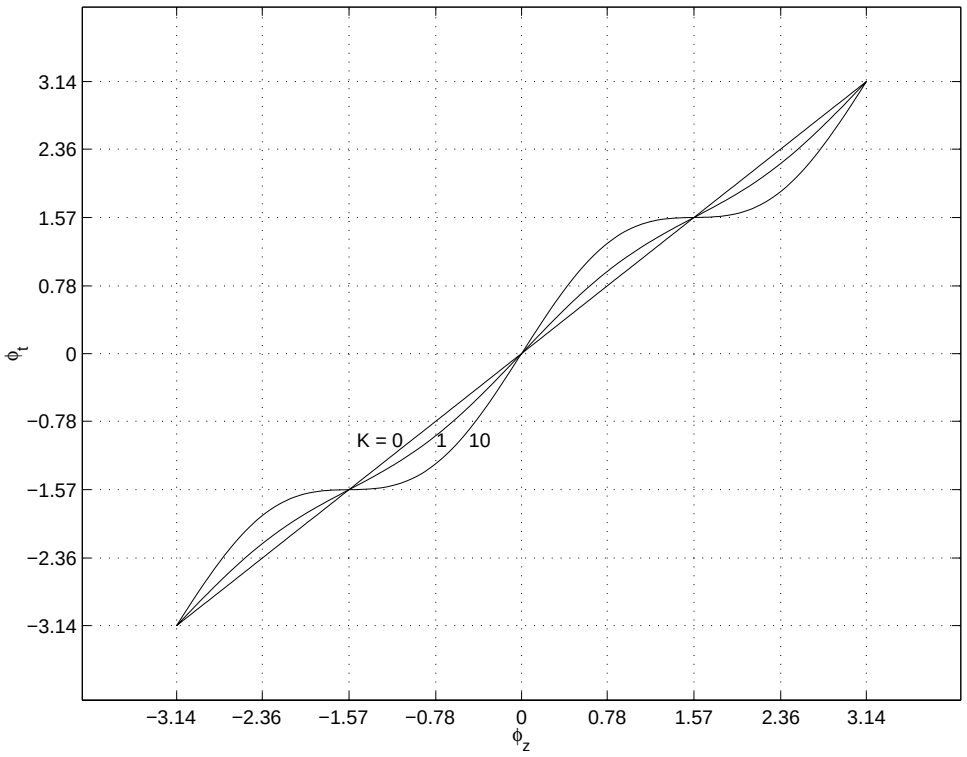

Figure 6.4.2: Observation phase ϕ_t versus emission phase ϕ_z, as given by Eq. (6.4.7), for $K = 0, 1, 10$; $\vartheta = 0$. Where the curves are almost horizontal, a large range of ϕ_z corresponds to a small range of ϕ_t.

terms return to their original values. Therefore ϕ_t also advances by 2π. Since $E_P(t)$, the electric field at observation point P at time t must be a periodic function (in the long undulator limit), when $E_P(t)$ is expressed in terms of ϕ_t it must be periodic with period 2π. But $E_P(t)$ is not, in general, a sinusoidal function. In fact, as K increases the electric field becomes progressively more peaked and therefore has progressively higher frequency components. Note also that, because $\omega_1(\vartheta)$ depends on ϑ, the harmonic frequencies are multiples of a fundamental frequency that depends on ϑ.

The leading cancellation within a single undulator period as K increases toward 1 and beyond is illustrated in Fig. 6.4.3. At any point on the viewing screen† there are contributions to the amplitude for every value of z but, especially as K increases, the greatest contributions at any angle come from regions near the points of tangency with the electron's trajectory. One sees from the figure that there are two such points per undulator

† Recall that, in a Fraunhofer picture, parallel rays converge to a single point on the viewing screen.

period. A procedure suggested by this feature is to calculate the amplitude from a full period (instead of from a half-period as previously) by summing the integrands from paired points before completing the integration. Then the complete undulator amplitude will be obtained as the sum of N_w (instead of the previous $2N_w$) phasors.

Another feature that can be inferred from Fig. 6.4.3 is that for $\theta \neq 0$ (as in the figure) the spacing between the two sources deviates from $\lambda_w/2$. This defeats the usual cancellation on even radiation harmonics, which leads to radiation peaks between the dominant, odd harmonic peaks.

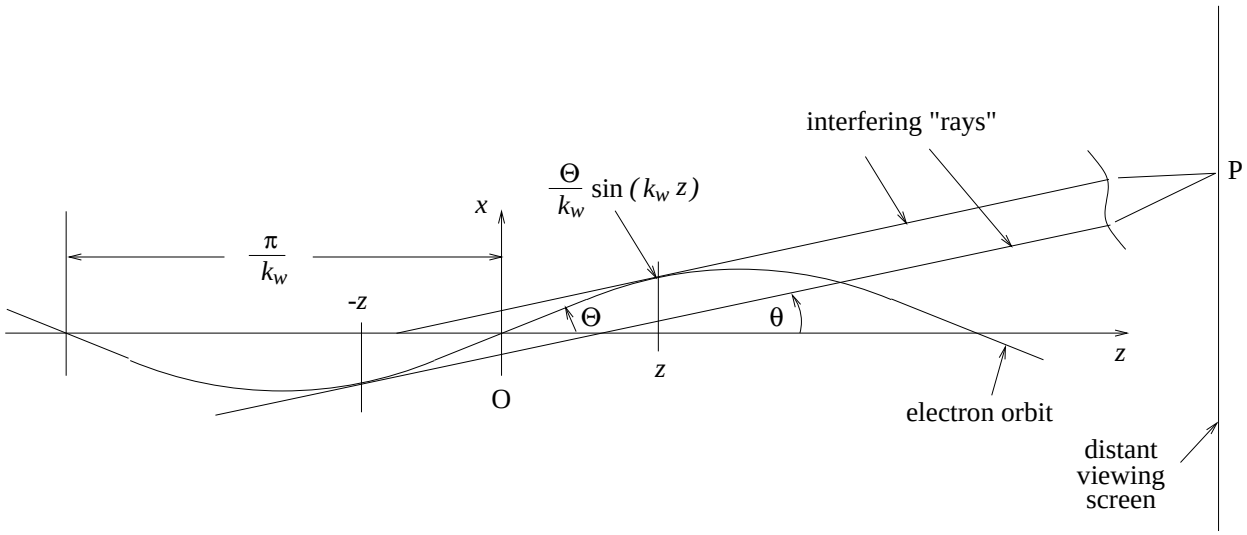

Figure 6.4.3: The contributions to the radiated amplitude at any angle are greatest in regions near the two points of tangency. Because of their opposite curvatures these amplitudes interfere destructively at low frequencies. The $n = 1$ resonance condition is satisfied when the electron delay (relative to photon) first converts this to constuctive interference. As K increases from zero, the two contributions become increasingly out of phase due to the electron's speed deficit and non-straight path.

Proceeding to the analytic calculation, the electric field is given by Eq. (2.1.5)

$$\mathbf{E}\left(\mathbf{r},t\right) = \frac{q}{4\pi\epsilon_0 c}\,\frac{1}{\mathcal{R}}\left[\frac{\widehat{\mathcal{R}}\times\left(\left(\widehat{\mathcal{R}}-\frac{\mathbf{v}}{c}\right)\times\frac{\dot{\mathbf{v}}}{c}\right)}{\left(1-\widehat{\mathcal{R}}\cdot\frac{\mathbf{v}}{c}\right)^3}\right]_{\text{ret.}} \tag{6.4.8}$$

and using Eq. (2.3.4), its transform is given by

$$\widetilde{\mathbf{E}}\left(\omega\right)=\frac{q}{4\pi\epsilon_0 c\mathcal{R}}\frac{1}{\sqrt{2\pi}}\int_{-\infty}^{\infty}e^{i\omega t}\left[\frac{\widehat{\mathcal{R}}\times\left(\left(\widehat{\mathcal{R}}-\frac{\mathbf{v}}{c}\right)\times\frac{\dot{\mathbf{v}}}{c}\right)}{\left(1-\widehat{\mathcal{R}}\cdot\frac{\mathbf{v}}{c}\right)^3}\right]_{\text{ret.}}dt\ . \tag{6.4.9}$$

Changing the integration variable from t to t_r and replacing the dt/dt_r factor using Eq. (6.2.19) yields

$$\widetilde{\mathbf{E}}\left(\omega\right)=\frac{q}{4\pi\epsilon_0 c\mathcal{R}}\frac{1}{\sqrt{2\pi}}\int_{-\infty}^{\infty}e^{i\omega t(t_r)}\frac{\widehat{\mathcal{R}}\times\left(\left(\widehat{\mathcal{R}}-\frac{\mathbf{v}}{c}\right)\times\frac{\dot{\mathbf{v}}}{c}\right)}{\left(1-\widehat{\mathcal{R}}\cdot\frac{\mathbf{v}}{c}\right)^2}dt_r\ . \tag{6.4.10}$$

We will use the result

$$\frac{\widehat{\mathcal{R}}\times\left(\left(\widehat{\mathcal{R}}-\mathbf{v}/c\right)\times\dot{\mathbf{v}}/c\right)}{\left(1-\widehat{\mathcal{R}}\cdot\mathbf{v}/c\right)^2}=\frac{d}{dt_r}\frac{\widehat{\mathcal{R}}\times\left(\widehat{\mathcal{R}}\times\mathbf{v}/c\right)}{1-\widehat{\mathcal{R}}\cdot\mathbf{v}/c} \tag{6.4.11}$$

Since this formula is critical, I exhibit the main step in its derivation:

$$\begin{aligned}\frac{d}{dt_r}\frac{\widehat{\mathcal{R}}\times\left(\widehat{\mathcal{R}}\times\mathbf{v}\right)}{1-\widehat{\mathcal{R}}\cdot\mathbf{v}}&=\frac{\widehat{\mathcal{R}}\times\left(\widehat{\mathcal{R}}\times\dot{\mathbf{v}}\right)}{1-\widehat{\mathcal{R}}\cdot\mathbf{v}}+\frac{\widehat{\mathcal{R}}\times\left(\widehat{\mathcal{R}}\times\mathbf{v}\right)}{\left(1-\widehat{\mathcal{R}}\cdot\mathbf{v}\right)^2}\widehat{\mathcal{R}}\cdot\dot{\mathbf{v}}\\&=\frac{\widehat{\mathcal{R}}\times\left(\widehat{\mathcal{R}}\times\dot{\mathbf{v}}\right)+\left(\mathbf{v}\cdot\widehat{\mathcal{R}}\right)\dot{\mathbf{v}}-\left(\dot{\mathbf{v}}\cdot\widehat{\mathcal{R}}\right)\mathbf{v}}{\left(1-\widehat{\mathcal{R}}\cdot\mathbf{v}\right)^2}\ ,\end{aligned} \tag{6.4.12}$$

where two terms have cancelled after expanding the triple cross product. Combined with the relation $\widehat{\mathcal{R}}\times\left(\mathbf{v}\times\dot{\mathbf{v}}\right)=\left(\widehat{\mathcal{R}}\cdot\dot{\mathbf{v}}\right)\mathbf{v}-\left(\widehat{\mathcal{R}}\cdot\mathbf{v}\right)\dot{\mathbf{v}}$, this yields Eq. (6.4.11). Since $\widehat{\mathcal{R}}$ is being held fixed in this calculation, we are neglecting the displacement of the electron off the undulator axis in the determination of $\widehat{\mathcal{R}}$. This assumes that $K\lambda_w << \mathcal{R}$, which will always be valid in practice. Substituting into Eq. (6.4.10), and replacing the triple cross product as in Eq. (2.1.6), we obtain

$$\widetilde{\mathbf{E}}\left(\omega\right)=\frac{q}{4\pi\epsilon_0 c\mathcal{R}}\frac{1}{\sqrt{2\pi}}\int_{-\infty}^{\infty}e^{i\omega t(t_r)}\frac{d}{dt_r}\left(\frac{-\mathbf{v}_\perp/c}{1-\widehat{\mathcal{R}}\cdot\mathbf{v}/c}\right)dt_r\ . \tag{6.4.13}$$

This formula can be further simplified by integrating by parts and again using Eq. (6.2.19);

$$\frac{\widetilde{\mathbf{E}}\left(\omega,\theta,\psi\right)}{\frac{q}{4\pi\epsilon_0 c\mathcal{R}}}=\frac{i\omega}{\sqrt{2\pi}}\int_{-\frac{N_w}{2}\frac{\lambda_w}{c}}^{\frac{N_w}{2}\frac{\lambda_w}{c}}e^{i\omega t(t_r)}\frac{\mathbf{v}_\perp}{c}dt_r\ . \tag{6.4.14}$$

In this step we have restricted the range of integration to the actual length of the undulator which is $N_w\lambda_w$. To make the transitions between inside and outside as graceful as possible we require N_w to be an *odd* integer. In component form, from Eq. (6.4.3), the transverse velocity is given by†

$$\frac{\mathbf{v}_\perp}{c} = \begin{pmatrix} \Theta\,\cos k_w z - \theta \\ -\psi \end{pmatrix} \ . \tag{6.4.15}$$

Substituting this into Eq. (6.4.14) and changing integration variable from t_r to ϕ_z using Eq. (6.4.7) yields

$$\frac{\widetilde{\mathbf{E}}\,(\omega,\theta,\psi)}{\frac{q}{4\pi\epsilon_0 c\mathcal{R}}} = \frac{i\omega}{\sqrt{2\pi}} \int_{-N_w\pi}^{N_w\pi} \exp\left(i\,\frac{\omega}{\omega_1\,(\vartheta)}\,\left(\phi_z + p\,\sin\phi_z + q\,\sin 2\phi_z\right)\right) \begin{pmatrix} \Theta\,\cos\phi_z - \theta \\ -\psi \end{pmatrix} \frac{d\phi_z}{k_w c}\,, \tag{6.4.16}$$

where N_w has to be odd. We can now exploit the periodic nature of the exponent to represent the integral as a sum;

$$\begin{aligned} \frac{\widetilde{\mathbf{E}}\,(\omega,\theta,\psi)}{\frac{q}{4\pi\epsilon_0 c\mathcal{R}}} = \frac{i}{\sqrt{2\pi}}\,\frac{\omega}{k_w c} \left(\sum_{j=-(N_w-1)/2}^{(N_w-1)/2} \exp\left(i\frac{\omega}{\omega_1\,(\vartheta)}\,2\pi\,j\right)\right) \\ \times \int_{-\pi}^{\pi} \exp\left(i\frac{\omega}{\omega_1\,(\vartheta)}\,\left(\phi_z + p\,\sin\phi_z + q\,\sin 2\phi_z\right)\right) \begin{pmatrix} \Theta\,\cos\phi_z - \theta \\ -\psi \end{pmatrix} d\phi_z \end{aligned} \tag{6.4.17}$$

This is the main result of the calculation. Since the integral is independent of N_w, one has obtained a useful factorization into a "phasor sum" part (which can be readily summed)

$$\begin{aligned} \sum_{j=-(N_w-1)/2}^{(N_w-1)/2} \exp\left(2\pi i\frac{\omega}{\omega_1\,(\vartheta)}\,j\right) &= \frac{\exp\left(-\pi i\,\frac{\omega}{\omega_1(\vartheta)}\,(N_w-1)\right) - \exp\left(\pi i\,\frac{\omega}{\omega_1(\vartheta)}\,(N_w+1)\right)}{1-\exp\left(2\pi i\,\frac{\omega}{\omega_1(\vartheta)}\right)} \\ &= \frac{\sin\left(N_w\pi\omega/\omega_1\,(\vartheta)\right)}{\sin\left(\pi\omega/\omega_1\,(\vartheta)\right)} \end{aligned} \tag{6.4.18}$$

and the "single period amplitude (which will, in general, have to be evaluated numerically)

$$\frac{i}{\sqrt{2\pi}}\,\frac{\omega}{k_w c} \int_{-\pi}^{\pi} \exp\left(i\frac{\omega}{\omega_1\,(\vartheta)}\,\left(\phi_z + p\,\sin\phi_z + q\,\sin 2\phi_z\right)\right) \begin{pmatrix} \Theta\,\cos\phi_z - \theta \\ -\psi \end{pmatrix} d\phi_z \ . \tag{6.4.19}$$

For frequencies close to resonance, using the definitions of Eq. (6.2.37),

$$\nu = \frac{1}{n}\,\frac{\omega}{\omega_1\,(\vartheta)} = 1 + \Delta\nu \ , \tag{6.4.20}$$

† Because both components of $\mathbf{v}_\perp$ are even functions of z their Fourier transforms are relatively real, which means they are in phase in all directions, which causes the radiation to be linearly polarized. This contrasts with the radiation from arc magnets, which is elliptically polarized.

the phasor sum can be approximated, as in Eq. (6.2.40), though the details are quite different because the integral now covers a full period of the undulator. One result of this is that both numerator and denominator vanish at $\Delta\nu = 0$ for values of n that are both even and odd. Exactly on resonance the value of the sum is

$$\sum\Big|_{\Delta\nu=0} = \frac{d/d\Delta\nu\,\sin\left(N_w\pi n\left(1+\Delta\nu\right)\right)}{d/d\Delta\nu\,\sin\left(\pi n\left(1+\Delta\nu\right)\right)}\Big|_{\Delta\nu=0} = N_w\,\left(-1\right)^{\left(N_w-1\right)n} = N_w\;; \tag{6.4.21}$$

the last step follows because N_w has been required to be odd. Near all resonances we have

$$\sum \approx N_w\,\frac{\sin\left(N_w\pi n\Delta\nu\right)}{N_w\pi n\Delta\nu} \equiv N_w\,\mathrm{sinc}\left(N_w\pi n\Delta\nu\right), \quad n = 0,1,2,3,\ldots\;. \tag{6.4.22}$$

(To recover the exact result from this approximation one need only replace the $N_w\,\mathrm{sinc}$ factor by expression (6.4.18).)

It is plausible to suppose, near any undulator resonance, that the dependence of $\widetilde{\mathbf{E}}(\omega,\theta,\psi)$ on ω (which is to say the dependence on $\Delta\nu$ for $\Delta\nu << 1$) is dominated by the phasor factor (6.4.22). (Since the approximate vanishing of the field for even n harmonics is built into the single period integral, for the dominant contribution we approximate only the odd n harmonics in this way.) Then, in integral (6.4.19), we make the replacement $\omega = n\omega_1(\vartheta)$ and get

$$\begin{aligned}
&\frac{i}{\sqrt{2\pi}}\,\frac{n\omega_1\left(\vartheta\right)}{k_w c}\int_{-\pi}^{\pi}\exp\left(i\,n\;\left(\phi_z + p\,\sin\phi_z + q\,\sin 2\phi_z\right)\right)\begin{pmatrix}\Theta\,\cos\phi_z - \theta\\ -\psi\end{pmatrix}d\phi_z\\
&\quad = i\sqrt{\frac{2}{\pi}}\,\frac{n\omega_1\left(\vartheta\right)}{k_w c}\int_{0}^{\pi}\cos\left(n\;\left(\phi_z + p\,\sin\phi_z + q\,\sin 2\phi_z\right)\right)\begin{pmatrix}\Theta\,\cos\phi_z - \theta\\ -\psi\end{pmatrix}d\phi_z\;.
\end{aligned} \tag{6.4.23}$$

For $\theta = 0$ the dominant (upper) integral can be evaluated analytically;

$$\begin{aligned}
&\frac{i}{\sqrt{2\pi}}\,\frac{n\omega_1\left(\vartheta\right)}{k_w c}\Theta\int_{0}^{\pi}\left(\cos\left(\left(n+1\right)\phi_z + nq\,\sin 2\phi_z\right) + \cos\left(\left(n-1\right)\phi_z + nq\,\sin 2\phi_z\right)\right)d\phi_z\\
&\quad = \frac{i}{\sqrt{2\pi}}\,\frac{n\omega_1\left(\vartheta\right)}{k_w c}\frac{\Theta}{2}\int_{0}^{2\pi}\left(\cos\left(\frac{n+1}{2}\xi + nq\,\sin\xi\right) + \cos\left(\frac{n-1}{2}\xi + nq\,\sin\xi\right)\right)d\xi\\
&\quad = i\sqrt{\frac{\pi}{2}}\,\frac{n\omega_1\left(\vartheta\right)}{k_w c}\frac{K}{\gamma}\,\left(J_{\frac{n+1}{2}}\left(-nq\right) + J_{\frac{n-1}{2}}\left(-nq\right)\right)\;.
\end{aligned} \tag{6.4.24}$$

Recombining factors we obtain

$$\frac{\widetilde{E}_{x,n}\left(\omega,0,\psi\right)}{\frac{q}{4\pi\epsilon_0 c\mathcal{R}}} \approx i\sqrt{\frac{\pi}{2}}\,\frac{n\omega_1\left(\vartheta\right)}{k_w c}\frac{K}{\gamma}\,N_w\,\mathrm{sinc}\left(N_w\pi n\Delta\nu\right)\,\left(J_{\frac{n+1}{2}}\left(-nq\right) + J_{\frac{n-1}{2}}\left(-nq\right)\right)\;, \tag{6.4.25}$$

which is valid only for odd n and for $\Delta\nu << 1$. The lower component of Eq. (6.4.23) can be evaluated for even n. It yields

$$\frac{\widetilde{E}_{y,n}(\omega,0,\psi)}{\frac{q}{4\pi\epsilon_0 c\mathcal{R}}} \approx i\sqrt{2\pi}\,\frac{n\omega_1(\vartheta)}{k_w c}(-\psi)\;N_w \operatorname{sinc}(N_w\pi n\Delta\nu)\;J_{\frac{n}{2}}(-nq)\;. \tag{6.4.26}$$

These formulas can serve to check the numerical evaluation of integral (6.4.23) in the $\theta = 0$ limit.

Recapitulating, the unapproximated, general K, undulator radiation formula derived in this section is

$$\begin{aligned}\frac{\widetilde{\mathbf{E}}(\omega,\theta,\psi)}{\frac{q}{4\pi\epsilon_0 c\mathcal{R}}} &= i\sqrt{\frac{2}{\pi}}\,\frac{\omega}{k_w c}\,\frac{\sin(N_w\pi\omega/\omega_1(\vartheta))}{\sin(\pi\omega/\omega_1(\vartheta))} \\ &\times\int_0^\pi \cos\left(\frac{\omega}{\omega_1(\vartheta)}\phi_z - \frac{\theta K}{\gamma}\frac{\omega}{ck_w}\sin\phi_z + \frac{K^2}{8\gamma^2}\frac{\omega}{ck_w}\sin 2\phi_z\right)\begin{pmatrix}\Theta\cos\phi_z-\theta\\ -\psi\end{pmatrix}d\phi_z\;.\end{aligned} \tag{6.4.27}$$

The factorization into phasor part and single period part is analogous to the similar factorization in Eq. (6.2.42). In particular the single period integral in the lower line is independent of N_w. The only dependence on N_w enters via the phasor factor which, except for inessential odd/even complication, is the same as in the earlier derivation. Furthermore, from the $N_w\operatorname{sinc}(N_w\pi n\Delta\nu)$ approximation to the phasor part, one sees that it is independent of angles once the frequency is expressed via the offset variable $\Delta\nu$. For practical wigglers, having say $N_w > 10$, this *sinc* approximation is valid in regions where the radiation is significantly large. In these regions the replacement $\omega/\omega_1(\vartheta) \to n$ in the integrand (as in Eq. (6.4.23)) is also legitimate, yielding

$$\widetilde{\mathbf{E}}(\omega,\theta,\psi) \approx \sum_{n=1,3,5,\ldots}\widetilde{\mathbf{E}}_n(\theta,\psi)\;nN_w\operatorname{sinc}\left(N_w\pi\left(\frac{\omega}{\omega_1(\vartheta)}-n\right)\right)\;, \tag{6.4.28}$$

where

$$\begin{aligned}\widetilde{\mathbf{E}}_n(\theta,\psi) &= i\,\frac{q}{4\pi\epsilon_0 c\mathcal{R}}\sqrt{\frac{2}{\pi}}\,\frac{2\gamma^2}{1+K^2/2+\gamma^2\vartheta^2}\times \\ &\int_0^\pi \cos\left(n\left(\phi_z - \frac{2\gamma\theta K\sin\phi_z}{1+K^2/2+\gamma^2\vartheta^2} + \frac{(K^2/4)\sin 2\phi_z}{1+K^2/2+\gamma^2\vartheta^2}\right)\right)\begin{pmatrix}\Theta\cos\phi_z-\theta\\ -\psi\end{pmatrix}d\phi_z\;.\end{aligned} \tag{6.4.29}$$

These features insure that the discussion in section 6.3 of energy interval definition and angular width of the radiation carries over unchanged to the exact, general K, radiation

pattern derived in this section. Until one approaches intensities at which free electron laser action (i.e. stimulated emission) becomes important, the only enhancement to the forward amplitude is the N_w factor coming from the phasor factor. After squaring this leads to a N_w^2 dependence for the on-resonance Poynting vector in any given direction. For a detector having fractional energy acceptance small compared to $1/N_w$ and tuned exactly on resonance, this leads to an N_w^2 rate dependence. For a detector having broad energy acceptance and therefore integrating over a range broad compared to the resonance line width, the rate is proportional to N_w. This behavior is consistent with the proposition that the total energy radiated from the undulator is given by the standard Schott formula (Eq. (6.2.14)), unenhanced by any interference effect.

6.5. Numerical/Graphical Representation of Undulator Radiation

The angular intensity pattern is proportional to $|\widetilde{E}_{n,x}|^2(\theta,\psi)$, which is given by Eq. (6.4.29). It is exhibited for $K = 1.5$, $n = 3, 5$, in Fig. 6.5.1 and Fig. 6.5.2.

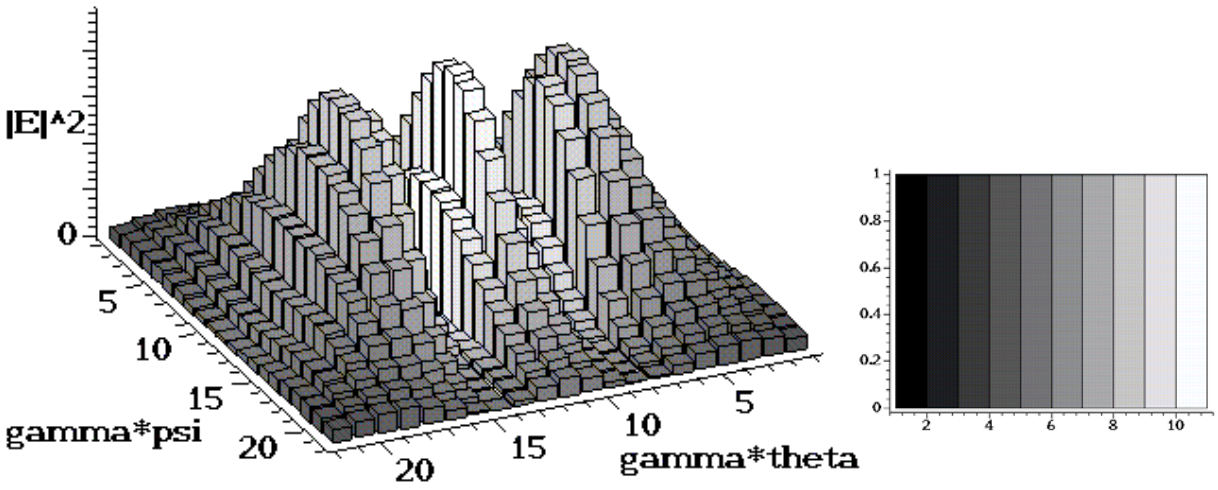

Figure 6.5.1: Histogram representation of undulator radiation: the height of each bin gives the value of $|\widetilde{E}_{3,x}|^2_{K=1.5}(\theta,\psi)$, as given by Eq. (6.4.29) (with factor $q/(4\pi\epsilon_0 c\mathcal{R})$. suppressed) at the appropriate value of $(\gamma\theta, \gamma\psi)$. Since the photon frequency ω is known as a function of the same independent-variable pair (θ,ψ) (Eq. (6.4.6)), it can be exhibited as a ratio $\omega/\omega_3(0)$ which is coded by the grayscale shading. The forward direction is marked by the highest tower which has $\omega/\omega_3(0) = 1$ and is therefore pure white. 'gamtheta' and 'gampsi' stand for $\gamma\theta$ and $\gamma\psi$. The bin widths are $\Delta\theta = \Delta\psi = 0.15/\gamma$. This data is independent of N_w.

Each histogram tower represents both $|\widetilde{E}_{3,x}|^2_{K=1.5}(\theta,\psi)$ and the ratio $\omega(\theta,\psi)/\omega_3(0)$. The intensity is represented by the height of the tower and the photon energy by its grayscale value. The bin widths are $\gamma\Delta\theta = \gamma\Delta\psi = 0.15$. A detector having these acceptances and centered, say, at the origin, would count only photons of frequency $\omega = \omega_3(0)$ (which makes the tower pure white.) Assuming the detector accepts all photons close to this energy (so the sinc-factor of Eq. (6.4.29) can be treated as a δ-function) the rate can

be read off from the vertical axis, but still needs multiplication by the factor nN_w from Eq. (6.4.29) and by the factor $\Delta\theta\,\Delta\psi$. (The vertical scale is not shown, but it extends uniformly from 0 to 2.5×10^8.) If the detector's fractional frequency acceptance is small compared to $1/N_w$ it is necessary to include the sinc-factor dependency of Eq. (6.4.29).

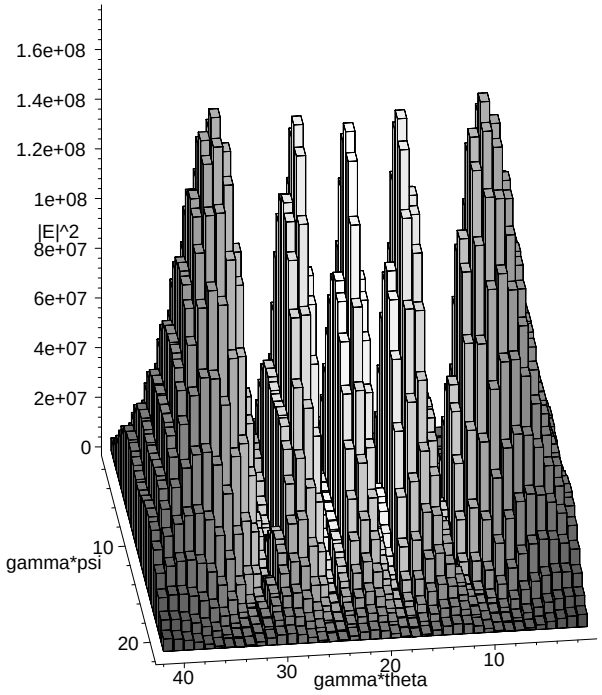

Figure 6.5.2: Same as previous figure except now $n = 5$ and bin spacings are $2\Delta\theta = \Delta\psi = 0.15/\gamma$. The θ-angular separation of fringe maxima is approximately $5 \times 0.075/\gamma = 0.375/\gamma$. The factor $\sin k_w z$ advances from 0 to 1 between north and south magnet poles, so the second term on the rhs of Eq. (6.4.5) gives a phase advance (at this angular separation, $n = 5$, $K = \Theta\gamma = 1.5$) equal to $5 \times 2\gamma \times 1.5 \times 0.375/\gamma \approx 2\pi$. This is why angular fringes are visible even with $N_w = 1$. For $N_w > 1$ it is only the central maximum that necessarily coincides with a multiple-pole maximum. A diffraction grating constructed from repeated double slits having a quarter wave plate in front of one of the slits could give a similar pattern.

There is an inevitable trade-off in which the undulator beam frequency $\omega_n(0)$ and intensity $|\mathbf{E}|^2$ are made as high as possible consistent with the machine energy γ and und undulator wave number k_w being as low as possible. For "cleaner" operation one prefers both the undulator parameter K and the harmonic number n to be as low as possible. (Until accelerator physics issues intrude, the bigger the better for N_w.) The first formula

governing this trade-offs is Eq. (6.4.6);

$$\frac{\omega_n(0)}{ck_w 2\gamma^2} = \frac{n}{1+K^2/2}\ , \tag{6.5.1}$$

by which the resonant frequency can be increased by increasing n but is unavoidably decreased by increasing K. The second key result, from Eqs. (6.4.24) and (6.4.7), (still suppressing the sinc factor and the factor $q/(4\pi\epsilon_0 c\mathcal{R})$) is

$$\frac{|\mathbf{E}_n|^2(0)}{\gamma^2} = \frac{\pi}{2}\left(\frac{2K\,n}{1+K^2/2}\right)^2\left(J_{\frac{n+1}{2}}\left(\frac{-nK^2/4}{1+K^2/2}\right)+J_{\frac{n-1}{2}}\left(\frac{-nK^2/4}{1+K^2/2}\right)\right)^2\ , \tag{6.5.2}$$

These formulas are evaluated for ranges of n and K, and the results exhibited numerically in the following table and graphically in Fig. 6.5.3. In each case in the table the upper number is given by Eq. (6.5.2) and the lower is given by Eq. (6.5.1).

n\K	0	.2	.4	.6	.8	1.0	1.2	1.4	1.6	1.8	2.0	2.4	2.6	2.8	3.0
1	0.	.25	.78	1.5	2.1	2.2	2.3	2.3	2.2	2.0	1.8	1.6	1.4	1.3	1.2
	1.	1.0	.91	.83	.77	.67	.59	.50	.43	.38	.33	.29	.26	.23	.20
3	0.	.49e-3	.022	.14	.61	1.1	1.7	2.2	2.4	2.6	2.7	2.4	2.4	2.2	2.1
	3.	3.0	2.7	2.5	2.3	2.0	1.8	1.5	1.3	1.2	1.0	.88	.79	.68	.60
5	0.	.60e-6	.30e-3	.012	.11	.31	.60	1.3	1.9	2.6	2.6	2.8	2.7	2.7	2.6
	5.	5.0	4.5	4.2	3.8	3.3	2.9	2.5	2.2	1.9	1.7	1.5	1.3	1.1	1.0
7	0.	.60e-9	.39e-5	.60e-3	.015	.11	.25	.86	1.4	1.8	1.9	2.7	3.1	2.8	2.6
	7.	7.0	6.4	5.8	5.4	4.7	4.1	3.5	3.0	2.7	2.3	2.1	1.8	1.6	1.4
9	0.	.58e-12	.46e-7	.33e-4	.0019	.023	.11	.34	.72	1.4	1.7	2.0	1.9	2.5	2.2
	9.	9.0	8.2	7.5	6.9	6.0	5.3	4.5	3.9	3.5	3.0	2.6	2.4	2.0	1.8
11	0.	.54e-15	.61e-9	.15e-5	.39e-3	.0044	.029	.22	.60	.55	1.8	1.9	1.9	2.6	2.9
	11.	11.	10.	9.2	8.5	7.3	6.5	5.5	4.8	4.2	3.7	3.2	2.9	2.5	2.2

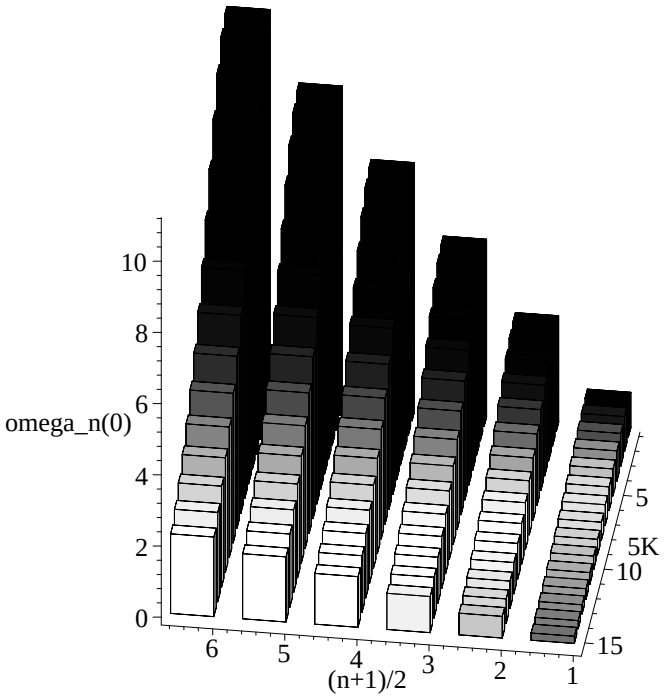

Figure 6.5.3: Histograms illustrating the dependence of undulator frequency (indicated by tower height) and intensity on resonance (indicated by tower grayscale) on undulator parameter $0 < K < 3.0$ and resonance order $n = 1, 3, 5, 7, 9, 11$. The grayscale is the same as in Fig. 6.5.1 and is normalized to 1 (white) in the lower left hand corner. Black regions have negligible flux.

An example may help to clarify this data. Consider the points $(n, K, \text{int.}, \text{freq.}) = (1, 0.2, 0.25, 1.0), (3, 0.6, 0.14, 2.5), (5, 0.8, 0.11, 3.8), (7, 1.0, 0.11, 4.7), (9, 1.2, 0.11, 5.3)$. These points have comparable intensities but, by increasing n and K together, it is possible to increase the beam frequency from 1.0 to 5.3 (in units of $ck_w 2\gamma^2$.) Being proportional to K^2, the total radiated beam power increases by a factor of 36 over this range. The beam is therefore much "cleaner" for low n values than for high. Calculations like this are useful in fixing the major storage ring and undulator parameters to achieve high brilliance. See chapter 9.

6.6. Approximation of the Integrals By Special Functions

The integrand in Eq. (6.4.27) can be Taylor expanded in terms of the (small) variable θ

$$\begin{aligned}\cos\left(n\phi + np\,\sin\phi + nq\,\sin 2\phi\right) = &\ \cos\left(n\phi + nq\,\sin 2\phi\right)\left(1 - \frac{n^2p^2}{4} + \frac{n^2p^2}{4}\,\cos 2\phi + \ldots\right) \\ &- \sin\left(n\phi + nq\,\sin 2\phi\right)\left(np\,\sin\phi + \ldots\right),\end{aligned} \tag{6.6.1}$$

and further terms can be derived easily. Here, motivated by Eq. (6.4.29), we have generalized the meaning of variable n by making the substitution

$$\frac{\omega}{\omega_1\left(\vartheta\right)} = n\ , \tag{6.6.2}$$

which means that n is now allowed to lie anywhere in the range $0 < n < \infty$ and, in particular, to not necessarily be an integer. Nevertheless, especially for large N_w, the *sinc* factor suppresses the complete expression when n is not close to an integer, so n can be thought of as being close to an integer.

Using abbreviation $\mathcal{C} \equiv \cos(n\phi + nq\,\sin 2\phi)$ we define standard integrals

$$I_{C0} = \int_0^\pi \mathcal{C}\,d\phi, \quad I_{C1} = \int_0^\pi \mathcal{C}\,\cos\phi\,d\phi, \quad I_{C2} = \int_0^\pi \mathcal{C}\,\cos 2\phi\,d\phi\ , \tag{6.6.3}$$

integrals $I_{S1}, I_{S2}, \ldots$, are defined similarly, but with $\mathcal{C}$ replaced by $\mathcal{S} \equiv \sin(n\phi + nq\,\sin 2\phi)$. The required integral is

$$\begin{aligned}&\int_0^\pi d\phi\,\cos\left(n\phi + np\,\sin\phi + nq\,\sin 2\phi\right)\left[\begin{pmatrix}\Theta\\0\end{pmatrix}\cos\phi + \begin{pmatrix}-\theta\\-\psi\end{pmatrix}\right] \\ &\quad= \begin{pmatrix}\Theta\left(1 - n^2p^2/8\right)\\0\end{pmatrix} I_{C1} + \begin{pmatrix}\Theta\,n^2p^2/8\\0\end{pmatrix} I_{C3} + \begin{pmatrix}-np\Theta/2\\0\end{pmatrix} I_{S2} \\ &\quad+ \begin{pmatrix}-\theta\left(1 - n^2p^2/4\right)\\-\psi\left(1 - n^2p^2/4\right)\end{pmatrix} I_{C0} + \begin{pmatrix}-\theta n^2p^2/4\\-\psi n^2p^2/4\end{pmatrix} I_{C2} + \begin{pmatrix}np\theta\\np\psi\end{pmatrix} I_{S1} + \ldots\ .\end{aligned} \tag{6.6.4}$$

I_{C1} was evaluated for odd n in Eq. (6.4.24), but it, and the other integrals, can now be expressed for arbitrary n and for positive integers j as

$$\begin{aligned}I_{Cj} &= \frac{1}{4}\int_0^{2\pi} \cos\left(\frac{n-j}{2}\,\xi + nq\,\sin\xi\right) d\xi + \frac{1}{4}\int_0^{2\pi} \cos\left(\frac{n+j}{2}\,\xi + nq\,\sin\xi\right) d\xi \\ I_{Sj} &= \int_0^\pi \sin\left(n\phi + nq\,\sin 2\phi\right)\,\sin j\phi\,d\xi \\ &= \frac{1}{4}\int_0^{2\pi} \cos\left(\frac{n-j}{2}\xi + nq\,\sin\xi\right) d\xi - \frac{1}{4}\int_0^{2\pi} \cos\left(\frac{n+j}{2}\xi + nq\,\sin\xi\right) d\xi\end{aligned} \tag{6.6.5}$$

All these integrals can be expressed in terms of the functions

$$\begin{aligned} \pi\,\mathbf{J}_\nu &= \int_0^\pi \cos\left(\nu\,\theta - z\,\sin\theta\right)\,d\theta \\ \pi\,\mathbf{E}_\nu &= \int_0^\pi \sin\left(\nu\,\theta - z\,\sin\theta\right)\,d\theta \end{aligned} \tag{6.6.6}$$

where $\mathbf{J}_i$ is known as an "Anger" function and $\mathbf{E}_i$ as a "Weber" function. (G. N. Watson, *Bessel Functions*, p.308.) These definitions are valid for general values of ν, but we will mainly use only integers or half-integer indices. Both functions are known to MAPLE and are presumably rapidly calculable. Bisecting the range, and replacing θ by $2\pi - \theta$ in the second integral, Watson gives the formula

$$\begin{aligned} \int_0^{2\pi} \cos\left(\nu\,\theta - z\,\sin\theta\right)\,d\theta &= \int_0^\pi \left(\cos\left(\nu\,\theta - z\,\sin\theta\right) + \cos\left(2\nu\pi - \nu\theta + z\sin\theta\right)\right)\,d\theta \\ &= 2\pi\,\cos^2\nu\pi\;\mathbf{J}_\nu\left(z\right) + \pi\,\sin 2\nu\pi\;\mathbf{E}_\nu\left(z\right)\;. \end{aligned} \tag{6.6.7}$$

In terms of these functions the required integrals are

$$\begin{aligned} I_{Cj} &= \frac{\pi}{2}\,\cos^2\left(\frac{n-j}{2}\pi\right)\;\mathbf{J}_{\frac{n-j}{2}}\left(-nq\right) + \frac{\pi}{4}\,\sin\left(\left(n-j\right)\pi\right)\;\mathbf{E}_{\frac{n-j}{2}}\left(-nq\right)\;, \\ &+ \frac{\pi}{2}\,\cos^2\left(\frac{n+j}{2}\pi\right)\;\mathbf{J}_{\frac{n+j}{2}}\left(-nq\right) + \frac{\pi}{4}\,\sin\left(\left(n+j\right)\pi\right)\;\mathbf{E}_{\frac{n+j}{2}}\left(-nq\right)\;, \\ I_{Sj} &= \frac{\pi}{2}\,\cos^2\left(\frac{n-j}{2}\pi\right)\;\mathbf{J}_{\frac{n-j}{2}}\left(-nq\right) + \frac{\pi}{4}\,\sin\left(\left(n-j\right)\pi\right)\;\mathbf{E}_{\frac{n-j}{2}}\left(-nq\right)\;, \\ &- \frac{\pi}{2}\,\cos^2\left(\frac{n+j}{2}\pi\right)\;\mathbf{J}_{\frac{n+j}{2}}\left(-nq\right) - \frac{\pi}{4}\,\sin\left(\left(n+j\right)\pi\right)\;\mathbf{E}_{\frac{n+j}{2}}\left(-nq\right)\;. \end{aligned} \tag{6.6.8}$$

6.7. Practical Evaluation of the Series

The Taylor expansion of Eq. (6.6.4) can be spelled out in general as follows:

$$
\begin{aligned}
f(m,j) &= \frac{\text{binomial}\left(m,(m-j)/2\right)}{m!\,2^{(m-1)}} \\
a(\eta,j) &= (-1)^{j/2}\sum_{0}^{i_{\max}}(-1)^{i}\,(\eta p)^{2i}\,f(2i,j)\,, \quad j=0,2,4,\ldots \\
a_0(\eta) &= a(\eta,0)/2, \\
b(\eta,j) &= (-1)^{(j-1)/2}\sum_{0}^{i_{\max}}(-1)^{i}\,(\eta p)^{(2i+1)}\,f(2i+1,j)\,, \quad j=1,3,5,\ldots \\
\gamma\widetilde{E}_x(\eta) &= \frac{K}{2}\left(2a_0(\eta)+a(\eta,2)\right)I_{C,1} \\
&\quad +\frac{K}{2}\sum_{i'=1}^{i_{\max}-1}\left(a\left(\eta,2i'\right)+a\left(\eta,2i'+2\right)\right)I_{C,2i'+1}+\frac{K}{2}\,a(\eta,2i_{\max})\,I_{C,2i_{\max}+1} \\
&\quad -\frac{K}{2}\sum_{i'=0}^{i_{\max}-1}\left(b\left(\eta,2i'+1\right)+b\left(\eta,2i'+3\right)\right)I_{S,2i'+2}-\frac{K}{2}\,b(\eta,2i_{\max}+1)\,I_{S,2i_{\max}+2} \\
&\quad -\gamma\theta\left(a_0(\eta)\,I_{C,0}+\sum_{i'=1}^{i_{\max}}a\left(\eta,2i'\right)\,I_{C,2i'}-\sum_{i'=0}^{i_{\max}}b\left(\eta,2i'+1\right)\,I_{S,2i'+1}\right) \\
\gamma\widetilde{E}_y(\eta) &= -\gamma\psi\left(a_0(\eta)\,I_{C,0}+\sum_{i'=1}^{i_{\max}}a\left(\eta,2i'\right)\,I_{C,2i'}-\sum_{i'=0}^{i_{\max}}b\left(\eta,2i'+1\right)\,I_{S,2i'+1}\right);
\end{aligned}
\tag{6.7.1}
$$

these expressions still need to be multiplied by the factor

$$
i\sqrt{\frac{2}{\pi}}\,\frac{\omega}{k_w c}\,\frac{\sin N_w\pi\eta}{\sin\pi\eta}\;; \tag{6.7.2}
$$

this factor (except for the i) is included for the following graphs. The maximum power of p retained in the expansion is $2i_{\max}+1$. For constant accuracy $i_{\max}$ has to increase with increasing $\gamma\vartheta$. At fixed K the ring structure depends only on $\gamma\vartheta$. Because an oscillatory function is being fit by a power series, the number of cycles fit is probably proportional to the highest power retained. From the example we have studied most carefully ($K=1.35$) a suggested rule of thumb is to choose $i_{\max}$ to be about four (or more) times the number of rings to be faithfully calculated, but this should be investigated in each case. The following three pairs of graphs illustrate these comments.

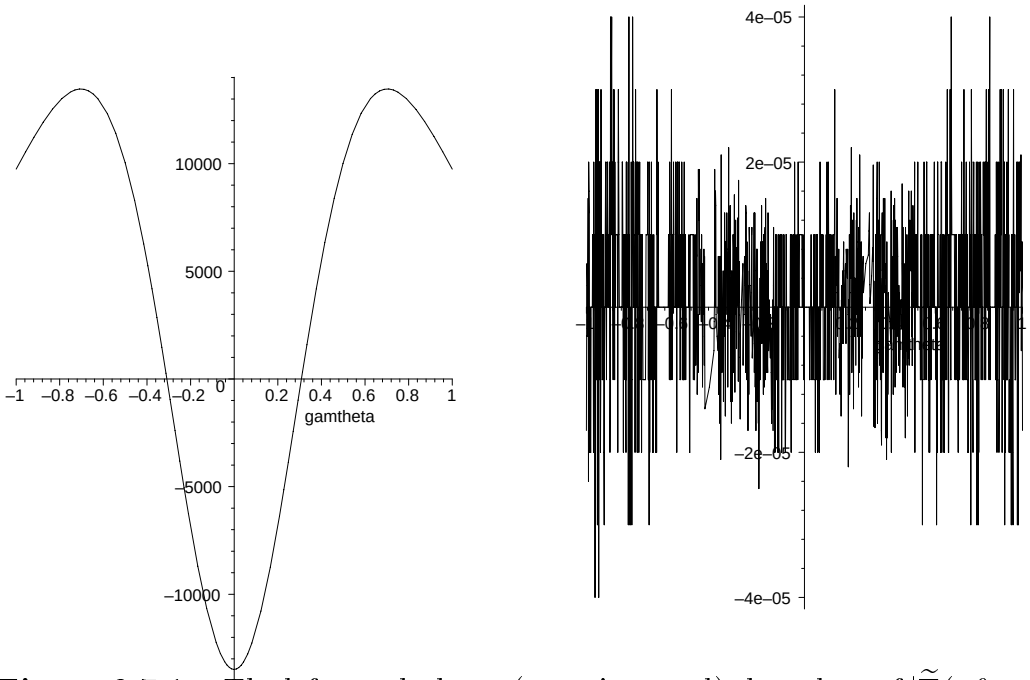

Figure 6.7.1: The left graph shows (superimposed) the values of $|\widetilde{\mathbf{E}}(\gamma\theta, \gamma\psi = 0.3, n = 3)|^2$ as given by integral (6.4.19) evaluated numerically and by using the method of section 6.7; $i_{\max} = 14$

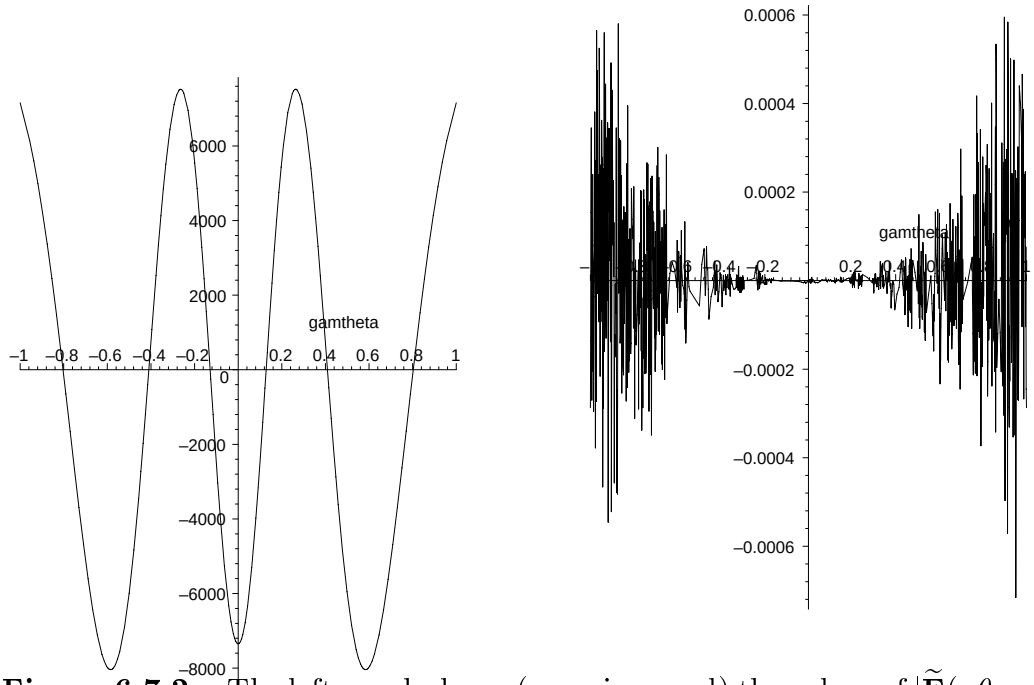

Figure 6.7.2: The left graph shows (superimposed) the values of $|\widetilde{\mathbf{E}}(\gamma\theta, \gamma\psi = -0.2, n = 7)|^2$ as given by integral (6.4.19) evaluated numerically and by using the method of section 6.7; $i_{\max} = 14$

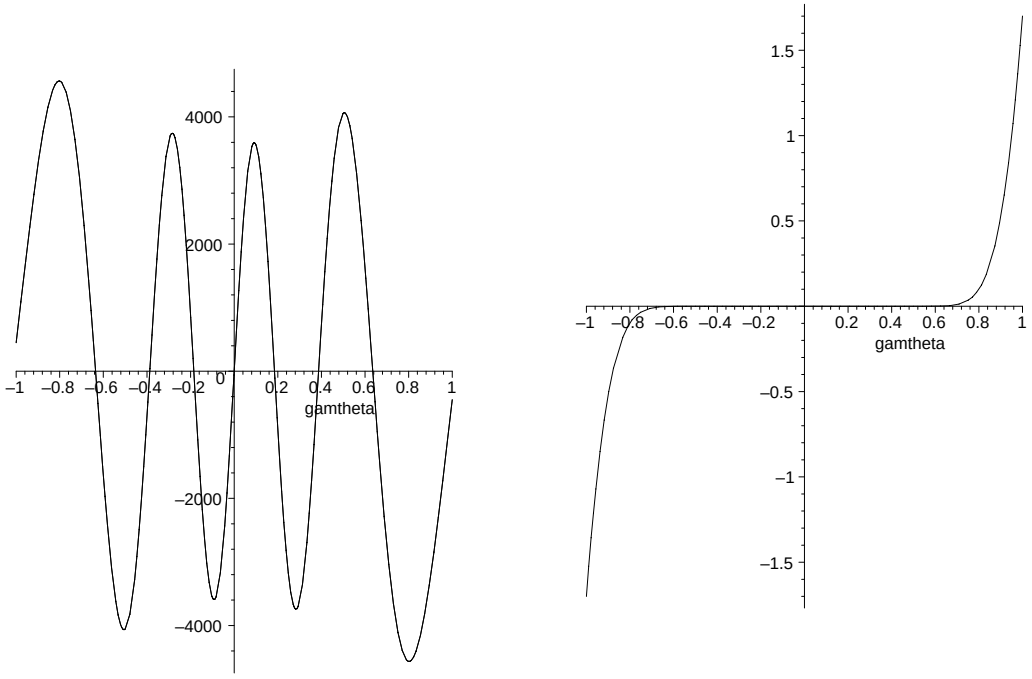

Figure 6.7.3: The left graph shows (superimposed) the values of $|\widetilde{\mathbf{E}}(\gamma\theta, \gamma\psi = 0.2, n = 10)|^2$ as given by integral (6.4.19) evaluated numerically and by using the method of section 6.7; $i_{\max} = 14$.

The fractional accuracy is excellent over the full range $-1/\gamma < \theta < 1/\gamma$ which includes essentially all the radiation. To obtain excellent accuracy in the experimentally relevant region of the central peak it is sufficient to use only the terms exhibited explicitly in Eq. (6.6.4).

Since θ, but not ψ, has been assumed small in deriving Eq. (6.6.4), its region of validity should be a narrow band centered on the ψ-axis. From Fig. 6.5.1 and Fig. 6.5.2 one knows that the radiation pattern is made up of parallel valleys separated by long mountains that are aligned with the ψ-axis. Since the variation with θ (at fixed ψ) is roughly sinusoidal (squared) one cannot expect a power series truncated to the terms shown explicitly in Eq. (6.6.4) to remain accurate outside the central three mountains. Nevertheless this truncated (and hence quite simple) form should be useful in practice because it it is the central mountain that is mainly used in most applications of undulator radiation.

6.8. Post-Monochrometer Profile

The beam from the undulator is typically passed through a monochrometer which passes only frequencies in a narrow band centered at, say,

$$\omega_{\text{mono.}} = n_{\text{mono.}}\,\omega_1\,(0)\,, \tag{6.8.1}$$

where $n_{\text{mono.}}$ is set to an integer or, typically, slightly below an integer. (For the example to be worked out shortly $n_{\text{mono.}} = 7.0$.) Substituting this into Eq. (6.6.2) yields

$$\eta\,(\vartheta) = n_{\text{mono.}}\,\frac{1 + K^2/2 + \gamma^2\vartheta^2}{1 + K^2/2} \tag{6.8.2}$$

as the appropriate parameter at which integral (6.6.4) is to be evaluated.† For large N_w we know that the phasor factor will suppress the field unless η is close to an integer; call it $n_{\text{harm.}}$ where

$$n_{\text{mono.}} \le n_{\text{harm.}} \le n_{\text{max.}}, \tag{6.8.3}$$

where $n_{\text{max.}}$ is the highest undulator harmonic that is kinematically possible or some arbitrarily chosen maximum value of interest. The analysis would be simplest for $n_{\text{mono.}} = n_{\text{max.}}$ but, in practice, it may be desirable to center the monochrometer on an undulator resonance lower than the maximum possible. (For the example to be worked out shortly $n_{\text{max.}} = 10$.) When this is done the harmonics for which $n_{\text{harm.}} > n_{\text{mono.}}$ yield circular ring profiles centered on the undulator axis, at angle $\vartheta_{\text{harm.}}$ given by solving Eq. (6.8.2) to obtain

$$\gamma\vartheta_{\text{harm.}} = \sqrt{\left(1 + \frac{K^2}{2}\right)\frac{n_{\text{harm.}} - n_{\text{mono.}}}{n_{\text{mono.}}}}\,. \tag{6.8.4}$$

The convergence of series (6.6.4) is worst for $n_{\text{harm.}} = n_{\text{max.}}$. To save computer time it is sensible to calculate only at points for which the phasor factor is not negligibly small. The larger N_w is, the slimmer are the rings in which there is any appreciable response. For example in generating Fig. 6.8.1 we have taken $\Delta n_{\text{harm.}} = \pm 1/N_w$ as the range over which the phasor factor is not negligible. This suppresses secondary diffraction rings having intensities in the several percent range.

† Note the surprising result that the argument of the Bessel-like functions entering the post-monochrometer profile, namely $\eta(\vartheta)\,q = n_{\text{mono.}}(K^2/4)/(1 + K^2/2)$, is independent of ϑ and hence of emission direction. This gives no important simplification because the indices depend on direction.

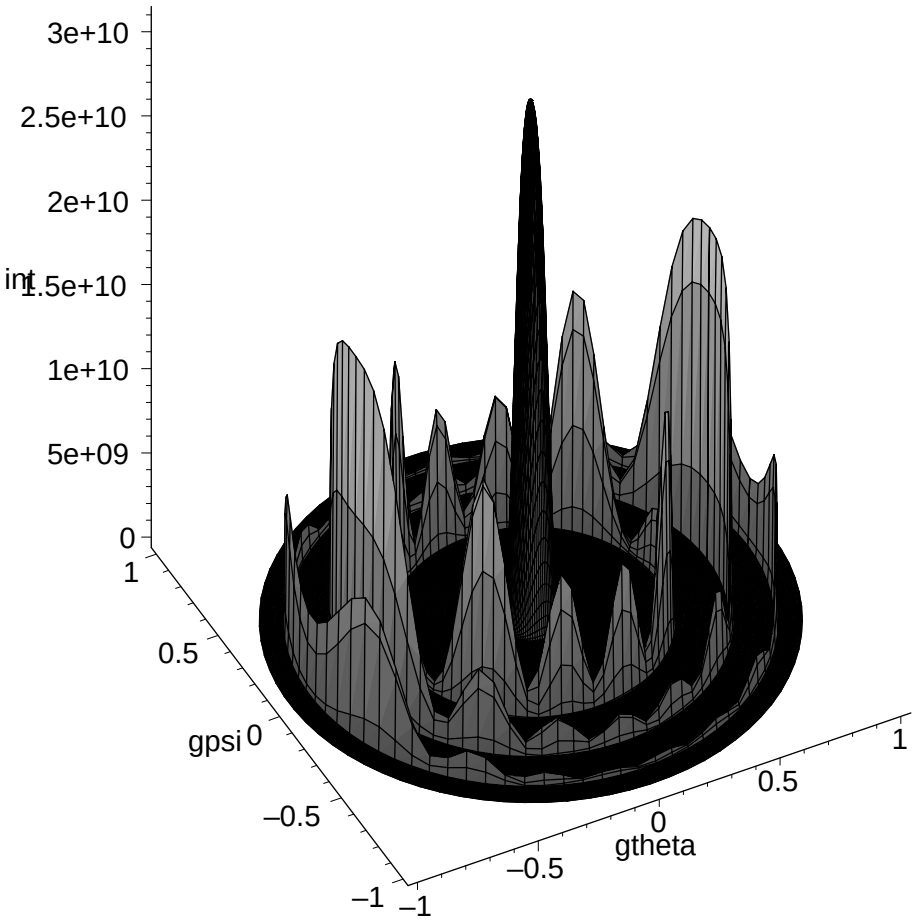

Figure 6.8.1: Spectrum for published ESRF configuration as recalculated using Eq. (6.6.4). Physical parameters were $E = 6\,\mathrm{GeV}$, $N_w = 20$, $\lambda_w = 46\,\mathrm{mm}$, $E_\gamma = 27\,\mathrm{keV}$. Calculational parameters are $N_w = 19$, $i_{\max} = 14$, $n_{\mathrm{mono.}} = 7$. This result can be directly compared with another calculation: www.esrf.fr/machine/support/ids/Public/CentralCone/CentralCone.html

6.9. Accelerator Physics Considerations

To complete the determination of intensity, brilliance, distribution functions and other parameters of the produced beam, it is necessary to address accelerator physics practicalities. For a start we assume the radiated power is small enough to make it legitimate to neglect degradation of the electron beam caused by the undulator deflections.

It is implicitly assumed in most discussions of synchrotron radiation (including this one) that the bend plane is horizontal and is designated as the x plane; the dominant field component is then E_x. (For the same reason) practical electron beams are usually ribbon-shaped, with transverse sigmas related by $\sigma_y << \sigma_x$. Because of this, it could turn out that vertical deflections would give superior performance for some purposes. I leave this as an open question, but continue to assume implicitly that the bend plane is horizontal.

6.9.1. Dependence of brilliance on electron beam emittance

For any one electron, it has been argued that the spectrum is rather insensitive to the particle's slope. In this sense the accelerator optics at the undulator is unimportant. It is true however, that the spike visible in Fig. 6.2.8 is as sharp as it is because a restricted range of angle ϑ has been assumed. Commonly, as mentioned earlier, one will wish to limit energy spread by exploiting the correlation between production angle and wavelength by limiting ϑ. For this to be effective the collimation has to take place at a distant location, where the transverse position is dominated by production angle rather than production position. A collimator at such a distant location will limit the ϑ range. Such an aperture will only be efficient if the spread of electron angles is not greater than the angular acceptance, which is about $\sqrt{\Delta\nu_{J,N_w}}/\gamma$. It may therefore be advantageous to reduce the electron cone angle $\sigma_{x'} = \sqrt{\epsilon_x/\beta_x}$, though doing this by increasing β_x will not increase the brilliance, because the spot size will be correspondingly increased.† If the reduced angular spread is obtained by reducing ϵ_x most of the improvement in angular acceptance will have been achieved when $\sigma_{x'} = \sqrt{\Delta\nu_{J,N_w}}/\gamma = 1/(\sqrt{N_w}\gamma)$. Accepting this as an equality, we obtain a "break point" below which the brilliance increases with decreasing emittance only because the

† Technically, for the r.m.s. angular spread of the electron beam, one should use $\sigma_{x'} = \sqrt{\epsilon_x\gamma_x}$ where $\gamma_x = (1+\alpha_x^2)/\beta_x$, but I will assume the undulator is at a "waist" where $\alpha_x = 0$.

spot size decreases;

$$\epsilon_{x,\mathrm{break}} = \frac{\beta_x}{N_w \gamma^2} = \frac{\beta_x}{(L_w/\lambda_w)\,\gamma^2} \qquad \left(\overset{\text{e.g.}}{=} 10^{-10}\,\text{m-rad.} \right) \tag{6.9.1}$$

for $N_w = 1000$, $\gamma = 10^4$, $\beta_x = 10\,\text{m}$.

In the $K << 1$ limit that has been discussed so far there is no essential distinction between horizontal and vertical displacements and angles, so the same estimates apply to $\sigma_{y'}$ and $\epsilon_{y,\mathrm{break}}$. Hence, for round beams, the brilliance varies inversely with electron emittance below the break point and inversely with the square of emittance above it.

For $\epsilon < \epsilon_{\mathrm{break}}$ the brilliance is given by formula (6.3.11), so a semi-empirical formula giving the brilliance through the full range of possible emittances is

$$\mathcal{B}_1 = \frac{3N_w\gamma^2}{\pi^2}\,\frac{P_1}{E_\gamma}\,\frac{1}{\sqrt{\beta_x\epsilon_x}\sqrt{\beta_y\epsilon_y}}\,\sqrt{\frac{1}{1+\epsilon_x/\epsilon_{x,\mathrm{break}}}}\,\sqrt{\frac{1}{1+\epsilon_y/\epsilon_{y,\mathrm{break}}}}\,. \tag{6.9.2}$$

As with all formulas so far, it is assumed that $K << 1$. It is always advantageous to reduce either or both of ϵ_x and ϵ_y, but below the break points the brilliance increases more slowly, proportional to $1/(\sqrt{\epsilon_x}\sqrt{\epsilon_y})$. This dependence is fairly weak, but it still justifies efforts to reduce ϵ_x unless this can only be accomplished by reducing the current in the electron beam. Reasons why such reduction is likely include the Touschek effect in circular machines or gun limitations in linear machines.

One "sanity check" that can be applied to the numerical value of $\epsilon_{x,\mathrm{break}}$ given in Eq. (6.9.1) is to test whether the value $\beta_x = 10\,\text{m}$ is appropriate. Unless one goes to special lengths such as breaking the undulator into sections to make room for focusing elements, storage ring stability will lead to a relation $\beta_x \approx L_w$ and, very roughly,

$$\epsilon_{x,\mathrm{break}} \approx \frac{\lambda_w}{\gamma^2} \qquad \left(\overset{\text{e.g.}}{=} 2\times 10^{-10}\,\text{m-rad,} \right) \tag{6.9.3}$$

which is consistent with Eq. (6.9.1) to the accuracy of the arguments. Note, however, that Eq. (6.9.3), unlike (6.9.1) is independent of β_x. This is relevant because, if it should prove possible to reduce ϵ_x arbitrarily, then Eq. (6.9.1) can be satisfied by reducing β_x proportionally. This would reduce the spot size, and hence increase the brilliance. But Eq. (6.9.3) shows that the practicalities of lattice design make this route less promising than might initially have been anticipated.

For the so-called "third generation light sources" such as ESRF and APS, vertical emittances as small as the emittance just calculated ($\epsilon_y \approx 10^{-10}$ m-rad at $\gamma = 10^4$) are actually achievable, but the minimum horizontal emittance is perhaps ten times greater. On the other hand, since typical wiggler lengths are not much greater than two meters and typical λ_w's greater than 2 cm, $N_w \approx 100$ is typical, in which case, according to Eq. (6.9.1), there is reduced benefit in reducing emittances below $\epsilon_{x,y} \approx 10^{-9}$ m-rad. One way of advancing "beyond third generation" is therefore to design electron accelerators that allow the insertion of undulators that are tens of meters in length.

Once a storage ring has been built one has little control over the emittances and one looks differently at Eq. (6.9.1), perhaps rearranging it into the form

$$\beta_x \gtrsim N_w \gamma^2 \epsilon_x \ . \tag{6.9.4}$$

When the radiation from the arcs of an accelerator that was designed for colliding beam physics is used parasitically, the ring is sometimes said to be a "first generation light source". After the installation of dedicated wigglers or undulators such a machine is promoted to the status of "second generation". As an example, consider CESR, for which $\gamma = 10^4$, $\epsilon_x = 2 \times 10^{-7}$ m-rad). Comparing Eq. (6.9.3), the emittance is above the break point by three orders of magnitude, which converts to a brilliance defect of six orders of magnitude. Viewed alternatively, with N_w equal to, say, 100, substitution into Eq. (6.9.4) yields $\beta_x \approx 2000$ m which, being some 200 times greater than typical values of β_x in the ring, is impractically large.

6.9.2. Dependence of Beam Brilliance on K

The flux of electrons in a beam with current I is I/e. Using Eq. (6.2.17), which gives the total energy emitted by a single electron from the $2N_w$ undulator poles, the total power radiated into the n-th harmonic is

$$P_n = f_n(K) \, \frac{I}{e} \, \frac{2}{\pi^{1/2}} \, \frac{C_\gamma E_e^4}{\lambda_w} \left(\frac{K}{\gamma} \right)^2 \, 2N_w \ , \tag{6.9.5}$$

where $f_n(K)$ is the fraction of the power radiated into the n-th harmonic. ($f_1(0) = 1$.) $f_1(K)$, crudely extracted from data in the Wiedemann paper mentioned above, is plotted in Fig. 6.9.1.

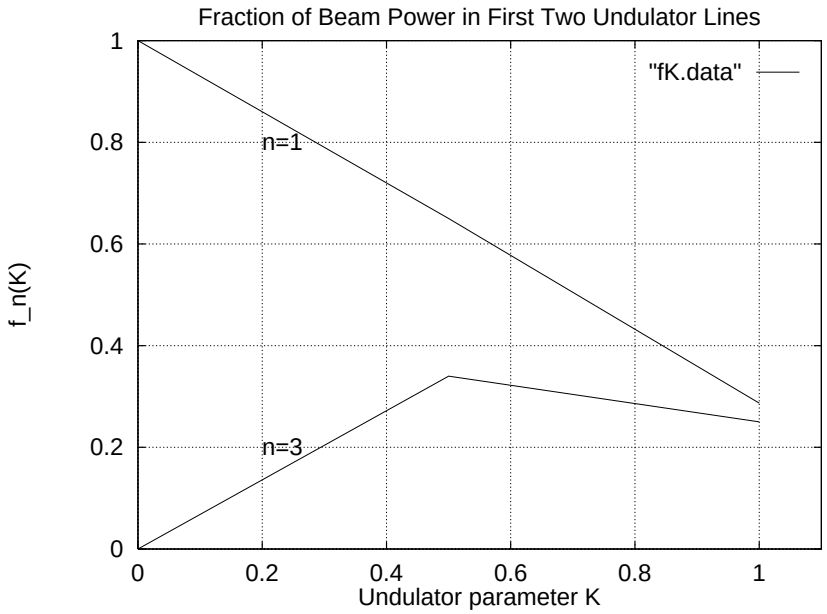

Figure 6.9.1: Plot of $f_1(K)$ and $F_3(K)$, the fraction of power radiated into the first two undulator lines, as a function of undulator parameter. Crudely extracted from figure 3 of the Wiedemann artucle in the Chao-Tigner handbook. ($f_1(K)$ has a different meaning in that article, and it is possible I am misinterpreting the data.)

Combining Eq. (6.9.5) with Eq. (6.9.2), the X-ray beam brilliance (in the $K << 1$ limit) is given by

$$\mathcal{B}_1(0) = f_1(0)\,\frac{I}{e}\,\frac{12}{\pi^{5/2}}\,\frac{C_\gamma E_e^3}{\lambda_w}\,K^2\,N_w^2\,\frac{E_e}{E_\gamma}\,\frac{1/\sqrt{\beta_x\epsilon_x}}{\sqrt{1+\epsilon_x/\epsilon_{x,\mathrm{break}}}}\,\frac{1/\sqrt{\beta_y\epsilon_y}}{\sqrt{1+\epsilon_y/\epsilon_{y,\mathrm{break}}}}\,. \qquad (6.9.6)$$

By increasing the K value from, say, $K = 0.1$ to, say, $K = 1$ this formula indicates that the brilliance will increase by two orders of magnitude. But there are at least four factors that make the brilliance depend on K less rapidly than this.

- From Fig. 6.9.1, one sees that the fraction of power in the fundamental line falls by a factor of 3 as K increases from 0.1 to 1.0.
- Because of the finite bend angle in the undulator, the "searchlight" beam from the electron is not always directed at the center of the X-ray collimator. Again one can define a "break point" K_{break} which separates the low K region in which the electron direction is within the collimator angle (so the flux and brilliance acquire the K^2 factor), from a high K region where only a fraction of the radiation swath passes through the collimator (so the flux and brilliance

acquire only a factor K). When the electron angle is maximum, its radiation is negligible, because it is at the position where the undulator field vanishes. In fact the radiation is dominated by an arc in which the intensity is more or less uniform but the angle varies from about $-\Theta/3$ to $\Theta/3$. The break point is therefore given roughly by

$$\frac{K_{\text{break}}}{\gamma} = 3\vartheta_{\text{nom.}} = 3\frac{\sqrt{0.001}}{\gamma} \ , \tag{6.9.7}$$

which is to say $K_{\text{break}} \approx 0.1$. According to this, the brilliance acquires a factor of about 10 (from this source) as K increases from 0.1 to 1.0. Because the electron excursion is horizontal, it makes sense for the collimator to be elliptical, say broader than than it is high by a factor of 10. In this case the flux could acquire the full $K^2 f_1(K)$ enhancement as K increases from 0.1 to 1.0 but, because the solid angle factor has been increased, the brilliance would be unchanged.

- In the increase from $K = 0.1$ to $K = 1$, according to Eq. (6.2.33), the factor $1 + K^2/2$ increases by 45%, and the peak X-ray energy shifts therefore from 12.4 keV to 8.7 keV. If we assume that E_e cannot be increased (because the storage ring is a its maximum energy) and λ_w cannot be changed (because the undulator has been built) it is difficult to assign a numerical penalty factor, or cost, to this energy reduction. Perhaps one would work on the $n = 3$ resonance line, and revise all the parameters accordingly. This may not be such a bad deal, because of the threefold relative energy narrowing of the line, even if the fraction of the beam power going into the $n = 3$ is low (about 1/4 according to Fig. 6.9.1) but I will not estimate the effect on the brilliance of the other factors.
- As explained previously, the angular beam width is proportional to $\sqrt{1 + K^2/2}$, so the collimation solid angle may have to be increased by 45% as K is increased from 0.1 to 1.0, with a corresponding loss of brilliance.

Ones assessment of the importance of these factors is subjective, and dependent on the details of actual detection apparatus. If increasing the aperture width by a factor of 10 is acceptable for the detection apparatus, increasing K from 0.1 to 1.0 yields a factor of at

least 10 in flux at constant brilliance, which seems attractive. But if the X-ray aperture has to be held fixed, both flux and brilliance (from the $n = 1$ line) increase only moderately as K is increased beyond about 0.1. Working on the $n = 3$ line with, say, $K = 1$ may be a favorable configuration, though. If it is important to keep the total X-ray beam power low, running on the lowest possible harmonic is favored.

Ignoring all but the first two of the factors listed above, and substituting from Eq. (6.9.1), the brilliance in the fundamental line is given by

$$\begin{aligned}&\mathcal{B}_1(K) \approx \\ &f_1(K)\,\frac{I}{e}\,\frac{12}{\pi^{5/2}}\,\frac{C_\gamma E_e^3}{\lambda_w}\,\frac{K^2}{1+K/0.1}\,N_w^2\,\frac{E_e}{E_\gamma}\,\frac{1/\sqrt{\beta_x\epsilon_x}}{\sqrt{1+N_w\gamma^2\epsilon_x/\beta_x}}\,\frac{1/\sqrt{\beta_y\epsilon_y}}{\sqrt{1+N_w\gamma^2\epsilon_y/\beta_y}}\,.\end{aligned} \tag{6.9.8}$$

(All quantities except those within the dimensionless ratio $C_\gamma E_e^3/\lambda_w$ are in MKS units.) In practice ϵ_y is likely to be below the break, and ϵ_x above the break. Should this be true, we get

$$\mathcal{B}_1(K) \approx \frac{I}{e}\,\frac{12}{\pi^{5/2}}\,\frac{C_\gamma E_e^3}{\lambda_w}\,\frac{K^2 f_1(K)}{1+K/0.1}\,N_w^{3/2}\,\frac{E_e}{E_\gamma}\,\frac{1}{\gamma\epsilon_x}\,\frac{1}{\sqrt{\beta_y\epsilon_y}}\,. \tag{6.9.9}$$

In the regime where this formula holds, there is strong incentive for reducing ϵ_x and (weaker) incentive for reducing ϵ_y and/or β_y.

The formula for flux is more complicated, especially because it depends strongly on the shape of the collimator, which will optimally be wider than it is high. But since the brilliance is reasonably insensitive to aperture shape, Eq. (6.9.8) may continue to be approximately valid for asymmetric apertures.

Even though some of the assumptions that have gone into Eq. (6.9.9) are probably already irresponsible, in the interest of further simplification, let us assume (as we did for β_x in deriving Eq. (6.9.3)) that $\beta_y = L_w = N_w\lambda_w$. Also, let us express emittances relative to the value 2×10^{-10} m-rad which is, on the one hand, probably achievable and, on the other hand, close to the break point that has been used in approximating the

emittance-dependent factors:

$$\begin{aligned}\mathcal{B}_1(K) &\approx \frac{I}{e}\frac{12}{\pi^{5/2}}\frac{C_\gamma E_e^3}{\lambda_w}\frac{K^2 f_1(K)}{1+K/0.1}N_w\frac{E_e}{E_\gamma}\frac{1}{\gamma}\left(\frac{2\times10^{-10}}{\epsilon_x}\right)\frac{1}{\sqrt{\lambda_w}}\sqrt{\frac{2\times10^{-10}}{\epsilon_y}}\frac{10^{15}}{2^{3/2}} \\ &\approx 0.62\times10^{19}\times0.686\times0.587\times0.411\times10^{6}\times10^{-4}\times7.07\times0.353\times10^{15} \\ &\times I\frac{K^2 f_1(K)}{1+K/0.1}N_w\left(\frac{2\times10^{-10}}{\epsilon_x}\right)\sqrt{\frac{2\times10^{-10}}{\epsilon_y}} \\ &\approx 2.56\times10^{23}\, I\frac{K^2 f_1(K)}{1+K/0.1}N_w\left(\frac{2\times10^{-10}}{\epsilon_x}\right)\sqrt{\frac{2\times10^{-10}}{\epsilon_y}}\,\mathrm{mm}^{-2}\mathrm{mr}^{-2}/0.1\%\mathrm{BW};\end{aligned} \tag{6.9.10}$$

a factor 10^{-12} entered in the last step to convert the brilliance into the conventional $\mathrm{mm}^{-2}\mathrm{mr}^{-2}$ unit. (This expression is not fully consistent with the assumptions made previously concerning the emittances, but it is approximately consistent when the ϵ_x factor is less than 1, and the ϵ_y factor is greater than 1.)

Curiously enough, after having included assumptions that supposedly follow from unassailable accelerator requirements, the brilliance depends only linearly on N_w. (This is probably because long undulators cause large beta functions which lead to large spot sizes.) This appears to weaken the case for going to Herculean lengths to increase N_w—for example, to obtain $N_w = 1000$ at $\lambda_w = 2\,\mathrm{cm}$ requires $L_w = 20\,\mathrm{m}$, and yields brilliance only five times greater than a 4 m undulator.

Specializing further, when parameters that have been suggested for the Cornell Energy Recovery Linac (I=0.1 A, K=1, E_γ=12.4 keV) are substituted, the anticipated brilliance is

$$\mathcal{B}_1 \approx 0.67\times10^{21}\,N_w\left(\frac{2\times10^{-10}}{\epsilon_x}\right)\sqrt{\frac{2\times10^{-10}}{\epsilon_y}}\,\mathrm{mm}^{-2}\mathrm{mr}^{-2}/0.1\%\mathrm{BW}\ . \tag{6.9.11}$$

This brilliance is somewhat higher than values obtained by Bilderback and Finkelstein using available computer programs, but too-optimistic assumptions have perhaps been made, not to mention likely blunders, since the results have not been checked.

6.9.3. Is the Forward Peak Subject to Line Narrowing?

The $2N_w$ undulator pulses resemble the emission from a linear, phased array, transmitting antenna. Even though the individual elements in such an array radiate more or less isotropically, when they are phased correctly, a narrow beam parallel to the array can be produced. To produce such a beam with free-space wavelength λ, because the wavefronts propagate at the speed of light, successive radiators should be phase shifted by (an odd multiple of) $\pi\lambda_w/\lambda$ to give constructive interference in the direction parallel to the array. (We continue to use alternating sign radiators spaced at $\lambda_w/2$.) The angular width of the radiation pattern can be defined to be the angle of the first interference minimum. For emission at (small) angle ϑ there is a phase shift $N_w\lambda_w\theta^2\pi/\lambda$ between radiation from first and last radiators. The condition for the vanishing of the amplitude from all $2N_w$ radiators is that this phase shift be 2π. That is

$$\theta_{\min} = \sqrt{\frac{1}{N_w}}\sqrt{\frac{\lambda}{\lambda_w}} = \frac{1}{\gamma}\frac{1}{\sqrt{2N_w}} \ , \tag{6.9.12}$$

where, in the last step, the relation $\lambda = \lambda_w/(2\gamma^2)$ has been used. This is indeed a small angle; for large N_w, it is much smaller than the cone angle $1/\gamma$ characterizing radiation from a single radiator.

The argument in the previous paragraph is fallacious however, since it assumed the radiation to be monochromatic, with wavelength independent of angle. In fact there is a large spread of wavelengths. At any angle the interference of all contributions at angle ϑ has already been accounted for in Eqs. (6.2.32) and Eq. (6.2.41). With Jackson, I therefore expect no fringes. This is certainly not intended to belittle the value of undulators in general. The narrowing proportional to $1/N_w$ of the frequency spectrum at fixed angle, say in the forward direction, is both uncontroversial and invaluable. Under ideal conditions it results in brilliance increasing as N_w^2.

Before leaving the question of whether fringes exist one can contemplate how such fringes might emerge from Jackson's, work-it-out-in-the-electron's-rest-system approach. For a start, one can question an assumption that is built into the Jackson picture, in spite of its being manifestly incorrect. I refer to the assumption that the electrons execute pure simple harmonic motion in their own rest frame when, in fact, they exhibit this motion only during the "time window" during which the wiggler is flying by. The width in time

of this window is $\Delta T'_w = N_w L_w/(\gamma c)$. The dipole radiation due to this oscillation will therefore be gated on for a time interval of length $\Delta T'_w$. At any angle the fields will be the product of a pure sinusoid and a square pulse. The frequency domain spectrum will therefore be the convolution of a single line (from the sinuisoid) and a $(\sin\omega)/\omega$ spectrum (from the square pulse). Qualitatively, the rest system frequency will be spread over a range $\Delta\omega'_w \approx 1/\Delta T'_w$.†

In the absence of the spread just described, the rest system dipole radiation is monochromatic; it is only after transformation back into the laboratory system that energy variation results and, even then, there is a one-to-one relation between frequency and angle. (This is because the laboratory system angle increases monotonically with increasing rest system angle.) At fixed laboratory angle the radiation is therefore not only monochromatic, but has unique phase. The presence of frequency spread in the electron's rest system changes this. Because of the spread of frequencies in the rest system there is the possibility of more than one contribution to the radiation at fixed laboratory angle. For example, one visualizes two rest system photons having different rest system frequencies and angles, but the same lab system frequencies and angles, and which could therefore interfere constructively of destructively. Unfortunately this is impossible, since the angle transformation from rest system to laboratory is independent of frequency. Therefore the laboratory frequency spectrum is the same as the rest system frequency spectrum (except for the scale of the frequency axis.) Nothing in this picture seems to predict the existence of angular fringes in the forward radiation.

Yet one more point can be made. All analyses of undulator radiation seem to employ the Fraunhofer picture, in which the detector is "at infinity". This assumption can be validated either by the image distance being large relative to all relevant source dimensions or by the presence of a parallel-to-point focusing lens. For undulator sources neither of these possibilities is fully available. X-ray lenses don't exist and focusing mirrors are problematical. And, especially with long undulators, the ratio of detector distance to undulator length may not be very large. It seems fair to say, therefore, that X-ray detectors are "out of focus" for observing interference fringes. This is just one more way in which any supposed fringes would be washed out.

† By this point it should be clear this description is equivalent to that given previously in section 6.2.3.

6.10. Treatment of Magnetic Wiggler Radiation as Thomson Scattering

There is a well-known treatment of undulator radiation as Compton back-scattering of the "photons" that are "produced" in a wiggler magnet. Since the frequency of these photons is zero, yet their wavelength is λ_w, they do not satisfy the relation between energy and momentum of *real* photons, and they are said to be *virtual*.

For a horizontal-bending undulator aligned with the z-axis, the only non-vanishing electric or magnetic field component is $B_y = B_0 \cos(k_w z)$. With electrons propagating at velocity $-v$ along the positive z-axis, it is useful to transform the wiggler field into the rest frame of the electron. The result is

$$\mathbf{E}' = -\gamma\, v\, B_y \cos\left(k_w \gamma \left(z' + v t'\right)\right) \hat{\mathbf{x}}, \quad \text{and} \quad \mathbf{B}' = -\frac{\mathbf{v}}{v^2} \times \mathbf{E}' \ . \tag{6.10.1}$$

This is very nearly the relation between $\mathbf{E}'$ and $\mathbf{B}'$ belonging to a plane-polarized plane wave, propagating in free space. In fact, in the limit $v \to c$ the correspondance becomes exact. Making the replacement $v = c$ yields what is known as the Weizsäcker-Williams approximation.

The wave just derived is said to be made up of "virtual" photons, and these photons can Compton scatter off the electrons. The (magnitude of) the rest energy of one of these virtual photons (calculated most easily in the laboratory frame, since the frequency vanishes there) is given by

$$|m_\gamma c^2| = \left| \sqrt{(\hbar\omega)^2 - (\hbar k_w)^2 c^2} \right| = \hbar k_w c \ . \tag{6.10.2}$$

Next consider the situation in the rest frame of the electrons. In this frame the photon energy is $E'_\gamma = \hbar k_w \gamma v$, since $k_w \gamma v$ is the (frequency) factor multiplying t' in the argument of the cosine factor in Eq. (6.10.1). If this energy is small compared to the electron rest energy,

$$E'_\gamma = \hbar k_w \gamma v << m c^2 \ , \tag{6.10.3}$$

(as will always be true for cases of interest to us) the incident and scattered photon energies are the same. It will be valid to neglect the virtual photon mass (calculated in Eq. (6.10.2)) if it is small compared to this energy;

$$\hbar k_w c \ \overset{?}{<<} \ \hbar k_w \gamma v \ , \tag{6.10.4}$$

which reduces to $\gamma >> 1$, and will be abundantly true in practice.

Condition (6.10.3) is also the condition for the validity of treating Compton scattering as Thomson scattering, for which the total cross section is

$$\sigma = \frac{8\pi}{3} r_e^2 = 0.665 \times 10^{-28}\,\mathrm{m}^2 \ . \tag{6.10.5}$$

where $r_e = 2.81784 \times 10^{-15}\,\mathrm{m}$. (See Eq. (2.21).) Though this cross section was calculated in the electron rest frame, the lab frame value is the same.

To calculate the radiation pattern in the laboratory it is necessary to write the angular distribution in the rest system of the electron, and then to transform it into the laboratory system. Though the scattered photons are mono-energetic in the electron rest system, this will no longer be true in the laboratory system. We can write down the maximum lab energy, since it corresponds to pure back-scattering. The result of Lorentz transforming the photon four-vector, $(\hbar\gamma k_w vc, 0, 0, \hbar\gamma k_w v/c)$, back to the lab frame, is a photon of energy

$$E_{\gamma,0} = \left(1 + \frac{v}{c}\right) \gamma^2\, \hbar k_w v \approx 2\gamma^2 \hbar k_w c \ . \tag{6.10.6}$$

Since $v \approx c$, the back-scattered wave length is less than the wiggler period λ_w by the factor $2\gamma^2$. This agrees with the undulator peak calculated using classical electrodynamics.

The energy and momentum components of the radiated photon in the electron rest system (primed coordinates) and laboratory system (unprimed coordinates) are related by the Lorentz transformation equations:

$$\begin{aligned} E'_\gamma \sin\vartheta' &= E_\gamma \sin\vartheta \\ E'_\gamma \cos\vartheta' &= \left(\cos\vartheta - \frac{v}{c}\right)\, \gamma E_\gamma \\ E'_\gamma &= \left(1 - \frac{v}{c}\cos\vartheta\right)\, \gamma E_\gamma \end{aligned} \tag{6.10.7}$$

Since E'_γ is independent of ϑ', the last of these equations yields E_γ as a function of ϑ;

$$E_\gamma\,(\vartheta) = \frac{E'_\gamma/\gamma}{1 - \frac{v}{c}\cos\vartheta} \approx \frac{E'_\gamma/\gamma}{1 - \left(1 - \frac{1}{2\gamma^2}\right)\left(1 - \frac{\vartheta^2}{2}\right)} \approx \frac{E_{\gamma,0}}{1 + \gamma^2\vartheta^2} \ . \tag{6.10.8}$$

This dependence of energy on angle is identical to that given in Eq. (6.2.35). This corroborates the equivalence of undulator radiation and Compton scattered radiation.

The discussion to this point has implicitly assumed $K << 1$. The main effect of finite K is described by Eq. (6.2.31) which gives the average electron velocity to be

$$\frac{\overline{v_z}}{c} \approx 1 - \frac{1}{2\gamma^2}\left(1 + \frac{K^2}{2}\right) \quad , \quad \overline{\gamma} \approx \frac{\gamma}{\sqrt{1 + K^2/2}} \ . \tag{6.10.9}$$

After this alteration, Eq. (6.10.8) becomes

$$E_\gamma(\vartheta) = \frac{E'_\gamma/\overline{\gamma}}{1-\left(1-\frac{1}{2\overline{\gamma}^2}\right)\left(1-\frac{\vartheta^2}{2}\right)} \approx \frac{2\gamma^2\left(\hbar c/\lambda_w\right)}{1+K^2/2+\gamma^2\vartheta^2} \ . \tag{6.10.10}$$

(Note that this formula agrees with Eq. (6.2.33).) This formula shows that increasing K causes a reduction in peak energy by factor $1+K^2/2$, and an increase in angular width by factor $\sqrt{1+K^2/2}$. However these effects have been calculated in the context of single photon interactions and relate only to the fundamental undulator peak. As K is increased higher harmonics become progressively more important and these can only be understood quantum mechanically as the coherent scattering of more than one photon.

Chapter 7.
Undulator Magnet Design

7.1. Introduction

For a given storage ring, with vacuum chamber height $2g$ required (by storage ring practicalities) to exceed a value of order one centimeter, there is a practical upper limit to the energy E_γ of x-rays that can be produced coherently and with large flux from the multiple poles of a symmetric undulator. This maximum energy is proportional to the square E_e^2 of the beam energy. For $E_e = 2.9\,\mathrm{GeV}$ the maximum energy is something like $15\,\mathrm{keV}$. The purpose of this report is to show that this upper limit can be increased substantially by using an asymmetric (defined below) undulator, and to suggest an electromagnet, permanent magnet, hybrid design for such an undulator.

The idea, illustrated in Fig. 7.1.1, is to produce very strong magnetic fields over very short intervals (spaced by somewhat larger intervals) in order to increase the "critical energy" without causing excessive beam deflection. Such strong magnetic fields require an electromagnet, but the weaker but longer, opposite sign fields (needed to cancel the overall field integral) can be produced by permanent magnet material.

From a symmetric undulator, because of the cancellation of adjacent pole amplitudes, only odd undulator harmonics contribute flux in the forward direction. For the asymmetric undulator this cancellation is largely suppressed, so the fluxes from even and odd harmonics will be comparable.

Analytic design formulas for both electromagnet and permanent magnet sections will be given and it is argued that the fields should approximately superimpose. But the interaction of electromagnet and permanent magnets is subtle so (obviously) a numerical study with both fields present simulataneously will be required.

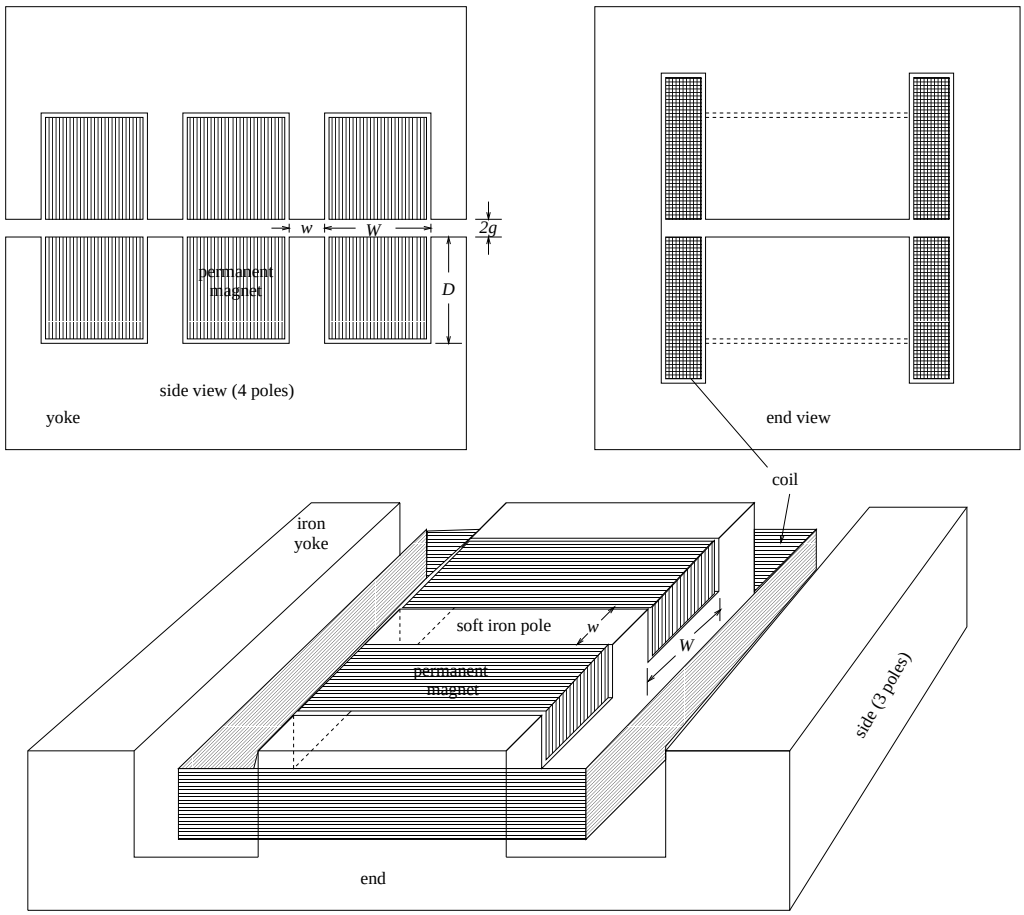

Figure 7.1.1: Schematic illustration of coil, yoke, and permanent magnetic material in a hybrid, electro-/permanent-magnet, asymmetric undulator. The mechanism to vary the gap height $2g$ is not shown; it will represent quite a design challenge.

7.2. Radiation Formulas

The main purpose of a storage ring "light source" is to produce x-rays. The so-called "critical photon energy" u_c for electon energy E_e in magnetic field B is given by

$$u_c = \frac{3}{4\pi}\, hc\, \gamma^3\, \frac{cB}{\gamma m_e c^2/e} = B\,[T]\, \left(\frac{E_e\,[\mathrm{GeV}]}{2.9\,[\mathrm{GeV}]}\right)^2\, 5.59\,\mathrm{keV}. \tag{7.2.1}$$

Roughly half of the radiated energy comes in the form of photons of energy exceeding u_c. For energies greater than u_c, the probability distribution (independent variable u/u_c) of photon energies is given approximately by

$$\frac{dP}{d\,(u/u_c)} \approx 0.24\, \frac{\exp\,(-u/u_c)}{\sqrt{u/u_c}}. \tag{7.2.2}$$

This factor has fallen by a factor of 35 for $u = 3u_c$, which makes $3u_c$ a kind of upper limit for what will be called "ideal operation". From an undulator Eq. (7.2.2) will provide the "envelope" of a "comb" of undulator resonances. In gross terms therefore (neglecting the comb structure), Eq. (7.2.2) will describe the photon energy distribution, independent of whether the radiation comes from bending magnet, wiggler or undulator. The total energy radiated per electron per unit length, dU/dz, also depends only on the local magnetic field, not the entire insertion device;

$$\frac{dU}{dz} = \frac{e^2}{6\pi\epsilon_0}\gamma^4 \left(\frac{cB}{\gamma m_e c^2/e}\right)^2 = B^2\,[T^2] \left(\frac{E_e\,[\mathrm{GeV}]}{2.9\,[\mathrm{GeV}]}\right)^2 10.6\,\mathrm{keV/m}. \tag{7.2.3}$$

From an undulator essentially all this energy potentially impinges on the physics apparatus. From a bending magnet or wiggler the energy is spread in a broad fan, most of which must be removed by collimation.

For $B = 1\,\mathrm{T}$, $E_e = 2.9\,\mathrm{GeV}$ the critical photon energy (5.59 keV) is, roughly speaking, at the dividing line above which x-rays are sufficiently energetic to pass through a vacuum window without unacceptable attenuation. For present purposes let us refer to photons with energies above 5 keV as "high energy x-rays". From Eqs. (7.2.1) and (7.2.2), if we require appreciable flux of high energy x-rays from a beam with energy E_e as low as 2.9 GeV it will be necessary to have magnetic fields of order 1 T or, preferably, greater. Such magnetic fields are at the high end, or beyond, of what is achievable with permanent magnet material. This requires the use of electromagnets, for which B can be as high as 2 T or superconducting magnets, which can have even higher fields.

Another important consideration is the extent to which "undulator" performance, in which the amplitudes from multiple poles sum coherently, can be achieved. In this regime essentially all the radiation is directed toward the physical apparatus using it (rather than in a broad spray) and, as well as the enhancement factor equal to the number of poles, there is strong forward peaking of the x-ray energies passed by a monochrometer. These features make the undulator beam "clean". An important parameter characterizing this behavior is $E^{(0)}_{1,\mathrm{edge}}$ the "edge energy" of the fundamental undulator resonance, for ideal, $K << 1$ undulator operation;

$$E^{(0)}_{1,\mathrm{edge}} = hc\,\frac{\gamma^2}{\lambda_w/2} = \left(\frac{E_e\,[\mathrm{GeV}]}{2.9\,[\mathrm{GeV}]}\right)^2 \left(\frac{1\,\mathrm{cm}}{\lambda_w/2\,[\mathrm{cm}]}\right) 3.99\,\mathrm{keV}; \tag{7.2.4}$$

(the factor 1/2 has been left explicitly in the factor $\lambda_w/2$ for later convenience in analysing an asymmetric undulator.) This edge energy is independent of B. So, surprisingly, the range of energies radiated coherently is independent of B (in the limit of "pure undulator operation" $K << 1$.) This is somewhat academic however, as one essentially never runs in the limit of pure undulator operation. In fact, satisfactory undulator operation can be achieved up to $K = 2$ or somewhat higher, and say, $n = 10$ (actually 9 or 11) where n labels the undulator harmonic. There is appreciable intensity into the higher harmonics only for $K \approx 1$ or greater. The edge energies of general harmonics are given by

$$E_{n,\text{edge}} = \frac{n}{1 + K^2/2} \left(\frac{E_e\,[\text{GeV}]}{2.9\,[\text{GeV}]} \right)^2 \left(\frac{1\,\text{cm}}{\lambda_w/2\,[\text{cm}]} \right) 3.99\text{keV}. \tag{7.2.5}$$

Since the undulator parameter K is proportional to B, the denominator factor $1 + K^2/2$ causes "diminishing returns" to set in as one attempts to increase the x-ray energies by increasing B. This sets a practical upper limit on K of order 2 or slightly higher if "clean beam" undulator performance is to be achieved.

For a fixed value of E_e, these consideration and the practicalities of magnet construction, set an upper x-ray energy limit for "clean" operation. It is necessary to reduce λ_w to the extent possible, but it is impractical for $\lambda_w/2$ to be less than the magnet gap height $2g$ which cannot be less than, say, 6 mm, without impairing storage ring operation. Also it is difficult to achieve small values of $\lambda_w/2$ using powered magnets requiring current-carrying coils around every pole. For the value $E_e = 2.9\,\text{GeV}$ featured in the formulas given so far, one needs values $\lambda_w < 2\,\text{cm}$, $B > 1\,\text{T}$ to obtain undulator operation in the range from 5 keV (easy) to 20 keV (hard); the most promising range of energies for "Physics Discovery". (A personal opinion.) Increasing E_e from 2.9 GeV would, of course, pay off handsomely in higher energy x-rays.

Formulas given in this section have assumed a "symmetric" undulator—equal pole lengths and equal but opposite field strengths. Relaxing this requirement makes the constraints more easily achievable.

7.3. A Hybrid, Electo-Permanent, Asymmetric Undulator

The stringent requirements just described can be relaxed by permitting the undulator to be "asymmetric", meaning that the magnetic field is strong and of one sign over a short section and weak with opposite sign over a long section; the length×strength products must be equal if the beams from the poles are to superimpose, and the electron beam is to suffer no net deflection. It will be argued that u_c (as given by Eq. (7.2.1)) needs only to be large in the strong field regions, and the factor $\lambda_w/2$ in Eqs. (7.2.4) and Eqs. (7.2.5) can, roughly speaking, be replaced by w, the length of the short, strong-field poles. The large values of B in those regions can be provided by electromagnet. The longer and weaker, opposite sign, fields can be provided by permanent magnets. Such a magnet design is described in this section.

A proposed hybrid, electo-permanent-magnet undulator is illustrated in Fig. 7.1.1. Its purpose is to produce a very strong vertical magnetic field in the short gap region between soft iron poles. The maximum X-ray energy that can be produced coherently from multiple magnet poles is dominated by the pole width w, which is therefore to be made as short as possible consistent with the product $B_0 w$ being sufficiently large. Since the maximum field B_0 is produced by an electromagnet, its value can approach 2 T. The purpose of the permanent magnet inserts is to produce magnetic field of opposite sign, needed because the undulator must produce no net bending. Most undulators are "symmetric" such that north and south pole widths are equal ($w = W$) and the field maxima are equal but opposite in sign. Here $w << W$ is being permitted. Since the maximum field achievable with permanent magnets is less than with electromagnets, and the permanent magnet has to overcome the (small) electromagnetic field between poles, the field in the permanent magnet sections will be less than between poles, with the result that $w < W$. For assessing the X-ray energies emitted from a symmetric undulator, the undulator period λ_w is the most important parameter. But for our asymmetric undulator it will be w rather than asymmetric undulator period $w + W$ that governs the high energy cut-off of the radiation. For improved field uniformity the gap height $2g$ should be as small as possible, but storage ring practicalities will make it impossible to reduce $2g$ below some minimum value such as 6 mm.

For purposes of first-cut design of such a magnet, a kind of superposition principle will be assumed. First the electromagnet field between soft iron poles will be calculated ignoring the permanent magnet material. Then the field due to the permanent magnet material will be calculated ignoring the electromagnet. The two field components will then simply be summed. Since ferromagnetism is thoroughly nonlinear, such superposition can only be approximate. Two features possibly invalidating this approach are demagnetization of the permanent magnets and saturation of the iron. Failure of superposition will be briefly considered below. Two extreme simplifying assumptions will be that the iron permeablility is infinite and the permanent magnet permeability is equal to the free space value μ_0.

7.4. Electromagnet Design

For the small values of gap height $2g$ that will undoubtedly be required, the magnetic field can be calculated by concentrating on the region between the iron pole and the magnet centerline. Half of this region is labelled "z-plane" in the upper part Fig. 7.4.1. The field will be calculated by conformal transformation, using the subsidiary complex w and t planes, also shown in Fig. 7.4.1. These figures, and the subsequent analysis, are copied from L. V. Bewley, *Two-Dimensional Fields in Electrical Engineering.*

In this approach any analytic function in any of the planes automatically satisfies the 2D Laplace equation in that plane, with the real and imaginary coordinates interpreted as Cartesian coordinates. In the $u + iv = w$-plane $\Re(\Phi(w)) = \Re(w)$ satisfies the boundary conditions $\Phi(0 + iv) = 0$, $\Phi(U + iv) = U$. $\Phi(w)$ is known as the "complex, magnetic scalar potential", and the magnetic field components are obtained from it by

$$-B_x + iB_y = \frac{d\Phi}{dz}, \tag{7.4.1}$$

which is a formula that follows because both divergence and curl of $\mathbf{B}$ vanish. In our case $\Phi \equiv w$.

The concatenated analytic transformation $w \to t \to z$, produces the desired boundaries and the appropriate boundary conditions in the z-plane. The tranformation $w \to t$ is

$$t = -e^{-i\pi w/U} = e^{\pi v/U}\left(\cos\frac{U-u}{U}\pi + i\sin\frac{U-u}{U}\pi\right), \tag{7.4.2}$$

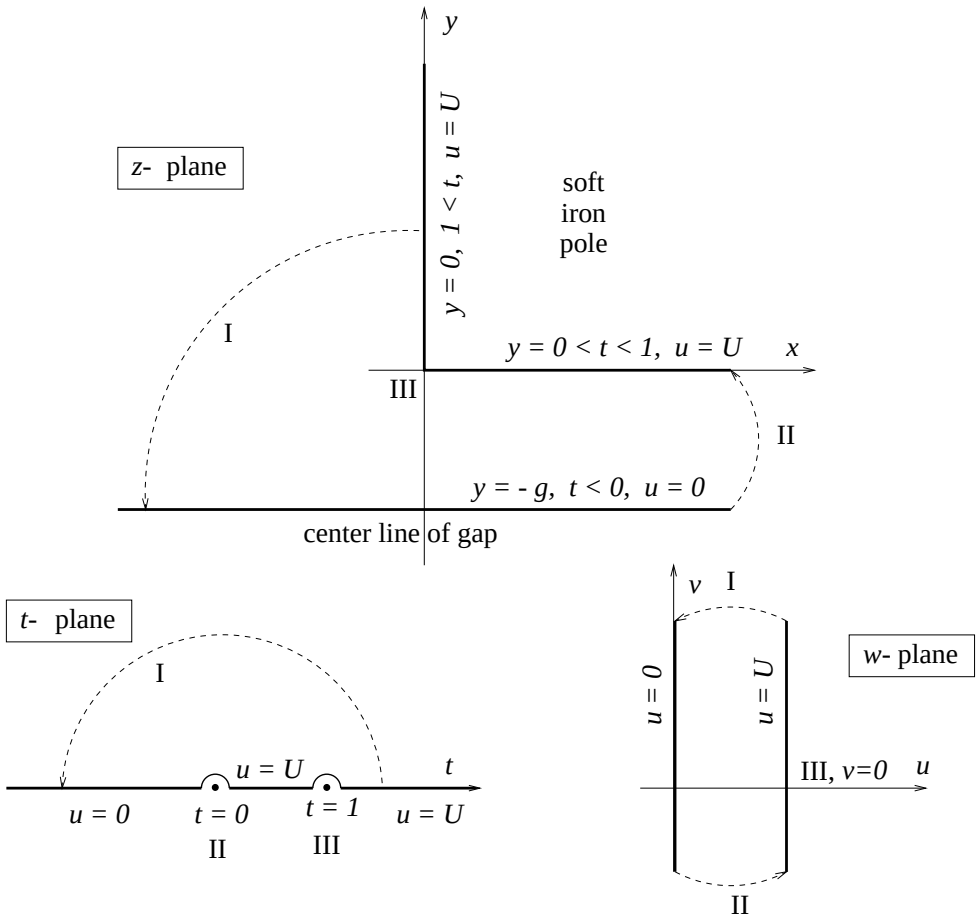

Figure 7.4.1: Complex planes used to determine the magnetic field in the region between one half pole and the centerline of the gap. At point III, the corner of the pole, $t = 1$ and $x = y = v = 0$.

On the boundaries this simplifies to

$$t = \begin{cases} -e^{\pi v/U} & \text{for } u = 0, \\ e^{\pi v/U} & \text{for } u = U. \end{cases} \tag{7.4.3}$$

The inverse transformation is

$$\frac{w}{U} = 1 + \frac{i}{\pi} \ln t = 1 - \frac{\theta}{\pi} - \frac{i}{\pi} \ln \rho, \tag{7.4.4}$$

where $t = \rho e^{i\theta}$. One can check that the function $\Re(w(t))$ satisfies the boundary conditions shown in the figure (U on the positive real t-axis, 0 on the negative real t-axis.) The further transformation $t \to z$ is given by

$$\begin{aligned} x + i\, y &= \frac{-2g}{\pi} \left(\sqrt{1-t} - \frac{1}{2} \ln \frac{1+\sqrt{1-t}}{1-\sqrt{1-t}} \right) \\ &= i\, \frac{2g}{\pi} \left(\sqrt{t-1} - \tan^{-1} \sqrt{t-1} \right), \end{aligned} \tag{7.4.5}$$

where the formula option permits the argument of the square root always to be chosen positive. Eliminating t from these formulas using Eq. (7.4.2) gives transformation formulas $(u, v) \to (x, y)$. v varies on contours of constant "potential" u, while on (orthogonal) field lines u varies and v is constant. Eqs. (7.4.5) therefore give the equations of both sets of curves in parametric form. Explicitly, the upper formula becomes

$$\frac{x + i\,y}{g} = \frac{-2}{\pi}\sqrt{1 + \exp\left(-i\pi w/U\right)} + \frac{1}{\pi}\,\ln\frac{1 + \sqrt{1 + \exp\left(-i\pi w/U\right)}}{1 - \sqrt{1 + \exp\left(-i\pi w/U\right)}}. \tag{7.4.6}$$

On the boundaries, the formulas reduce to

$$\begin{aligned}
\frac{y}{g} &= \frac{2}{\pi}\sqrt{e^{\pi v/U} - 1} - \frac{2}{\pi}\tan^{-1}\sqrt{e^{\pi v/U} - 1} \quad 1 < t, 0 < v, w = U + iv, \quad \text{pole side,} \\
\frac{x}{g} &= \frac{-2}{\pi}\sqrt{1 - e^{\pi v/U}} + \frac{1}{\pi}\,\ln\frac{1 + \sqrt{1 - e^{\pi v/U}}}{1 - \sqrt{1 - e^{\pi v/U}}}, \quad 0 < t < 1, v < 0, w = U + iv, \quad \text{pole face,} \\
&= \frac{-2}{\pi}\sqrt{1 + e^{\pi v/U}} + \frac{1}{\pi}\,\ln\frac{1 + \sqrt{1 + e^{\pi v/U}}}{1 - \sqrt{1 + e^{\pi v/U}}}, \quad t < 0, w = iv, \quad \text{centerline.}
\end{aligned} \tag{7.4.7}$$

The third of these relations is plotted in Fig. 7.4.2 and Fig. 7.4.3 shows a complete field plot.

Using Eq. (7.4.1) the field is given by

$$B_x - iB_y = -\frac{dw}{dz}; \tag{7.4.8}$$

In the process of deriving these transformations these two derivatives appeared:

$$\frac{dz}{dt} = i\,\frac{g}{\pi}\,\frac{\sqrt{t-1}}{t}, \quad \frac{dw}{dt} = i\,\frac{U}{\pi}\,\frac{1}{t}. \tag{7.4.9}$$

We therefore have

$$\begin{aligned}
B_x + iB_y = &-\left(\frac{dw}{dz}\right)^* = -\left(\frac{dw}{dt}\,\frac{dt}{dz}\right)^* = -\left(\frac{U}{g\sqrt{t-1}}\right)^* \\
&= \frac{-U}{g}\left[e^{\pi v/U}\left(\cos\frac{U-u}{U}\pi - i\,\sin\frac{U-u}{U}\pi\right) - 1\right]^{-1/2}.
\end{aligned} \tag{7.4.10}$$

We are primarily interested in the value of B_y along the centerline where $u = 0$;

$$\frac{B_y g}{U} = \frac{1}{\sqrt{1 + e^{\pi v/U}}}, \tag{7.4.11}$$

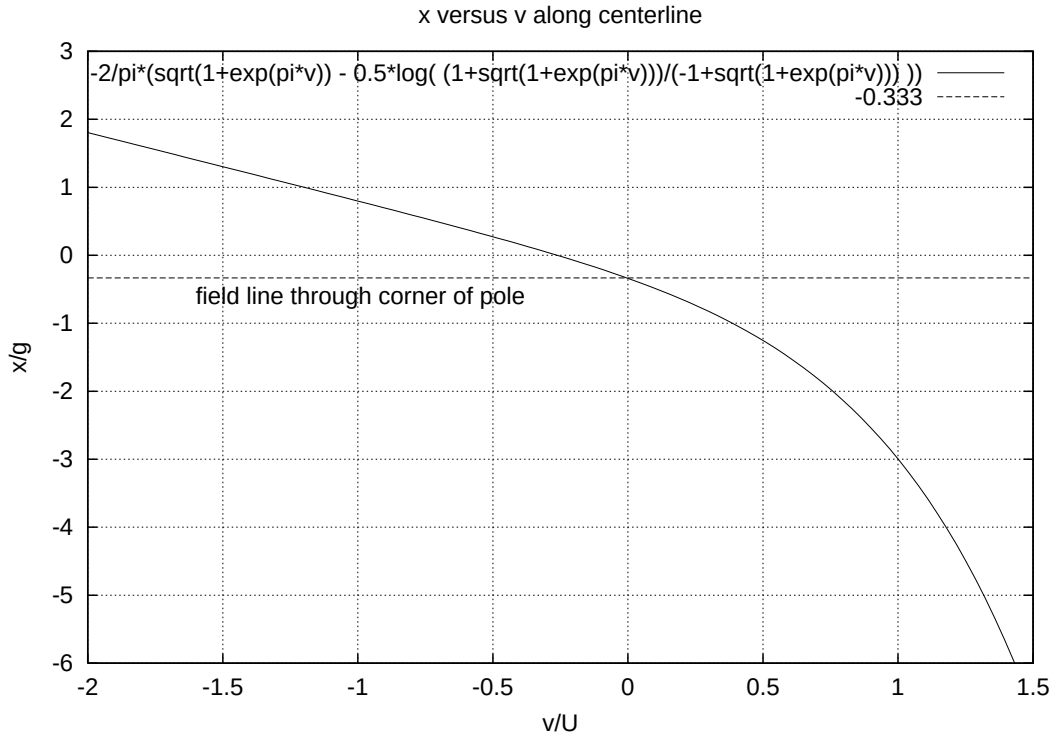

Figure 7.4.2: Relation between x and v along the centerline. Note that the $v = 0$ contour (the one leaving the corner of the pole) intersects the centerline at a slightly negative value of $x = -0.333g$. As v becomes more positive, the constant v contour bulges out more and more (i.e. x becomes increasingly negative.)

and along the pole face where $u = U$;

$$\frac{B_y g}{U} = \frac{1}{\sqrt{1 - e^{\pi v/U}}}, \tag{7.4.12}$$

The absolute value of the magnetic field is given by

$$\frac{|\mathbf{B}|g}{U} = \left[e^{2\pi v/U} - 2e^{\pi v/U} \cos\frac{U-u}{U}\pi + 1 \right]^{-1/4}. \tag{7.4.13}$$

Substituting from Eq. (7.4.11) into the third of Eqs. (7.4.7) yields

$$\frac{x}{g} = \frac{-2}{\pi}\left(\frac{U}{B_y g} - \frac{1}{2}\ln\frac{B_y g/U + 1}{-B_y g/U + 1} \right), \quad t < 0, \quad \text{along the centerline.} \tag{7.4.14}$$

The inverse of this formula gives the magnetic field profile along the centerline of the magnet; it is plotted in Fig. 7.4.4. Because $x = 0$ corresponds to the pole edge, rather than the pole center, it is necessary to specify the position of the pole center. For a wide

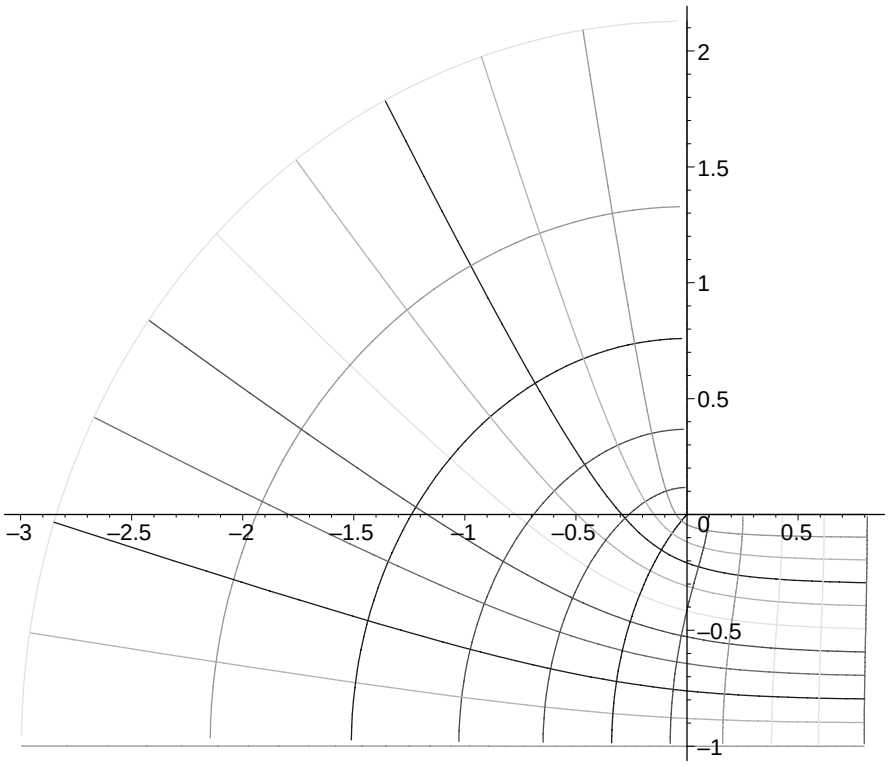

Figure 7.4.3: Field plot for the ranges $0 < u < 1$, $-1 < v < 1$. By the spacing between curves of constant v the field magnitude at $(0, 2g)$ is roughly one fifth of the field in the gap. This suggests that D/g should be at least 2 or g/D should be less than 0.5.

pole (in appropriate units) $B_y g/U$ approaches 1 in the interior of the pole. Since we want the pole to be as slender as possible a choice, such as shown in the figure, with full pole width equal to full gap $2g$ seems appropriate since the field is within 2% of its full value at $x = -g$. In the spirit of making σ_z as small as possible this is an aggressively small choice. But an even somewhat smaller choice could be made without much loss of central field relative to nominal.

Also plotted in Fig. 7.4.4 is an empirical (Gaussian) fit of the form

$$B_y = \frac{(Bg)_{\text{nom.}}}{g} \exp\left(-\frac{(x - w/2)^2}{2\,(1.6)^2\, g^2}\right); \tag{7.4.15}$$

This is an extremely crude fit, that doesn't properly combine the pole width and field spreading in the gap except at the one point where the fit was made. So it can be expected to give the dependence on g over only a very small range. More properly the parameters should be fit for various values of g holding w fixed. Of course saturation also invalidates

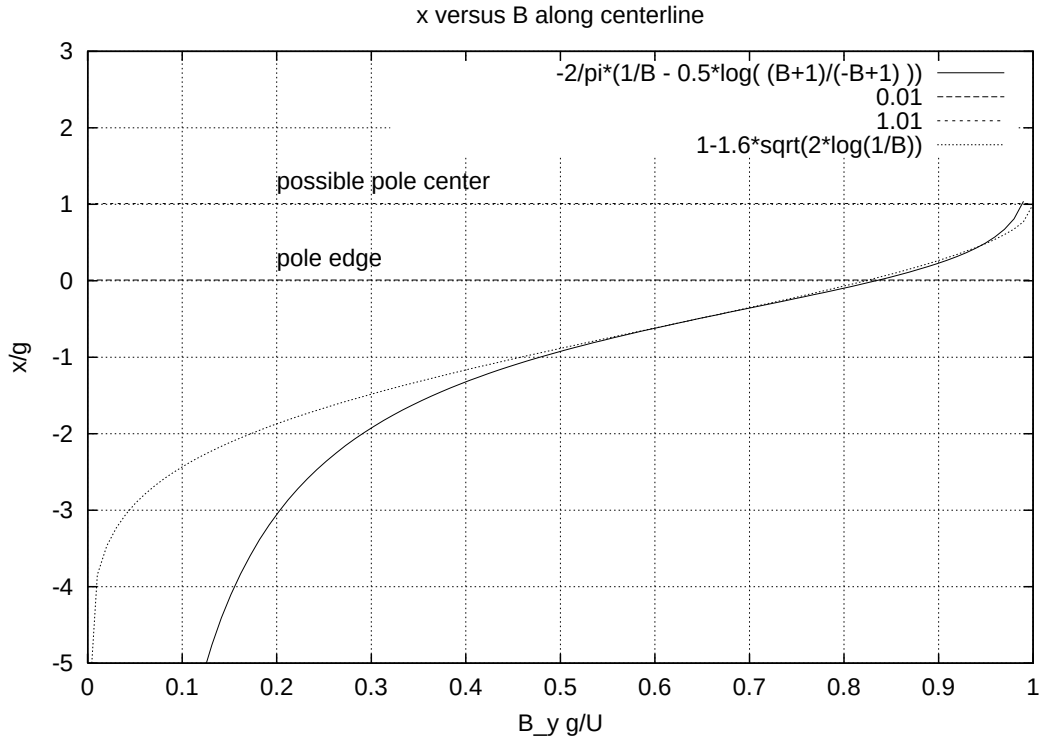

Figure 7.4.4: Magnetic field profile along the centerline due to one half pole. The pole edge is at $x = 0$. The pole width can be as little as $2g$ (the case shown) with only 2% field reduction from the nominal (thick pole) value. Also shown is a Gaussian fit that applies for this particular choice of pole width.

the formula for small g. Nevertheless, for subsequent calculations, I will use the value

$$\sigma_z = 1.6\, g, \quad \left(\stackrel{\text{e.g.}}{=} 0.51\,\text{cm for } 2g = 0.6\,\text{cm.} \right) \tag{7.4.16}$$

7.5. Permanent Magnet Design—Small Gap Limit

The magnetic field in the permanent magnet sections can be estimated while referring to Fig. 7.5.1. Assuming constant magnetization M (directed up in the figure) within the permanent magnet material, the permanent magnet block can be modelled by bound surface current densities M flowing in and out of the page. In this picture the material itself is replaced by free space, of permeability μ_0. The B-field will therefore resemble that of a rectangular solenoid, more or less uniform in the interior of these current sheets. Assuming $g << W$ the outward bowing of the fields in the gap region should be modest

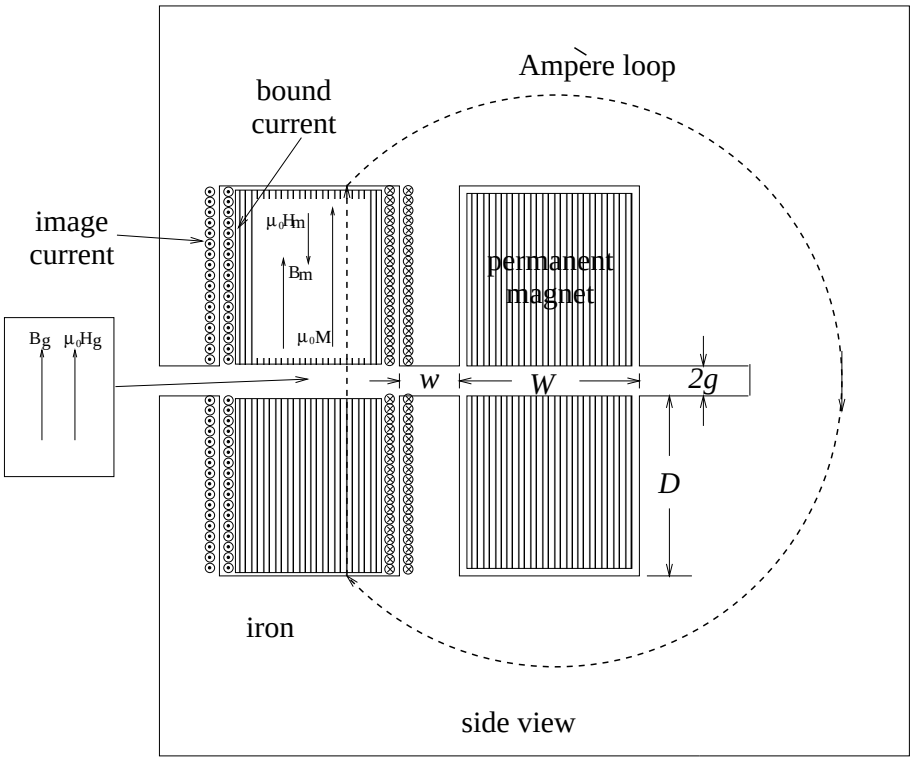

Figure 7.5.1: Two adjacent permanent magnet sections, separated by an iron pole, are shown. The Ampère loop links the "bound" current of the permanent magnet and the "image" current in the iron, but no "free" current.

and will be neglected. As a result

$$B_g = B_m \tag{7.5.1}$$

where subscripts g and m stand for "gap" and "magnetic material"; also B_w will be the magnetic field between the iron poles (which is currently being neglected.) Treating the iron as ideal, there is no contribution within the iron region to the Ampèrian loop integral along the path shown so this loop links zero true current.† From this and Eq. (7.5.1) the

† In fact the Ampère loop also links the current in the main dipole coil, but I am assuming $D >> g$, and hence that negligible flux from the main coil actually passes through the permanent magnet blocks. Of course this is wrong, especially adjacent to the corners of the iron poles where the "fringe fields" pass through the corners of the permanent magnet blocks. In the present approximation this is being neglected. It will be (crudely) accounted for later. The error becomes fractionally less significant for $W >> w$. Since one will be striving to make B_w as large as possible it may be necessary, for obtainable magnet material, even to allow the magnet block corners to be demagnetized by the main dipole current. This may make it tricky to maintain zero field integral, because of hysteresis, for example, as the gap height is changed. At worst the beam steering caused by the device can be adjusted empirically to zero by varying the main dipole current while viewing the closed orbit in the storage ring.

equation of the "load line" is obtained;

$$2gH_g + 2DH_m = 0, \quad \text{so} \quad B_m = -\frac{D}{g}\,\mu_0 H_m. \tag{7.5.2}$$

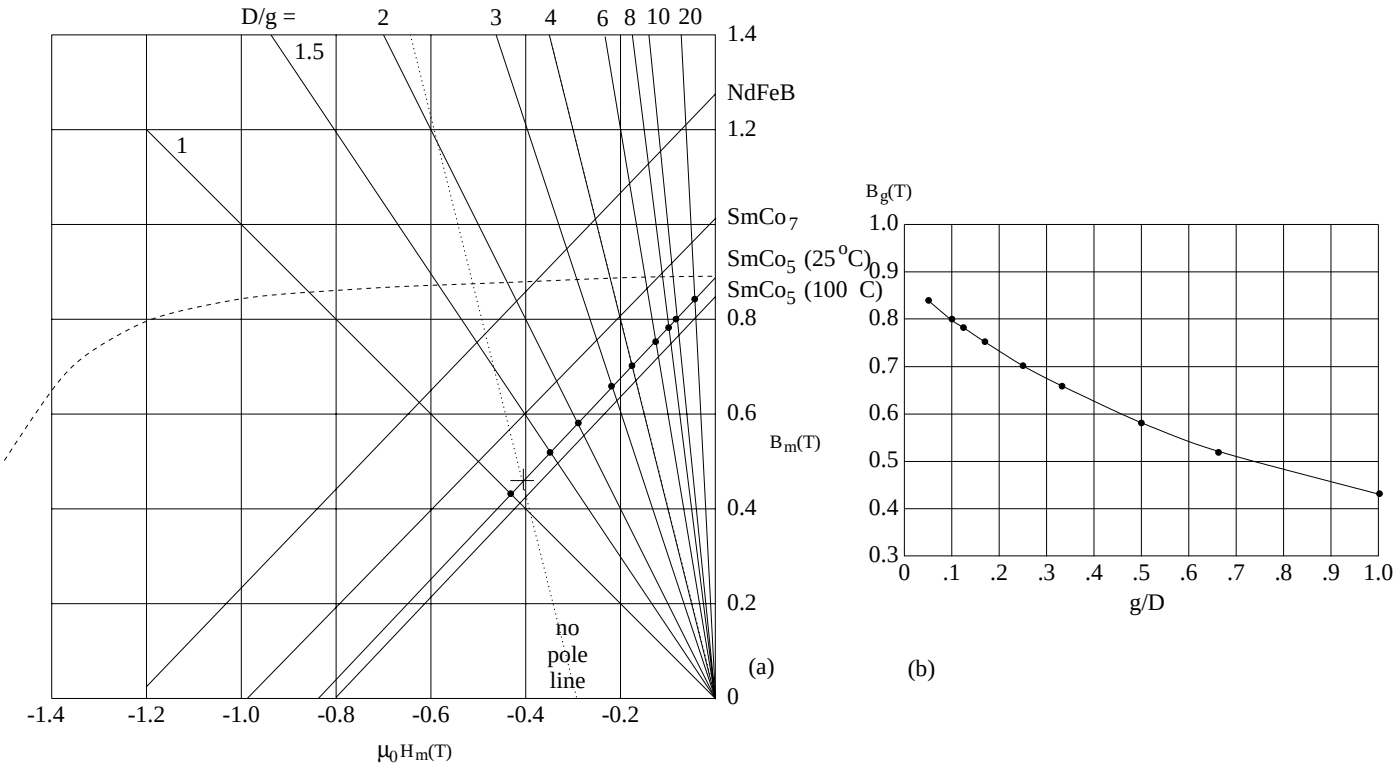

Figure 7.5.2: (a) Demagnetization curves for various permanent magnet materials. From P. Campbell, *Permanent Magnet Materials and Their Applicatation,* Cambridge University Press, 1994. Also shown are load lines given by Eq. (7.5.2) and their intersections with the $SmCo_5$ load line for various values of D/g. The dashed curve gives the magnetization $\mu_0 M$. (b) The corresponding dependence of B_g, the field in the gap, on g/D.

Load lines for various values of D/g are plotted in Fig. 7.5.2. Also shown are their intersections with the demagnetization curve for $SmCo_5$. This seems to be the material of choice because of its extremely large value of coercive force, which is the intersection of the dashed curve with the horizontal axis; in the units of the figure the intercept is at about 2 T. Maximizing this parameter will minimize the problem of irreversible demagnetization due to the electromagnet field.

Demagnetization curves for other materials are also shown. By using NdFeB, fields almost 50% higher could be achieved. But there seems to be little reason to push for

the highest possible field, since this would only reduce the ratio W/w proportionally. This would permit more complete periods per unit length of undulator, and hence higher total flux, but it would also exaggerate importance of the problematical regions close to the iron poles, both because of demagnification and their greater fractional importance. Fig. 7.5.2(b) shows the dependence of B_g on g/D. A polynomial fit to the data is

$$B_g\,[T] = 0.8704 - 0.7359\,(g/D) + 0.2974\,(g/D)^2\,. \tag{7.5.3}$$

7.6. Combined Electro- and Permanent-Magnet Fields

Fig. 7.5.2 suggests that the peak field at minimum g can be $B_g \approx 0.8\,\mathrm{T}$, with $g/D = 0.1$. However the dependence of B_g on g is rather weak at this point; the dependence is slower than the $1/g$ dependence of the iron pole fields. This suggests that the operating point should be chosen closer to the center of the range shown in Fig. 7.5.2(b). Tentatively I take $g/D = 0.25$ and therefore $B_g = 0.7$. Then, selecting $B_w = 1.6\,\mathrm{T}$ would seem to require $W/w \approx 2.5$. But the "stray flux" through the permanent magnet material from the electromagnet has been ignored. A feeble attempt to estimate this effect is indicated by the dotted line labelled "no pole line" in Fig. 7.5.2. If there were no iron poles then, effectively the gap would be five times greater and the B-field five times less, or about 0.3 T. This reduces the permanent magnet field by roughly 1/3. Furthermore the reduction in the corners is even greater. To compensate I select $W/w \approx 5$. These tentative choices are indicated in Fig. 7.6.1.

7.7. Estimated High Energy X-Ray Flux

In the high energy region this undulator is intended to service the flux will be dominated by the high field regions. According to Eq. (7.4.15) the magnetic field in these regions is given by

$$B\,(z) = B_0\,\exp\left(-\frac{z^2}{2\,(1.6g)^2}\right). \tag{7.7.1}$$

I will neglect all fields other than this. From Eq. (7.2.1), assuming a field $B_0 = 1.6\,\mathrm{T}$ can be achieved, the critical energy will be $u_c \approx 9\,keV$ and there will be "ideal" (defined above) flux up to about 27 keV.

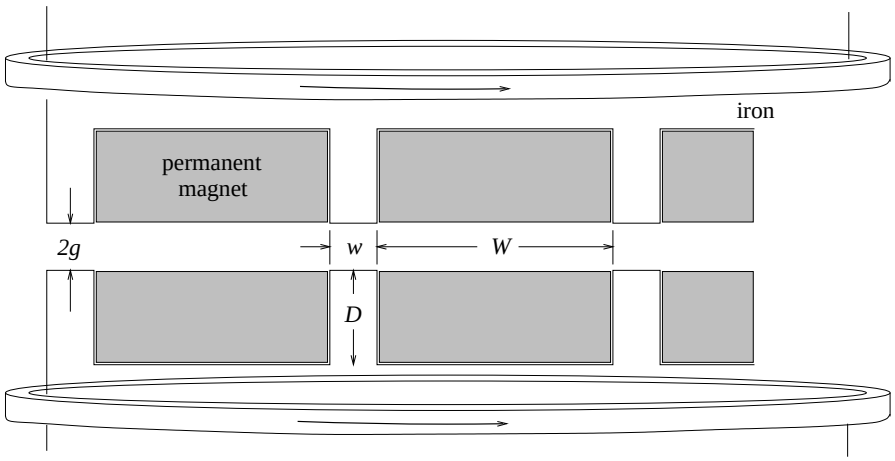

Figure 7.6.1: Pole profile of the asymmetric undulator. The relative dimensions shown are a tentative starting point for a more careful analysis that accounts for the interaction of electro and permanent magnet effects. The electromagnet coils are shown schematically only as a reminder of their presence.

One can introduce a kind of symmetric "comparison undulator" for which the fields within one half period more or less match Eq. (7.7.1). Its undulator wavelength would be

$$\lambda_{w,\text{comp.}} \approx 2\pi\sigma_z = 1.6\pi\,(2g)\,, \quad \left(\overset{\text{e.g.}}{=} 3\,\text{cm for } 2g = 6\,\text{mm.}\right) \tag{7.7.2}$$

The comparison K value would then be

$$K_{\text{comp.}} = 0.934\,B_0\,[\text{T}]\;\lambda_{w,\text{comp.}}\,[\text{cm}] \begin{pmatrix} \overset{\text{e.g.}}{=} 2.8\,B_0\,[\text{T}] \;\text{ for } 2g = 6\,\text{mm,} \\ \overset{\text{e.g.}}{=} 4.6 \;\text{ for } B_0 = 1.6\,[\text{T}]\,. \end{pmatrix} \tag{7.7.3}$$

This comfortably exceeds anything one would need in practice. Compared to the comparison undulator, the total power radiated from the asymmetric undulator of the same total length will be reduced by a factor equal to twice the ratio of periods (the ratio of poles per unit length)

$$\frac{N_{\text{asym.}}}{N_{\text{comp.}}} = \frac{1}{2}\,\frac{\lambda_{w,\text{comp.}}}{w+W} \approx \frac{1}{2}\,\frac{1.6\pi\,(2g)}{2g+10g} \approx 0.4. \tag{7.7.4}$$

In calculating post-monochrometer beam brilliance this factor may have to be squared to account for the reduced number of poles. As mentioned before, the fluxes into even and odd undulator harmonics will be comparable. This means the flux into any particular odd harmonic will be reduced by another factor of two over and above the reduction given by Eq. (7.7.4). On the positive side of the ledger, the presence of even harmonics will

ameliorate the problem of "holes" in the spectrum; a nuisance associated with running in the low order harmonic region.

Chapter 8.
The Microwave Undulator

Essentially all existing wigglers and undulators are made using conventional magnets, either electromagnets or permanent magnets. Nevertheless, in this chapter, the concentration will be on a "microwave undulator". This relies heavily on the content of the previous chapter, which describes features that are common to any undulator or wiggler. This chapters uses material that was written to advocate the development of a microwave undulator at CESR. The following abstract summarizes the content of the chapter.

Abstract. High order diffraction maxima from a magnetic undulator can extend the spectrum produced in a synchrotron X-ray source to high energy, but the resulting beam has (undesirably) high power relative to the flux of useful X-rays. Making the undulator period short can concentrate the beam power in the useful spectral range, but a magnetic undulator with ideal radiation properties usually has a gap height too small for satisfactory operation at existing storage rings. To overcome these limitations it is here proposed to replace the magnetic undulator field by an electromagnetic wave, propagating in a waveguide that serves also as the accelerator vacuum pipe. Because the "undulator" can pass through lattice focusing elements, it can be long yet inexpensive. For achievable microwave power, flux and brilliance can be achieved up to (almost) the limit that defines ideal undulator operation. By controlling microwave properties, the energy, flux, and state of polarization of the X-ray beam can be tuned (within microseconds) independent of storage ring parameters, and without disrupting the circulating beam. The controls for these parameters can therefore be put in the hands of the separate experimenters in separate beam lines. A possible design is given for an X-ray source centered on 12.4 keV X-ray energy, along with numerical estimates of its expected performance at the Cornell Electron Storage Ring (CESR), modified to maximize brilliance, and running at 5.1 GeV. The radiation from this system is analysed both classically, as undulator radiation, and quantum mechanically, as Compton scattering.

8.1. Introduction

The narrow band of energies, mentioned in the abstract as being ideal for X-ray diffraction, is limited on the high energy side by difficulty in making optical elements in that range, by excessive heating, by longterm damage, and by unwelcome backgrounds. The low energy limit is due to excessive attenuation in vacuum windows, protective covers and thick samples. The attenuation length of few keV photons is so short as to cause unacceptable attenuation but, because of the extremely rapid energy dependence of attenuation length, a factor of ten increase in energy largely overcomes this problem. One therefore seeks a photon beam centered on, say, $E_\gamma = 12.4\,\mathrm{keV}$,† as brilliant as possible, consistent with being as monochromatic as possible. The use of undulators to produce beams of this sort at electron storage rings is by now well understood, but the undulator period is too short to be practical for most storage rings. The apparatus proposed here is intended to supercede such an undulator in order to produce a beam that has brilliance, large both on an absolute basis and relative to total beam power, and is non-intrusive on the circulating beam.

It is difficult for λ_w to be small enough to satisfy Eq. (6.1.1) because of the inevitable fringing between the poles and a correspondingly too-small gap height requirement. One can contemplate using higher order interference maxima but, since the electron's trajectory through a standard undulator is essentially sinusoidal, the higher orders are extremely weak. The apparatus proposed to overcome the disadvantages of conventional is shown in Fig. 8.1.1.

As illustrated also in Fig. 8.1.2 our *microwave undulator* consists of a powerful microwave beam, propagating in a rectangular waveguide, through which the bunch of electrons or positrons passes. Depending on the propagation mode in the waveguide and whether the beam is a traveling or a standing wave, the microwave beam can be idealized as a superposition of two, four, or eight monochromatic plane waves. There is a close analogy between a conventional magnetostatic undulator and a standing wave beam, since the spatial dependence of their deflecting fields (at fixed time) are the same. But, to the extent the electron and microwave beams are parallel, the transverse force due to the

† The choice of $E_\gamma = 12.4\,\mathrm{keV}$ as nominal energy corresponds to a wavelength $\lambda_\gamma = 1\mathring{A}$ and to the (mnemonic) approximation $1\mathring{A} \to 12345\,\mathrm{eV}$.

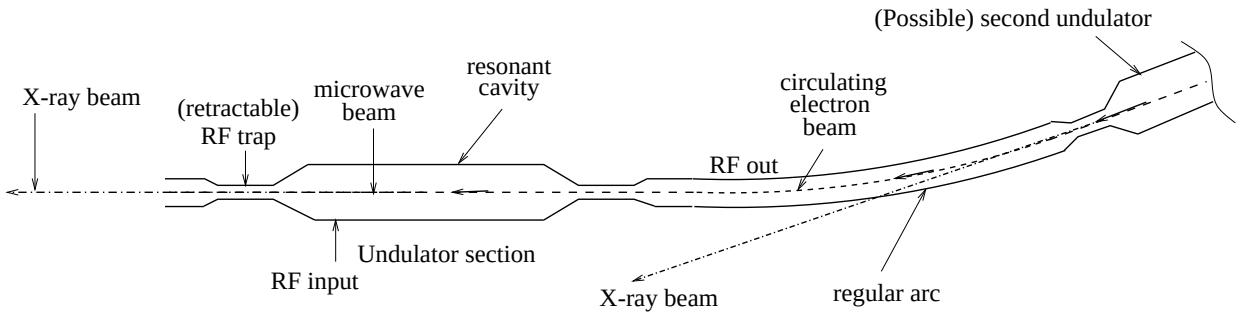

Figure 8.1.1: Microwaves in the "undulator" collide with circulating electrons. The useful microwaves propagate approximately anti-parallel to the electrons.

parallel-traveling beams are negligible (because electric and magnetic forces cancel) and, to calculate the X-ray production, it is only necessary to consider the anti-parallel microwave beam. Any one of these anti-parallel fields is characterized by "guide wavelength" λ_g, and its fields depend on position and time as $\cos(2\pi z/\lambda_g - \omega_{\rm rf} t)$. For an electron whose position is given by $z = -vt$ (where $v \approx c$) the field dependence is $\cos((2\pi/\lambda_g + \omega_{\rm rf}/v)z)$, which implies

$$\frac{1}{\lambda_w} = \frac{1}{\lambda_g} + \frac{\omega_{\rm rf}/\left(2\pi\right)}{v} \approx \frac{1}{\lambda_g} + \frac{1}{\lambda_{\rm rf}} \ , \tag{8.1.1}$$

yielding "effective wiggler wavelength" λ_w in terms of λ_g and "free space wavelength" $\lambda_{\rm rf}$. For waves traveling approximately parallel to the guide axis, this yields $\lambda_w \approx \lambda_{\rm rf}/2$. So our nominal 12.4 keV energy, requires an RF generator yielding free space wavelength $\lambda_{\rm rf} \approx 2\lambda_w = 4\,{\rm cm}$, i.e. 7.5 GHz. Corresponding to Eq. (6.2.13) we have

$$\sigma_z = \frac{\lambda_w}{2\pi} = \frac{1}{2\pi}\,\frac{\lambda_g \lambda_{\rm rf}}{\lambda_g + \lambda_{\rm rf}} \ . \tag{8.1.2}$$

For our nominal 12.4 keV energy, $\sigma_z = 1/\pi\,{\rm cm}$. In practice, we anticipate $\lambda_g \approx \lambda_{\rm rf}$ and therefore $\sigma_z \approx \lambda_{\rm rf}/(4\pi)$.

For purposes of estimating X-ray beam fluxes using traveling waves, we can use traditional undulator formulas with undulator period λ_w given by Eq. (8.1.1). In this picture the microwave beam is treated (classically) as an external force field that causes electrons to oscillate transversely. The analysis of the next few sections will therefore apply equally

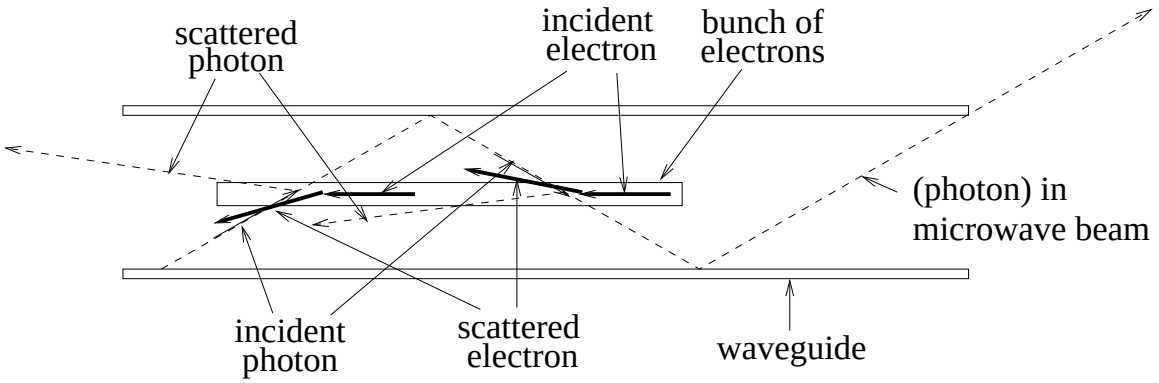

Figure 8.1.2: Microwave undulator configuration. An electron beam collides with a traveling (or standing) microwave beam. The microwave beam can be thought of as a superposition of plane waves that reflect repeatedly off the conducting walls of the waveguide.

to conventional undulators and wigglers, and language from the latter field will be employed.† Later, when the radiation is calculated quantum mechanically, the microwave beam will have to be treated as the appropriate superposition of plane waves.

8.2. Radiation Intensity From Microwave Undulator

Certain intensity limits are inherent to the ideal operation of an undulator. Based on Eq. (6.2.34), the maximum deflection angle satisfies $\Delta\Theta < 1/(2\gamma) = 0.05\,\mathrm{mr}$, a fairly modest angle. But, since this deflection occurs over a short length, the local curvature may be substantial. The maximum total energy radiated, as a fraction of radiation per turn, can be related to $\Delta\Theta$ using Eq. (6.2.17);

$$\frac{U_{\rm tot}}{U_0} = \frac{2N_w}{\pi^{3/2}}\,\frac{R_0}{\sigma_z}\,\Delta\Theta^2 \quad \left(\stackrel{\rm e.g.}{=} \frac{2N_w}{2\pi^{3/2}}\,\frac{90}{0.01} \times \frac{10^{-8}}{4} \approx 0.4\times 10^{-5}\ (2N_w) \right) \ . \tag{8.2.1}$$

What makes the undulator promising, in spite of this relatively low upper limit, is the "short magnet enhancement"† that shifts all the radiated energy into a narrow high energy band. As well as the factor $2N_w$ explicitly exibited in Eq. (8.2.1), the beam brilliance

† In fact, the next few sections amount to being a tutorial on convevtional undulators.

† It is this short magnet enhancement that enables the CERN proton ring diagnostics, referred to previously. In their case (because they have protons) the rate of *visible* photons is enhanced by some 23 orders of magnitude (according to Coisson.) This gigantic enhancement is possible only because of the large proton to electron mass ratio. For an electron ring like CESR, since the critical energy u_c is already in the few keV range, the enhancement is enormously less; the energy radiated per unit energy for $u = 4u_c$ is roughly ten times less than for $u = u_c$, so the number of photons radiated per unit energy falls by about 40 over the same range.

acquires another factor $2N_w$ from the diffractive line narrowing. It seems therefore, that one need not be unduly discouraged concerning the intensity limit that follows from condition (6.2.34).

For the microwave undulator the maximum achievable deflection is determined by the maximum power P propagating along the waveguide. For propagation in the TE_{10} mode (which is the propagating mode with lowest cut-off frequency) the power is given by[12]

$$P = \frac{|E_{\max}|^2}{Z_0}\,\frac{ab}{2}\,\sqrt{1-\left(\frac{\lambda_{\rm rf}}{2a}\right)^2} \tag{8.2.2}$$

where $Z_0 = \sqrt{\mu_0/\epsilon_0} = 377\,\text{ohms}$, $E_{\max}$ is the maximum electic field, and a and b are waveguide dimensions. The wave can be represented as the sum of two waves, directed at angles θ on one or other side the axis, where

$$\cos\theta = \sqrt{1-\left(\frac{\lambda_{\rm rf}}{2a}\right)^2}\ . \tag{8.2.3}$$

In this mode the cut-off wavelength is $2a$. Since we favor waves propagating more or less parallel to the waveguide axis, $\theta << \pi$, we will have $\lambda_{\rm rf} << 2a$, so the square root factor in Eq. (8.2.2) will be approximately 1. For example, $a = \lambda_{\rm rf}$ will yield $\cos\theta = 0.866$, $\theta = 30°$.

The total deflection per half period also depends on the particular waveguide propagation mode but, for simplicity, let us consider only the case of propagation exactly parallel to the waveguide axis. (As a matter of fact, there is no such mode, but short wavelength modes can propagate approximately parallel to the guide.) The motion of a charged particle in an electromagnetic wave is analyzed in Appendix A. According to Eq. (A.19), the maximum deflection angle is given by

$$\Delta\Theta = \frac{dx}{d\Phi}\Big|_{\max}\frac{d\Phi}{dz} \approx \frac{2\omega_{\rm rf}}{c}\,\frac{e\,E_{\max}}{\mathcal{L}\,m\,\omega_{\rm rf}^2} = \frac{1}{\gamma}\,\frac{\lambda_{\rm rf}}{2\pi}\,\frac{E_{\max}}{mc^2/e} \quad \left(\approx \frac{1}{\gamma}\,\frac{\lambda_{\rm rf}}{2\pi}\,\frac{E_{\max}\,(\mathrm{MV/m})}{0.511\,\mathrm{MV}}\right)\ . \tag{8.2.4}$$

Since RF field gradients as high as $100\,\mathrm{MV/m}$ are physically achievable (if only for brief pulses) it is possible to briefly achieve deflections $\Delta\Theta \sim 1/\gamma$, which is as large as is consistent with ideal undulator operation.

But, for CW operation, it is more meaningful to relate $\Delta\Theta$ to microwave power. To avoid the extravagance of supporting CW power P, it is sensible to establish a standing wave pattern† in a (long) waveguide resonator of length L_w. There is a possible advantage

† A ring resonator configuration could support only forward-traveling waves, with similar power considerations.

to making this tube circular, so that arbitrarily-polarized, linear, circular, etc., waves could be established. But, to simplify the discussion, we are considering only a rectangular tube of width a and height b, carrying the TE_{10} mode. Using a superconducting RF cavity may also be attractive, but the following numerical estimate will assume the waveguide is made of room temperature copper. This choice would be especially convenient because the waveguide could be continuous through the magnets making up the beam line, and hence could be made almost arbitrarily long without disrupting the lattice optics seriously.

The power $P(z)$ of a wave propagating in the $+z$ direction in a waveguide satisfies

$$-\frac{dP}{dz} = 2\alpha P \ , \tag{8.2.5}$$

which means that $2\alpha P$ can be interpreted as the power per meter flowing into the walls. Neglecting end losses, the external power $P_{\mathrm{ext.}}$ required to maintain a standing wave (sum of equal but opposite traveling waves) in a guide of length L_w therefore satisfies

$$\frac{P_{\mathrm{ext.}}}{P} = 4\alpha L_w \ . \tag{8.2.6}$$

In the TE_{10} mode α (the inverse of the distance over which E and H fall by $1/e$) is given by

$$\alpha = \frac{1}{b}\sqrt{\frac{\pi}{Z_0 \sigma \lambda_{\mathrm{rf}}}}\,\frac{1+\frac{2b}{a}\left(\frac{\lambda_{\mathrm{rf}}}{2a}\right)^2}{\cos\theta}, \tag{8.2.7}$$

where the numerical values appropriate for room temperature copper are $\sigma_{\mathrm{cu}} = 4.0 \times 10^7/\mathrm{ohm/m}$ and $\pi/(Z_0\sigma) = \pi/(376.7 \times 4.0 \times 10^7) = 2.08 \times 10^{-10}\,\mathrm{m}$. We obtain, in this case, using $\lambda_{\mathrm{rf}} = a = 0.04\,\mathrm{m}$, $b = 0.02\,\mathrm{m}$,

$$\begin{aligned}\frac{P_{\mathrm{ext.}}}{P} &= \frac{4L_w}{b}\sqrt{\frac{2.08\times10^{-10}\,(m)}{\lambda_{\mathrm{rf}}\,(m)}}\,\frac{1+\frac{2b}{a}\left(\frac{\lambda_{\mathrm{rf}}}{2a}\right)^2}{\cos\theta} \\ &\left(\overset{\text{e.g.}}{=} \frac{4L_w\,(m)}{0.02\,(m)}\sqrt{\frac{2.08\times10^{-10}}{0.04}}\,\frac{1.25}{0.866} = \frac{L_w\,(\mathrm{m})}{48.1\ (\mathrm{m})}\ .\right)\end{aligned} \tag{8.2.8}$$

Returning to the estimate of radiated power, using Eq. (8.2.2) and Eq. (8.2.8), $\Delta\Theta^2$ can be expressed as

$$\Delta\Theta^2 \approx \frac{1}{\gamma^2}\,\frac{1}{\sqrt{1-\left(\frac{\lambda_{\mathrm{rf}}}{2a}\right)^2}}\,\frac{1}{2\pi^2}\,\frac{\lambda_{\mathrm{rf}}^2}{ab}\,\frac{P}{\left(mc^2/e\right)^2/Z_0} \quad \left(\approx \frac{1}{\gamma^2}\,\frac{1}{2\pi^2}\,\frac{\lambda_{\mathrm{rf}}^2}{ab}\,\frac{P_{\mathrm{ext.}}\,(MW)}{693.1\,\mathrm{MW}}\,\frac{48.1\ (\mathrm{m})}{L_w\,(\mathrm{m})}\ .\right) \tag{8.2.9}$$

For an external power level $P_{\rm ext.} \approx 1\,{\rm MW}$, this factor will be about $10^{-3}/\gamma^2$. In this case the X-ray flux per unit length will be less than from a $K = 1$ (the largest value consistent with "ideal" behavior) undulator by a factor of one thousand. For a superconducting waveguide this factor could be much closer to one. In absolute terms, from Eq. (8.2.1), the total radiated power is given by

$$\frac{U_{\rm tot}}{U_0} = \frac{2N_w}{2\pi^{7/2}}\,\frac{R_0}{\sigma_z}\,\frac{1}{\gamma^2}\,\frac{1}{\sqrt{1-\left(\frac{\lambda_{\rm rf}}{2a}\right)^2}}\,\frac{\lambda_{\rm rf}^2}{ab}\,\frac{P}{\left(mc^2/e\right)^2/Z_0}\ . \tag{8.2.10}$$

The power radiated from an undulator of length $L_w = N_w\lambda_w$ can be estimated by recalling that the pure antiparallel assumption leads to $\lambda_w \approx 2\lambda_{\rm rf}$ and $\sigma_z \approx \lambda_{\rm rf}/(4\pi)$. With these approximations we obtain for $U_{\rm tot}$, the power radiated by a single electron,

$$\frac{U_{\rm tot}}{U_0} \approx \frac{4}{\pi^{5/2}}\,\frac{L_w\,R_0}{ab}\,\frac{1}{\gamma^2}\,\frac{P_{\rm ext.}\,(MW)}{693.1\,{\rm MW}}\,\frac{P}{P_{\rm ext.}}\ . \tag{8.2.11}$$

Since the final factor causes this to be independent of L_w, contrary to what one might have expected, the power of the produced X-ray beam (per unit of external microwave power) will be independent of L_w. Nevertheless, high brilliance will favor large L_w. (The formulas determining power that have been given will also become more nearly valid as L_w is increased.)

For beam current I, the number of electrons traversing the undulator per second is $I/e = 0.62\times10^{19}\,/{\rm A/s}$. Because the width of the energy spectrum is inversely proportional to the number of undulator periods N_w, and the flux is reckoned per tenth percent bandwidth, there is a sensitive dependence of "flux" $\mathcal{F}'$ on N_w. Let us assume that N_w, though large, is small enough that the fractional energy width (at fixed angle) exceeds one tenth percent. Then (to accuracy not better than a factor of two) the flux acquires a rough factor $N_w/10^3$, and the flux per tenth percent bandwidth (at all energies and angles, but with peak value $h\nu = 12.4\,{\rm keV}$) is given by

$$\begin{aligned}\mathcal{F}' = \frac{U_{\rm tot}}{h\nu}\,\frac{I}{e}\,\frac{N_w}{10^3} &\approx \frac{4}{\pi^{5/2}}\,\frac{L_w\,R_0}{ab}\,\frac{U_0}{h\nu}\,\frac{I}{e}\,\frac{1}{\gamma^2}\,\frac{P_{\rm ext.}\,(MW)}{693.1\,{\rm MW}}\,\frac{P}{P_{\rm ext.}}\,\frac{N_w}{10^3}\\ &\left(\overset{\rm e.g.}{=} 0.229\,\frac{0.885\times10^{-4}\times5.11^4\times10^9}{0.04\times0.02\times1.24\times10^4}\,\frac{0.62\times10^{19}}{10^8\times693.1\times0.0208}\,\frac{N_w}{10^3}\right.\\ &\left.= 0.60\times10^{16}\,\frac{N_w}{10^3}\,\frac{\rm photons/s}{\rm MW\text{-}A}\ .\right)\end{aligned} \tag{8.2.12}$$

The power ratio estimate of Eq. (8.2.8) has been used. For $L_w = 10\,\mathrm{m}$, $N_w = 10/0.02$, about half of the photons will fall within the nominal 0.1% bandwidth. Taking $I = 0.1\,\mathrm{A}$, the flux† (including all angles) will be

$$\mathcal{F}'_{0.1\mathrm{A}} = 3.0 \times 10^{14}\,\frac{\mathrm{photons/s/0.1\%BW}}{\mathrm{MW}}\ . \tag{8.2.13}$$

On economic grounds a continuous power of $P_{\mathrm{ext.}} = 1\,\mathrm{MW}$ would probably be tolerable but, in practice, even "CW operation" would employ a duty factor far less than 1, so 1 MW seems like a conservative estimate for the microwave power (assuming this power level can be supported without breakdown.) Of course it would give a big improvement to use superconducting waveguide instead of the copper that has been assumed. Ignoring the dependence of energy on angle, the X-ray beam power corresponding to Eq. (8.2.13) is $\mathcal{P} \approx 2 \times 3 \times 10^{14} \times 1.24 \times 10^4 \approx 10^{19}\,\mathrm{eV/s}$ at 1 MW.

For comparison purposes, Fig. 8.2.1 shows performance of a conventional, 5 mm gap, undulator as reported by Walker.[13] This is just a crude fit, crudely extrapolated, and it refers to operation at $E_e = 1.5\,\mathrm{GeV}$. The flux at 12.4 keV is down by about three orders of magnitude from the value given in Eq. (8.2.13). On the other hand, the X-ray beam power, (given in the caption to the figure) is about $10^{19}\,\mathrm{keV/s}$. According to these estimates, the flux from the microwave undulator is three orders of magnitude greater even though the beam power is three orders of magnitude less.

8.3. Accelerator Physics Considerations

To complete the determination of intensity, brilliance, distribution functions and other parameters of the produced beam, it is necessary to address accelerator physics practicalities. For a start, because the radiated power is so weak, it seems safe to neglect degradation of the electron beam caused by the microwave (except due to peripheral effects such as requiring too small vacuum tube dimensions or causing vacuum degradation due to microwave heating.)

† As mentioned previously, the beam power is being accounted for as if made up of full-energy photons so, to obtain the actual number distribution in angle and energy of photons, Eq. (8.2.13) would need to be manipulated. Without this having been done, Eq. (8.2.13) is not very useful for making comparisons with other X-ray sources. The symbol $\mathcal{F}'$, rather than $\mathcal{F}$, is intended to be a reminder of this unconventional usage.

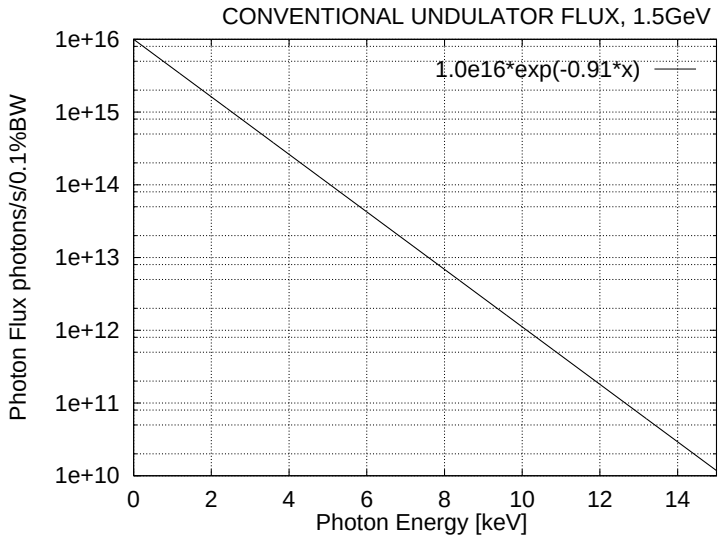

Figure 8.2.1: Fit to flux from conventional wiggler[13] operating with 5 mm gap and beam energy $E = 1.5\,\mathrm{GeV}$. The straight line crudely approximates 8 diffraction maxima in the range up to 10 keV and extrapolates to 15 keV. Integrating over the distribution given in the key yields a total beam power $\mathcal{P} \approx 10^{19}\,\mathrm{keV/s}$.

One can envisage a waveguide undulator passing right through some of the magnets making up the accelerator lattice. An example of the lattice optics of a sequence of six minimum emittance cells, is shown in Fig. 9.4.1. An waveguide undulator as long as 15 meters could be placed within the zero-dispersion central straight section. (The purpose of having zero dispersion is to minimize the influence of the undulator on the circulating beam.)

It is implicitly assumed in most discussions of synchrotron radiation (including this one) that the bend plane is horizontal and is designated as the x plane; the dominant field component is then E_x. (For the same reason) practical electron beams are usually ribbon-shaped, with transverse sigmas related by $\sigma_y << \sigma_x$. Because of this, it could turn out that vertical deflections would give superior performance for some purposes I leave this as an open question, but continue to assume implicitly that the bend plane is horizontal.

For any one electron, it has been argued that the spectrum is rather insensitive to the particle's slope. In this sense the accelerator optics at the undulator is unimportant. It is true however, that the spike visible in Fig. 6.2.8 is as sharp as it is because a restricted range of angle ϑ has been assumed. Commonly one will wish to limit line broadening

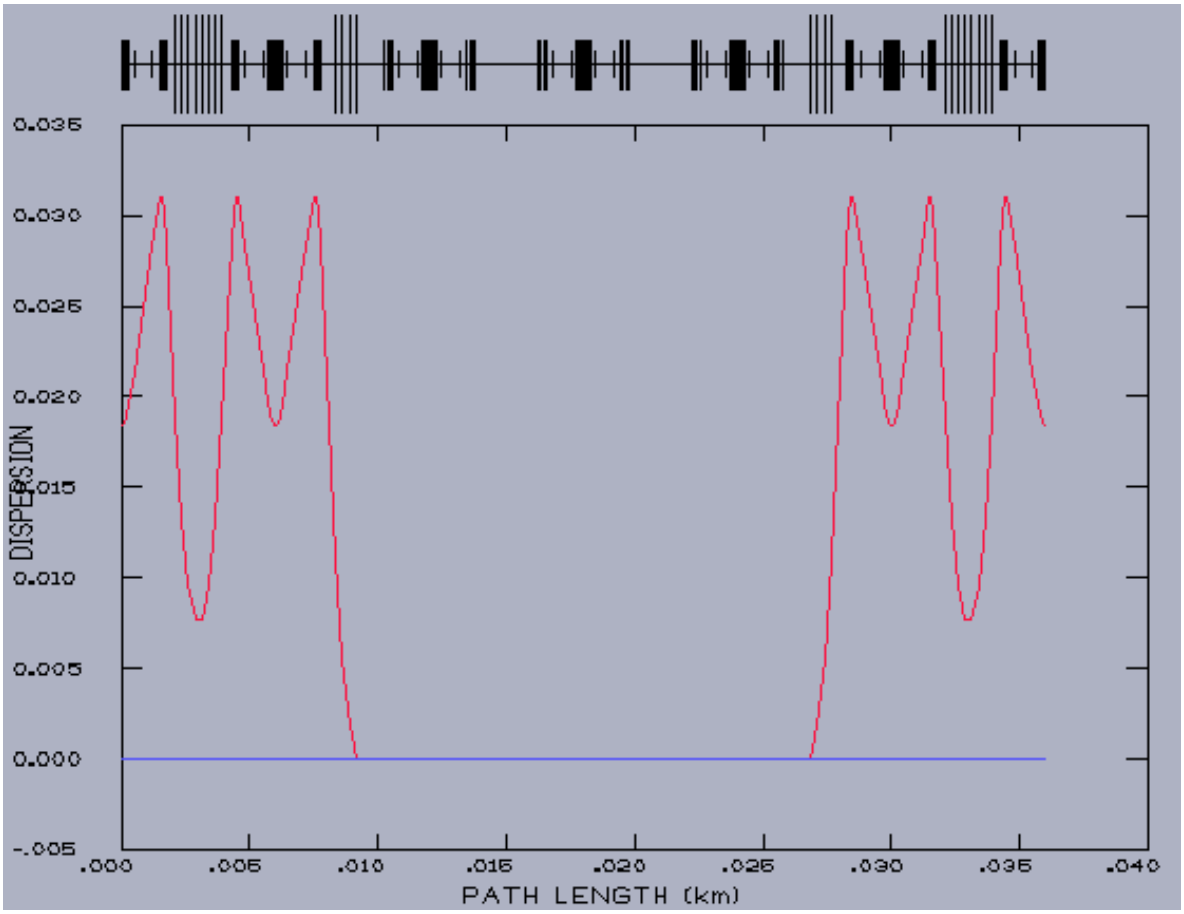

Figure 8.3.1: Six consecutive minimum emittance cells, with the second and fifth cells modified to provide zero dispersion in the third and fourth cells. Bending magnets, quadrupoles, and sextpoles are indicated by long medium and short hatch marks in the schematic above the graph.

by exploiting the correlation between production angle and wavelength by limiting ϑ. It therefore seems sensible to perform collimation at a large distance where the transverse position is dominated by production angle rather than production position. A collimator at such a position will limit the ϑ range. Such an aperture will only be effective if the spread of electron angles is small compared to $1/\gamma$.

The spatial and angular width parameters that influence the brilliance are contained in the product

$$\sigma_{\gamma,x}\sigma_{\gamma,x'}\sigma_{\gamma,y}\sigma_{\gamma,y'} = \sqrt{\beta_x\epsilon_x}\sqrt{\frac{\epsilon_x}{\beta_x}+\frac{f}{\gamma^2}}\sqrt{\beta_y\epsilon_y}\sqrt{\frac{\epsilon_y}{\beta_y}+\frac{f}{\gamma^2}} \approx \sqrt{\beta_x\epsilon_x}\sqrt{\beta_y\epsilon_y}\,\frac{f}{\gamma^2} \qquad (8.3.1)$$